Characterizing Water on Early Mars through the Geomorphic Analysis,

Crater-Age Dating, and Sediment Transport Modeling

of Valley Networks and Deltas

by

Monica Renee Theilen Hoke

B.S. Florida Institute of Technology, 2000

M.S. Florida Institute of Technology, 2003

M.S. University of Colorado, Boulder, 2008

A thesis submitted to the

Faculty of the Graduate School of the

University of Colorado in partial fulfillment

of the requirement for the degree of

Doctor of Philosophy

Department of Astrophysical and Planetary Sciences

2011

This thesis entitled:
Characterizing water on early Mars through the geomorphic analysis, crater-age dating, and
sediment transport modeling of valley networks and deltas

written by Monica Renee Theilen Hoke
has been approved for the Department of Astrophysical and Planetary Sciences

_____

Dr. Brian M. Hynek

_____

Dr. Philip J. Armitage

_____

Dr. David A. Brain

_____

Dr. Bruce M. Jakosky

_____

Dr. Gregory E. Tucker

Date: _____

The final copy of this thesis has been examined by the signatories, and we
Find that both the content and the form meet acceptable presentation standards
Of scholarly work in the above mentioned discipline.

Hoke, Monica R. T. (Ph.D., Astrophysical and Planetary Sciences)

Characterizing water on early Mars through the geomorphic analysis, crater-age dating, and

sediment transport modeling of valley networks and deltas

Thesis directed by Assistant Professor Brian M. Hynek

ABSTRACT

The presence of valley networks across much of the ancient surface of Mars, together with the locations and morphologies of the ancient Martian deltas and paleolakes, provides strong evidence that the Martian surface environment was once capable of sustaining liquid water at the surface. Many of the largest valley networks have characteristics consistent with their formation primarily by precipitation and surface runoff. However, the timing and duration of clement conditions on Mars has remained unclear.

Ten of the largest valley networks on Mars were mapped, crater-age dated, and analyzed to understand changes in fluvial erosion during early Martian history. Crater-age dating of individual valley networks revealed ages that cluster in the Late Noachian and Early Hesperian, consistent with their formation during a period of enhanced fluvial erosion and incision on Mars. Formation timescales of the valley networks were investigated through the use of three different sediment transport models, the Darcy-Weisbach flow velocity equation, and a variety of parameters to encompass a range of possible formation conditions. With runoff rates similar to intense storms in arid regions on Earth, the minimum formation timescales of these Martian valley networks range from 10^5 to 10^7 years. Shorter formation timescales require hurricane-scale flows that, if minimized with assumptions of continuous formation unlike even terrestrial rates, could complete large valley network formation in as little as 200 to 5000 years, though this is not the preferred interpretation. Investigating the effects of changing hydrologic and sedimentary conditions on Martian delta formation with 3-D modeling indicates that significant off shore sedimentation is common, particularly with high river discharge scenarios. These results have important implications for the formation timescales of the deltas and the lack of identifiable deltas on Mars today.

While the results of this thesis do not support impact-induced climate change as the mechanism for creating precipitation sufficient to incise the large valley networks, neither do they extend the amount of time required to form the features beyond their range in age, consistent with hypotheses that precipitation was constrained to a relatively short period of Martian history near the Noachian-Hesperian boundary, approximately 3.6 to 3.8 Ga.

DEDICATION

I dedicate this dissertation to the memory of my grandparents: Joseph Oran Edmonds, Betty Bonigene Edmonds, Grace Marjorie Theilen, and John Wallace Theilen. Granpa Joe, you were an amazing man who could (and did) do anything. Grandma Betty, I will always cherish your many fantastic stories. Grandma Marge, your devotion to your family was always an expression of your love. Grandpa John, your words follow me in every stage of my life: Pride, Integrity, Perseverance. Yours was truly a great generation, and I am continuously amazed at how fully you lived your lives.

I also dedicate this dissertation to my son, Calvin Theil Hoke, and to my niece, Kelsey Morgan Theilen. As your great-grandpa John would have said, whatever in life you do, always to yourself be true.

ACKNOWLEDGEMENTS

have helped me on my path to where I am today. Thank you, Henryk Goreki, Dan Simmons,

Kim Stanley Robinson, and Joss Whedon for sharing your brilliant ideas with the world.

Table of Contents

Contents

List of Tables

List of Figures

1 Introduction

The possibility of liquid water on other planets has for generations sparked imaginations and directed the focus of scientists and engineers, as well as politicians and the public. The simple H_2O molecule has played such an important role in forming the planets of our solar system, shaping the Earth's surface, and facilitating the origin and evolution of life that NASA focused its Mars exploration program on finding water. This focus began with Giovanni Schiaparelli's 1877 drawings of "canali" on Mars that inspired the excited, though flawed, interpretation of artificially-built canals (Lowell, 1906), was confirmed with the first Mariner 9 images showing a natural fluvial history on Mars' surface (e.g. Baker, 1982; Masursky, 1973; Mutch et al., 1976), and continues with the Mars Science Laboratory that launches in November 2011 to assess Mars' habitability. Mars offers the potential to answer fundamental questions regarding the role of water in planetary atmosphere, surface, and interior evolution; the potential for life, present and past; and the opportunity to someday inhabit her ancient shores.

Water was delivered to Mars in much the same way that it reached Earth 4.5 billion years ago, through the mixing of the outer solar system's volatile-rich proto-planetary material with the growing inner solar system's terrestrial planets. Over time, much of that initial water supply has been lost to the surface and to space (e.g. Jakosky and Phillips, 2001). While atmospheric loss to space by impact ejection affects all atmospheric constituents equally, loss due to thermal escape and solar wind stripping preferentially removes lighter isotopes. Measurements of the deuterium to hydrogen ratios show a considerable enrichment in the heavier deuterium isotope, indicating a significant amount of Mars' initial water has been lost to space (e.g. Jakosky and Phillips, 2001).

Unlike Earth, what remains of Mars' water inventory is frozen at its poles, on its surface, and in its underground. When the Phoenix lander scratched the surface of the northern plains at

68.22° North latitude in 2008, it found a frozen water ice table mere centimeters below the surface (Smith et al., 2009). These results supported the decades of research that hypothesized the presence of ground ice, as evidenced by permafrost features (e.g. Carr and Schaber, 1977), polygonally patterned crust (e.g. Seibert and Kargel, 2001), crater ejecta patterns (e.g. Strom et al., 1992), ground ice modeling (e.g. Leighton and Murry, 1996; Mellon and Jakosky, 1995), and orbital measurements of hydrogen in the soil (e.g. Boynton et al., 2002).

Though the currently thin, 5 mbar atmosphere contains little water (Smith, 2002), some water and carbon dioxide are cycled between the poles and low latitudes throughout the Martian year, allowing water vapor to accumulate into clouds in the Martian sky and form layers of frost and snow that cover the ground (e.g. Smith et al., 2009). Recent swings to higher obliquity may have redistributed significant water ice on the Martian surface (e.g. Haberle et al., 2003; Mischna et al., 2003), driving the formation of glacial deposits at low latitudes (e.g. Head et al., 2005). Looking further back in time, the water that is now locked in frozen stores at its poles and within the Martian surface and subsurface may have once traveled the globe in an active hydrological cycle, moving sediment and altering the surface as it went.

1.1 Liquid water early in Martian history: On the move

Water left its trace in a much larger way earlier in Martian history, attributing to a more significant role in shaping the surface then than now. This role is most pronounced with the enormous outflow channels that scar the surface where water erupted from the equatorial underground and flowed downhill to the northern lowlands (Baker et al., 1992) in periodic bursts during the Hesperian (the middle epoch in Martian history that lasted approximately 3.0 to 3.7 billion years ago (Hartmann and Neukum, 2001)), and into the Amazonian (the current Martian

epoch, extending from ~3.0 Gyr to present (Hartmann and Neukum, 2001) (e.g. Ivanov and

Head, 2001; Nelson and Greeley, 1999; Rotto and Tanaka, 1995)).
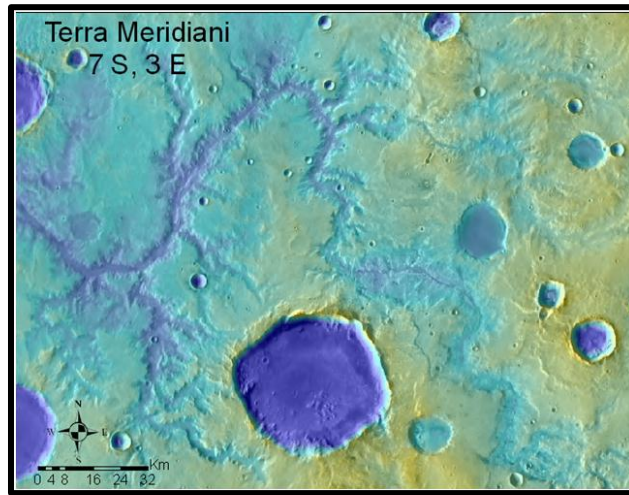
Figure 1. The valley network centered at 7°N latitude and 3°E longitude is shown in co-registered Mars Orbiter Laser Altimeter (MOLA) topography and Thermal Emission Imaging System (THEMIS) daytime infrared (IR) data.

Networks of valleys (Figure 1) similar in appearance to dried-up versions of Earth's river

systems incise much of the southern highlands on Mars. Most, though not all, of the Martian

valley networks are located on ancient surfaces, and they appear to have formed during a final

stage of fluvial erosion that occurred sometime during the Late Noachian (~3.7 to 3.8 Gyr) or

Early Hesperian (~3.7 to 3.6 Gyr) epochs (e.g. Howard et al., 2005; Hynek and Phillips, 2001,

2003; Hynek et al., 2010; Irwin et al., 2005a). These drainage features are significantly smaller

than the outflow channels and are generally believed to have formed 1) in a warmer, thicker

atmosphere by precipitation and runoff of water on the surface; 2) by liquid water seeping out of

the ground, causing headward growth by sapping; or 3) a combination of precipitation and

groundwater sapping (e.g. Baker and Partridge, 1986; Carr, 1995, 1996; Craddock and Howard,

2002; Howard et al., 2005; Hynek and Phillips, 2001, 2003; Pieri, 1980; Sharp and Malin, 1975).

Evidence for the formation mechanism(s) can be found in the geomorphic features of the valleys (Carr, 1996). Some valleys appear to be immature in plan form with few and/or stubby tributaries, consistently sized valleys that do not widen downstream, and alcove-like heads that suggest formation by the headward propagation of the valley through groundwater sapping (e.g. Baker and Partridge, 1986; Goldspiel et al., 1993; Malin and Carr, 1999; Pieri, 1976). Alternatively, Martian valley characteristics attributed to formation by precipitation and surface runoff include densely spaced, dendritic tributaries that often reached up to drainage divides and widths and depths that generally increase downstream (e.g. Carr, 1996; Craddock and Howard, 2002; Hynek and Phillips, 2003). These characteristics suggest the valleys formed from a widespread source of water, as would occur by precipitation, and that the erosive capability of the surface runoff increased as tributaries intersected and combined discharges downstream.

Often, the interior valley cross section shape is attributed to the formation mechanism. Groundwater sapping processes tend to form box-, or U-shaped canyons with relatively flat floors and steep walls, whereas precipitation and runoff produce more V-shaped valleys. Many Martian valleys have both U- and V-shaped profiles (Williams and Phillips, 2001). This may be an indication that both groundwater and precipitation processes contributed to the formation of the valley networks. If precipitation and surface runoff formed the valleys, some infiltration and ground water sapping also likely played a role. Likewise, if groundwater sapping was the dominant formation mechanism, precipitation may have been necessary for the aquifer to refill. Many researchers have described evidence for reactivation of the valley networks and a shift from precipitation-dominated to groundwater sapping-dominated regimes toward the end of their formation (Baker and Partridge, 1986; Williams and Phillips, 2001). However, the interior cross section may also be a reflection of the preservation state of the valley, with pristine V-shaped

valleys degrading to U-shapes as they experience wall collapse and infilling. Many processes

have affected the valley networks since their formation, including impacts, eolian transport, mass

wasting, and mantling by dust, impact ejecta, and/or volcanic ash, and the valley networks are

found in different degrees of preservation (e.g. Carr, 1996; Craddock and Howard, 2002; Irwin

and Howard, 2002; Irwin et al., 2008; Howard, 2007; Hynek and Phillips, 2003).

These different formation mechanisms are characterized by very different amounts and

rates of water needed to form the valleys, which in turn, suggest very different climate conditions

that characterize the timing of their formation (Carr, 1996). The interpretation of the valleys as

having formed from precipitation and surface runoff often invokes conditions that are much

warmer and wetter than on Mars today; conditions that are sometimes compared to arid, semi-

arid, and temperate regions on Earth (e.g. Barnhart et al., 2009; Hynek and Phillips, 2001;

Stepinski and Stepinski, 2005). The duration of clement conditions may have persisted

throughout the Noachian, particularly during the Late Noachian when it is assumed most of these

features formed, or they may have occurred as one or more short bursts of intense fluvial activity

(e.g. Howard et al., 2005; Irwin et al., 2005a). Invoking drastically different climatic conditions

on Mars during a time when the sun was less luminous made the warm, wet conditions for valley

formation difficult to explain (Carr, 1996).

Many researchers argued that warm, wet conditions were not required to form the

Martian valley networks and that their formation was a result of groundwater sapping, which can

operate under less favorable conditions (e.g. Baker and Partridge, 1986; Pieri, 1980). Some even

suggested that Mars has always been cold and dry and that the valleys formed by groundwater

sapping due to geothermal heating (Carr and Malin, 2000; Goldspiel and Squyres, 2000; Gulick

and Baker, 1990). However, transporting the eroded rocks out of the valley poses a problem for

groundwater sapping scenarios (Craddock and Howard, 2002; Lamb et al., 2006). And the lack

of continued valley formation throughout Martian history suggests conditions on Mars were

indeed different from today (Craddock and Howard, 2002).

It was noted in early studies that the regions between networks were largely undissected,

attributing the lack of incision to localized water sources of low discharge (e.g. Carr, 1995;

Malin and Carr, 1999). Carr (1995) produced a global map of Martian valley networks from

Viking-based Mars Digital Image Mosaic (MDIM) data that that was dominated by immature

widely spaced valleys with few tributaries. The Carr (1995) results supported the interpretation

that these features formed primarily by groundwater sapping associated with fluvial (e.g. Pieri,

1980; Sharp and Malin, 1975) or mass wasting (Carr, 1995) processes.

With improved quality and resolution of data from the Mars Global Surveyor, Mars

Odyssey, Mars Express, and Mars Reconnaissance Orbiter missions, many additional studies

were able to analyze the valley networks in greater detail. Hynek and Phillips (2003) identified

up to an order of magnitude more valleys in these systems, with tributaries that reached up to

drainage divides and drainage densities comparable to some terrestrial precipitation-fed systems.

Within some of the Martian valleys, interior channels and terraces are observed, hypothesized to

have formed by rivers (Craddock and Howard, 2002). Many valleys follow a meandering path

indicative of slow-moving rivers that, upon reaching a bend, deposit sediment on the inside bank

and preferentially erode the outside bank. Recently, a global map of Martian valley networks

was created that updated the Carr (1995) Viking data-based version using primarily the Thermal

Emission Imaging System (THEMIS) daytime infrared (IR) data and Mars Orbiter Laser

Altimeter (MOLA) data (Hynek et al., 2010). This new map identified many more valleys in the

previously undissected regions and found that nearly every region of the Noachian-aged surface below 60° latitude contained significant dissection by valleys (Hynek et al., 2010).

These observations have led many researchers to conclude that valley networks formed primarily by precipitation and surface runoff (e.g. Craddock and Howard, 2002; Howard et al., 2005; Hynek and Phillips, 2003; Irwin et al., 2005a), and that earlier observations of widely-spaced tributaries and undissected inter-valley surfaces were, at least in part, due to limitations of Viking data (e.g. Hynek et al., 2010).

However, high-resolution MOC images have shown a lack of fine-scale incision associated with the valley networks (Carr and Malin, 2000), which should be present in precipitation-formed systems. The lack of small tributaries may be a result of high infiltration rates of the Martian soil (Baker and Partridge, 1986), resistance of the surface to erosion (e.g. Craddock and Howard, 2002), or removal through geological processes including eolian deposition, dust and volcanic ash mantling, impact crater ejecta, and impact crater gardening (e.g. Craddock and Howard 2002; Hynek and Phillips 2003; Irwin and Howard 2002; Irwin et al 2008).

The formation of valley networks through precipitation and surface runoff processes would have produced extensive erosion and deposition on the surfaces the valley networks incise. Indeed, large regions of the Noachian highlands have had several hundreds of meters of surface material removed and crater floors filled (Carr, 1996; Craddock and Howard, 2002; Craddock et al., 1997; Forsberg-Taylor et al., 2004; Howard et al., 2005; Hynek and Philips, 2001). These high erosion rates during the Noachian, interpreted as being a the result of precipitation and surface runoff, are estimated to be approximately 1000 times higher than

currently on Mars (Craddock and Howard, 2002; Craddock and Maxwell, 1993; Hynek and Phillips, 2001; Golombek et al., 2006).

1.2   <u>Where the Waters Pool</u>

The valley networks are spatially and temporally coincident with impact craters that have been interpreted to have once contained lakes and seas (e.g. Cabrol and Grin, 1999; Fassett and Head, 2008a; Irwin et al., 2005a; Ori et al., 2000; Scott et al., 1995). These crater paleolakes are characterized by degraded states in which their rims are lowered and their basins filled, often reducing crater depths significantly and creating an abrupt change in slope from the crater wall to a relatively flat crater floor (Irwin et al., 2005a). Fluvially-formed terraces that rim the crater interior as well as inlet valleys, with or without outlet valleys, are often used to identify the crater as having been altered by a standing body of water (e.g. Cabrol and Grin, 1999; Fassett and Head, 2008a; Irwin et al., 2005a; Ori et al., 2000). Although some of these interpretations have been subsequently reinterpreted as having had volcanic origins (e.g. Leverington and Maxwell, 2004; Squyres et al., 2004), recent comparison of the global distribution of valley networks (Hynek et al., 2010) and valley-fed open-lake basins on Mars (Fassett and Head, 2008a) show a correlation between paleolake formation and regions of high drainage density, placing the basins in regions of known past fluvial activity.

Some of the crater paleolakes contain deposits of sedimentary material that are interpreted to be fan and deltas deposits, formed at the mouth of valleys where they open into the basins. Deltas, which are the deposited sediment from a river that slows upon entering a body of water, such as a lake, sea, or ocean, are found across Mars at mostly low latitudes on primarily Noachian-age terrain (e.g. Cabrol and Grin, 1999, 2000; Di Achille and Hynek, 2010a; Irwin et al., 2005a; Ori et al., 2000). The Martian deltas come in many shapes and sizes, presumably

8

reflecting a range of formation conditions and preservation states. The meandering channels (now inverted), layering, and multi-lobed shape of Eberswalde Delta (e.g. Malin and Edgett, 2003; Moore et al., 2003; Pondrelli et al., 2010; Wood, 2006) and the Jezero deltas (e.g. Ehlmann et al., 2008; Fassett and Head, 2005) suggest deposition of clay, sand, and gravel in a lacustrine environment with temporal variations in the composition of grain size of the supplied sediment, lake levels, and flow discharge rates. Interestingly, layers of gravel and boulders up to a few meters in diameter are also seen within the layers of Eberswalde and Jezero deltas (Ehlmann et al., 2008; Howard et al., 2007; Pondrelli et al., 2008; Schieber, 2007), suggesting at least some of the Martian deltas contain grain sizes that range from clay to boulders. These observations point to varied formation conditions that at times supported the slow deposition of the smaller grains and at other times were capable of transporting larger rocks.

Alternatively, some deltas have characteristics that arguably suggest a simpler, shorter formation scenario. Nepenthes is a well-preserved Gilbert delta (de Pablo and Pacifici, 2008) with a smooth cone-shaped flat top surface and a steep frontal scarp. This type of sedimentary deposit forms when a river enters into a body of water, slows, and deposits its load in a semi-circular fan-shaped body with relatively flat upper surfaces and steep distal fronts (Gilbert, 1885). The Nanedi delta deposit that nearly fills its small crater has fine layers a few meters thick and steep 50-m high, well rounded distal edges that may indicate depositional lobes in a lacustrine environment (Hauber et al., 2009). Kleinhans et al. (2010) concluded that both the Nepenthes and Nanedi deltas formed from a dilute bedload-dominated flow as a result of a single event, as evidenced by well-preserved shorelines. The Tyras deposit also appears to be composed of primarily fine-grained material and has two scarps that may have been carved by wind-generated waves, suggesting this fan-delta experienced a complicated formative history

characterized by changing paleolake levels (Di Achille et al., 2006). Others, however, interpret the stair-step topography similar to that of Tyras and other deposits as having formed by high discharges of both bedload and suspended load sediment over short periods of time during single outflow events (e.g. Kleinhans et al., 2010; Kraal et al., 2008).

Ori et al. (2000) described evidence for several Gilbert-type deltas in craters on Mars and argued that their formation cannot have been by one or a few very high energy cataclysmic flooding events. Rather, due to the complex nature of some of the Martian deltas and the interpretation that terraces were formed by wave action, the lakes must have been present for several thousands of years, at a minimum. If the Eberswalde and Jezero deltas formed intermittently by seasonal or ephemeral flows, their formation may have taken thousands to millions of years (e.g. Fassett and Head, 2005; Moore et al., 2003). However, if continuous formation conditions are evoked, formation timescales can drop by several orders of magnitude (e.g. Fassett and Head, 2005; Hauber et al., 2009; Jerolmack et al., 2004; Kleinhans et al., 2010).

Most of the previous efforts to determine possible formation timescales of the Martian deltas relied on bulk flow and transport calculations of a single grain size, and assumed that all of the sediment supplied to the system was deposited in, and remained on, the delta. Often, continuous formation conditions are assumed, and, not surprisingly, very short timescales result. However, deposition of sediment in a lacustrine environment and their formative timescales can be affected by many parameters not incorporated in the more simplified treatments, including basin topography (i.e. bathymetry), sediment grain sizes, sediment concentrations, and river characteristics.

The water that presumably formed the valley networks and outflow channels would have flowed into the northern lowlands where they deposited their sediment loads (e.g. Lucchitta et al,

1986) and possibly collected into an ocean (e.g. Baker et al., 1991; Head et al., 1999; Parker et al., 1989). Some of the evidence for a northern ocean, which is still highly debated (Ghatan and Zimbelman, 2006; Kargel et al., 1995; Malin and Edgett, 1999; Tanaka, 1999; Withers and Neumann, 2001), includes potential shorelines (Parker et al, 1989, 1993), topographic smoothness within the northern plains and roughly constant elevation along proposed shorelines (Head et al., 1999), and the elevation of delta deposits, particularly those in open basins that border the dichotomy between the southern highlands and the northern lowlands (Di Achille and Hynek, 2010a).   Although the presence of a northern ocean is neither required nor excluded by many of the other ancient fluvial features found on Mars, the active hydrological cycle that it would create (Soto et al., 2010) fits into the formation scenarios of many valley networks and deltas. Describing how such an environment that is so different from what exists today could have formed and persisted on Mars remains an important open question in Martian research.

1.3   Climate

The formation of large drainage networks, alluvial fans, and deltas during this period indicates sustained flows of water (Howard et al., 2005), suggesting the early Martian atmosphere during which most of the valley networks formed was either continuously or episodically warmer, thicker, and wetter than today. Episodic changes in atmospheric temperature, pressure, and humidity may have been driven by changes in obliquity and orbit, impact events, and volcanic activity (e.g. Baker, 2001; Baker et al., 1991; Carr, 1996; Jakosky and Phillips, 2001; Jakosky et al., 1995; Phillips et al., 2001; Segura et al., 2002).

Making a case for an early Martian atmosphere that sustained the flow of liquid water on its surface has been challenging for many researchers over many decades (e.g. Haberle et al., 1994; Kasting, 1991; Mischna et al., 2000; Soto and Richardson, 2009). Mars would have

required a substantially thicker atmosphere composed of greenhouse gases in order to increase the surface temperature enough to allow liquid water to persist. Sources of greenhouse gases such as carbon dioxide, sulfur dioxide, and water may have come from volcanic outgassing, which is known to have been widespread on Mars during the Noachian and Hesperian (e.g. Jakosky and Phillips, 2001; Phillips et al., 2001). However, a thick CO_2 atmosphere would produce clouds that would increase the Martian albedo and reduce warming (Kasting, 1991). Forget and Pierrehumbert (1997) and Mischna et al (2000) incorporated into their models the ability of CO_2 ice clouds to also reflect surface thermal radiation back to the surface, though the overall effect was probably not enough to increase surface temperatures (Jakosky et al., 2005).

During the first billion years of our solar system's history, during which Mars formed most of the fluvial features we see today, the sun's output was 30% less than it is today (Gough, 1981; Newman and Rood, 1977) and the spectrum peaked in the ultraviolet rather than the visible. The extreme ultraviolet (EUV) radiation radiated by the young sun was up to 20 times greater 4.1 billion years ago than it is today (Ribas et al., 2005; Tian et al., 2009). The high EUV radiation at this time in Martian history would have destroyed upper atmospheric CO_2 and other molecules, resulting in upper atmospheric heating and expansion. Due to Mars' low gravity, this atmospheric heating and expansion left the atmospheric constituents vulnerable to increased thermal escape of the atmosphere, preventing a CO_2-dense greenhouse atmosphere from forming (Tian et al., 2009). As the sun matured, the EUV flux decreased, allowing a dense CO_2 atmosphere to form for the first time in the late Noachian (Tian et al., 2009). This delayed ability of the Martian atmosphere to develop an effective greenhouse agrees with the analysis of Irwin et al. (2005a) and other researchers that Mars experienced a period of intense fluvial

activity for a brief period during the Late Noachian and Early Hesperian during which time valleys were incised, paleolakes filled, and deltas formed.

A carbon-rich atmosphere supporting precipitation would produce carbonate deposits on the surface as atmospheric carbon was dissolved in water droplets and transported to the surface in rain (Pollack et al., 1987). Evidence for some carbonates are found in the global Martian dust, which contain up to 5% carbonates (Bandfield et al., 2003). It is possible significant stores of carbonates are also located under the surface, either transported into the crust by circulating groundwater or buried by subsequent processes. Evidence for layers of buried carbonates exposed within an impact crater suggests extensive carbonate deposits may be present beneath impact ejecta and volcanic resurfacing on Mars (Michalski and Niles, 2010). Carbonates may also have been destroyed by ultraviolet radiation (Clark, 1979; Mukhin et al., 1996) or reactions with sulfuric acid (e.g. Catling, 1999; Clark, 1999), or never formed due to the presence of a reducing atmosphere (e.g. Craddock and Howard, 2002; Fairen et al., 2004). Mars' atmosphere likely had significant amounts of SO_2 and H_2S from volcanic outgassing (Johnson et al., 2008), which would have led to the formation of sulfuric acid, thus preventing carbonate formation.

Interactions of the primarily basaltic Martian crust with acidic water would have eventually broken down the basalt into phyllosilicates or sulfate minerals. Abundant water-altered minerals have been detected on the surface of Mars (Bibring et al., 2006; Murchie et al., 2009; Taylor et al., 2006), but not in the areas of highest valley density (Hynek et al., 2010). The water-altered minerals may be missing, at least in part, due to eolian and impact processes (Hynek et al., 2010), but it is still surprising that the regions receiving significant precipitation are missing the mineralogical evidence of their watery past.

Not all salts are missing from the dissected surfaces of Mars, though. Using THEMIS thermal infrared images, Osterloo et al. (2008, 2010) identified chloride salts in 640 locations across Noachian and Hesperian-aged terrain that correspond to regions of valley network incision (Hynek et al., 2010) and valley-fed paleolakes formation (Fassett and Head, 2008a). The chloride salts are found primarily in topographic lows, and some appear to have been buried and subsequently exposed and eroded. This may explain why large regions containing the salts are not observed.

An alternative method of creating warm, wet conditions on early Mars has been proposed to have been achieved by impacting bolides (Segura et al., 2002, 2008; Toon et al., 2010). Although large impacting bolides will eject atmospheric gases to space, thus representing a significant source of atmospheric loss early in Martian history (e.g. Brain and Jakosky, 1998), they can also provide a source of heating and volatiles to the planetary surface. Segura et al. (2002, 2008) showed that the temporary warming of the surface following an impact would have allowed evaporation and/or melting of frozen reservoirs of water in the poles and subsurface. The significant amount of volatiles delivered to Mars by large impactors would have also created a temporary steam atmosphere, which would have rained out and, combined with the surface heating and sustained evaporation, would have created a global hydrological cycle lasing months to years (Segura et al., 2002). The Segura et al (2008) model of impact-induced climate change from impactor-diameters of 30 to 100 km is characterized by a brief period of continuous precipitation lasting 0.5 to 3 years, respectively. This period is then followed by intermittent precipitation due to active hydrological cycles created from evaporation, condensation, and precipitation lasting up to decades until the surface temperature falls below freezing and the atmospheric moisture is lost to condensation at the poles. As the impact-induced climate change

14

affects Mars globally and not just near the impact site, an impact anywhere on the surface could be used to explain the formation of valley networks during the limited time following the impact event. However, it is not clear that the timing or duration of impact-induced warming is sufficient to produce many of the large Martian valley networks.

1.4   <u>**Understanding the "when, where, how, and how long" of water on early Mars**</u>

All of the above discussion suggests that Mars was once very different than it is today; that perhaps Mars experienced precipitation that flowed into rivers, and where the rivers met the sea, deltas formed. The timing and duration of clement conditions on Mars, however, has remained unclear. Knowing when the Martian valley networks formed tells us when Mars was potentially warmer and wetter and, possibly, habitable. Estimations of how long it took the valley networks and deltas to form provides important constraints on the duration of the clement climate that was needed to sustain liquid water on the Martian surface. These were the goals of the research presented in this thesis.

The Martian valley networks have often been assigned an age based on the age of the surface on which they occur and superposition relationships with other geologic features (e.g. Carr, 1996; Carr and Clow, 1981). Determining the ages of actual valley formation, however, provides much more precise constraints on the timing and duration of warmer, thicker atmospheric conditions. In Chapter 2 (Hoke and Hynek, 2009), valley network ages were determined through crater counting on the valley networks themselves, providing a minimum age bound on the end of their formation. With the global THEMIS daytime IR dataset and MOLA topography, craters down to a few hundred meters across that overlap the valley networks were identified, allowing a more precise crater age dating of the valley networks themselves that is independent of the surrounding surface on which they lie (Hoke and Hynek,

2009). Since valley networks have limited surface areas, their crater densities were determined

with a method tailored for counting craters on narrow linear features (Tanaka, 1982). Due to the

limited number of craters that were able to be counted on smaller valley networks, only the

largest or most extensive valley networks were analyzed in this work.

While the crater-age dating revealed valley network-specific ages that cluster in the Late

Noachian and Early Hesperian and show a range in ages that span tens of millions of years

(Hoke and Hynek, 2009), it is uncertain how long thicker and warmer atmospheric conditions

were needed to produce the valley networks. In Chapter 3 (Hoke et al., 2011), the formation

timescales of the Martian valley networks are investigated through the use of three different

sediment transport models, the Darcy-Weisbach flow velocity equation, and a variety of

parameters to encompass a range of possible formation conditions. This is done specific to each

of seven of the largest valley networks in the Terra Sabaea, Arabia Terra, and Meridiani regions

of Mars, all of which have characteristics consistent with their formation primarily by

precipitation and surface runoff (Hoke and Hynek, 2009). To better represent past Martian

conditions, the use of terrestrial empirical relationships were minimized, when possible. As

well, an analysis of an analogous terrestrial river system was completed with the same methods.

Finally, the valley network-specific sediment transport rates and formation timescales were

compared with prior age-dating of the valley networks through crater density analysis (Hoke and

Hynek, 2009) to understand the state of the climate at this time in Martian history.

In Chapter 4, delta formation timescales as a function of varying sediment and river

characteristics were explored. Several researchers have performed analyses that addressed the

timing and duration of formation, however there is much disagreement on the conditions and

duration of delta formation on Mars. Formation timescales of the Martian deltas span weeks or

months (e.g. Hauber et al., 2009; Kleinhans et al., 2010; Kraal et al., 2008) to thousands or millions of years (e.g. Di Achille et al., 2006; Fassett and Head, 2005; Moore et al., 2003; Ori et al., 2000) depending on the delta characteristics, discharge rates, degree of intermittency, and methods used by the researchers.

For this study I used Sedflux 2.0, a 2-D and 3-D basin-filling model that uses event-based time stepping (e.g. seasons) to determine the spatial and temporal deposition of multi-grained sediment load from a river into a standing body of water while tracking sediment properties such as grain size, density, porosity, etc. Sedflux, which is managed by the Community Surface Dynamics Modeling System (CSDMS) at the Institute for Alpine and Arctic Research (INSTAAR) of the University of Colorado (e.g. Hutton and Syvitski, 2008; Syvitski and Hutton, 2001), creates a framework within which individual process-response models operate. Delta formation was modeled under Martian conditions in an effort to understand their formation conditions and timescales.

By comparing our valley network crater-age dating results with the valley network and delta formation timescales, we are able to provide important constraints on the duration of the clement climate that was needed to sustain liquid water on the Martian surface.

2 Roaming zones of precipitation on ancient Mars as recorded in valley networks

Abstract: The ten largest valley networks in the Terra Sabaea, Arabia Terra, and Meridiani Planum regions of Mars were mapped, crater-age dated, and analyzed by geomorphology, stream order, and drainage density to understand changes in fluvial erosion during early Martian history. All of these networks demonstrate characteristics consistent with formation by precipitation. Many appear to be in different stages of preservation, with both highly eroded and pristine valleys sometimes appearing in the same network. In some cases, the valley network morphologies and crater-age dating indicate multiple periods of formation. The results from this research place precipitation-driven formation of the Martian valley networks in Terra Sabaea, Arabia Terra, and Meridiani Planum in the Late Noachian and Early Hesperian epochs (~3.6 to 3.8 billion years ago). Our age estimates do not extend into earlier or later Martian history, and the spread in these ages indicates they did not all form, or cease formation, at the same time. The difference in age between the oldest and youngest valley networks in Terra Sabaea, Arabia Terra, and Meridiani Planum analyzed in this work is ~210 Myr, ±50 Myr. Within this range are valley networks that have distinctly separate ages and those that appear to be coeval. This research suggests the Late Noachian and Early Hesperian were characterized by roaming zones of precipitation that occurred during either continuously warmer and thicker atmospheric conditions or intermittently clement conditions, with precipitation occasionally returning to previously rainy regions and overall continuing near Meridiani Planum longer than in Terra Sabaea.

2.1 <u>Introduction</u>

The presence of valley networks across much of the ancient surface of Mars is the most significant indicator that the Martian surface environment was once capable of sustaining long-duration flowing water under drastically different atmospheric conditions. These drainage features are generally believed to have formed in a warmer, thicker atmosphere by: 1) precipitation and runoff of water on the surface; 2) liquid water seeping out of the ground, causing headward growth by sapping; or 3) a combination of precipitation and groundwater sapping [Sharp and Malin, 1975; Pieri, 1980; Gulick and Baker, 1990; Carr, 1995, 1996; Goldspiel and Squyres, 2000; Carr and Malin, 2000; Hynek and Phillips, 2001, 2003; Craddock and Howard, 2002; Howard et al., 2005]. Evidence for the formation mechanism(s) can be found in the geomorphic features of the valleys [Carr, 1996]. Densely spaced, dendritic systems

with valleys that reach up to drainage divides and increase in width and depth downstream suggest formation by precipitation and surface runoff. Widely spaced systems with few tributaries, consistently sized valleys, and alcove-like heads suggest formation by the headward propagation of the valley through groundwater sapping. However, these features may also be a reflection of the surface layer resistance to erosion by surface runoff, and they may therefore still suggest formation by precipitation.

Drainage systems can be quantitatively described by a series of parameters, including stream order, stream length, and drainage density. Determination of these parameters is greatly affected by the ability to identify the small, shallow tributaries. For Mars, the ability to identify small tributaries depends on the resolution and coverage of the data used to map the valley networks as well as the preservation of these small, shallow tributaries from infilling [e.g. Hynek and Phillips, 2003]. Using the Viking-based Mars Digital Image Mosaic (MDIM) (~230 m/pixel) data, Carr [1995] produced a global map of valley networks that was dominated by immature, widely spaced valleys with few tributaries, which supported the interpretation that these features formed primarily by groundwater sapping associated with fluvial [e.g. Sharp and Malin, 1975; Pieri, 1980] or mass wasting [Carr, 1995] processes. With improved quality of images from the Mars Global Surveyor (MGS) Mars Orbiter Camera (MOC) (240 m/pixel) [Malin and Edgett, 2001] combined with gridded topography from the MGS Mars Orbiter Laser Altimeter (MOLA) (~30 cm/pixel vertical resolution and ~460 m/pixel horizontal resolution at the equator) [Smith et al., 2001], Hynek and Phillips [2003] identified up to an order of magnitude more valleys in these systems, with tributaries that reached up to drainage divides and drainage densities comparable to some terrestrial precipitation-fed systems. These observations supported the interpretation that precipitation and surface runoff played a bigger role than

19

groundwater sapping in the formation of these Martian valley networks [Hynek and Phillips, 2003].

The Thermal Emission Imaging System (THEMIS) instrument onboard the Mars Odyssey (MO) spacecraft is a multispectral camera that provides imaging in both the visible (VIS) and thermal infrared (IR) [Christensen et al., 2004]. THEMIS currently provides near-global coverage of the Martian surface in the IR with ~100 m/pixel resolution. Although the THEMIS daytime IR global mosaic (230 m/pixel) used in this research provides comparable resolution to earlier datasets, the daytime IR data provide greater contrast between sunlit and shaded surfaces than do Viking or MOC images, allowing more detail to be seen in the valleys with the THEMIS daytime IR dataset. Compared to MOC Wide Angle and Viking, more small tributaries, multiple flow paths, terraces, and anabranching channels have been observed. Other datasets of higher resolution are available, such as MOC Narrow Angle (1.5 to 12 m/pixel), THEMIS VIS (18 m/pixel), High Resolution Stereo Camera (HRSC) (<30 m/pixel), and High Resolution Imaging Science Experiment (HiRISE) (<1 m/pixel), but they provide insufficient coverage of the surface to allow complete mapping of the networks. The MGS MOLA global gridded data can be used to automate mapping of the networks [e.g. Stepinski and Collier, 2004], but the horizontal resolution is too coarse to provide the level of detail needed in this study. Combining THEMIS daytime IR and MOLA topographic data improves the identification of valley networks over THEMIS or MOLA alone, resulting in a superior dataset for accurate mapping and analysis of the valley networks on Mars.

Most, though not all, of the Martian valley networks are located on ancient surfaces, and they appear to have formed during a final stage of fluvial erosion that occurred sometime during the Late Noachian (~3.7 to 3.8 Gyr) or Early Hesperian (~3.7 to 3.6 Gyr) epochs [e.g. Hynek and

Phillips, 2001, 2003; Howard et al., 2005; Irwin et al., 2005a; Hynek et al., 2008]. Extensive

erosion and local deposition that removed several hundred meters of surface material and filled

crater floors occurred throughout the highlands, including the Terra Sabaea, Arabia Terra, and

Meridiani Planum regions where this research is focused [Craddock et al., 1997; Hynek and

Philips, 2001; Craddock and Howard, 2002; Howard et al., 2005]. The formation of large

drainage networks, alluvial fans, and deltas during this period indicates sustained flows of water

[Howard et al., 2005], suggesting the early Martian atmosphere during which most of the valley

networks formed was either continuously or episodically warmer, thicker, and wetter than today.

Episodic changes in atmospheric temperature, pressure, and humidity may have been driven by

changes in obliquity and orbit, impact events, and volcanic activity [e.g. Baker et al., 1991;

Jakosky et al., 1995; Carr, 1996; Baker, 2001; Jakosky and Phillips, 2001; Phillips et al., 2001;

Segura et al., 2002]. Indeed, many authors have discussed evidence for multiple epochs of

valley network activity [e.g. Baker and Partridge, 1986; Grant and Schultz, 1990; Grant, 2000;

Williams and Phillips, 2001; Harrison and Grimm, 2005; Howard et al., 2005; Irwin et al.,

2005a]. Many researchers [e.g. Baker and Partridge, 1986; Williams and Phillips, 2001;

Harrison and Grimm, 2005] describe the reactivation of older, precipitation-formed valleys by

the headward extension of pristine valleys through sapping processes. Meanwhile, other

researchers [e.g. Howard et al., 2005; Irwin et al., 2005a] describe a change from widespread

fluvial erosion and significant infilling of the highlands during the Noachian to a late-stage of

increased runoff and intense valley formation characterized by integrated networks and the

deposition of deltas and fans during the Late Noachian to Early Hesperian. As the valley

networks formed, they were affected by impacts, eolian transport, mass wasting, and mantling by

dust, impact ejecta, and/or volcanic ash; all processes that have continued to modify the valley

networks through Martian history to varying degrees [e.g. Carr, 1996; Craddock and Howard, 2002; Irwin and Howard, 2002; Howard, 2007].

The Martian valley networks have often been assigned an age based on the age of the surface on which they occur and superposition relationships with other geologic features [e.g. Carr and Clow, 1981; Carr, 1996]. This method of age-dating represents a maximum age. Determining the ages of actual valley formation, however, provides much more precise constraints on the timing and duration of warmer, thicker atmospheric conditions. This work can be done through crater counting on the valley networks themselves, providing a minimum age bound on the end of their formation. Crater counting on valley networks is made difficult by the small areal extent of the valley networks, allowing fewer craters to be counted. Even so, crater counting on Martian valley networks has been done for decades so as to better constrain the timing of their formation. Pieri [1980] compared crater counts on valley networks with surrounding terrain to determine their relative ages and got different ages depending on the crater diameters used in crater counting. He found that the valley networks appeared younger than the surrounding terrain at larger crater diameters and older than the surrounding terrain at small crater diameters. The unexpected result at small crater diameters (<1km) is likely due to the inclusion of younger inter-crater plains in the crater counts for the surrounding terrain. Baker and Partridge [1986] observed differences in preservation state for the Martian valley networks, and they performed crater counting on these networks using three separate methods while treating pristine and degraded valleys separately. They defined pristine valleys as being relatively fresh-appearing with steep valley walls, and they defined degraded valleys as having scalloped or rilled walls and greater, indistinct valley widths. Their results vary depending on the method of determining which craters should be included in the count and how the sampling
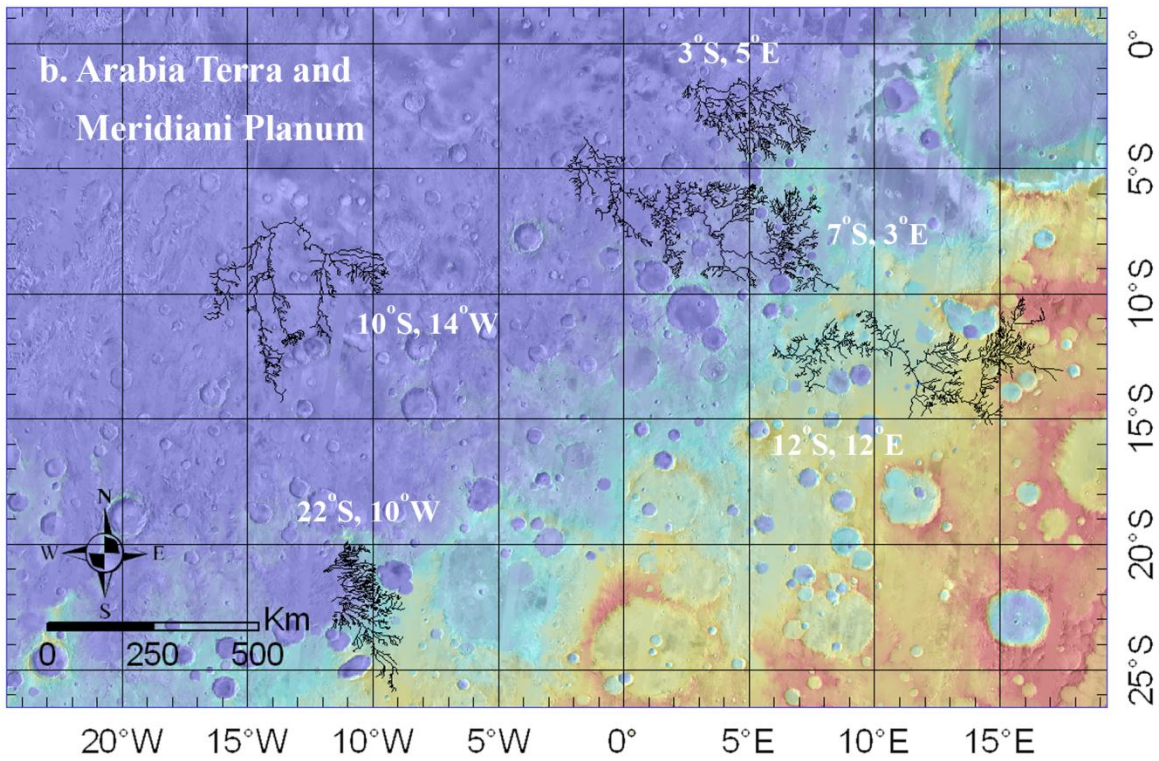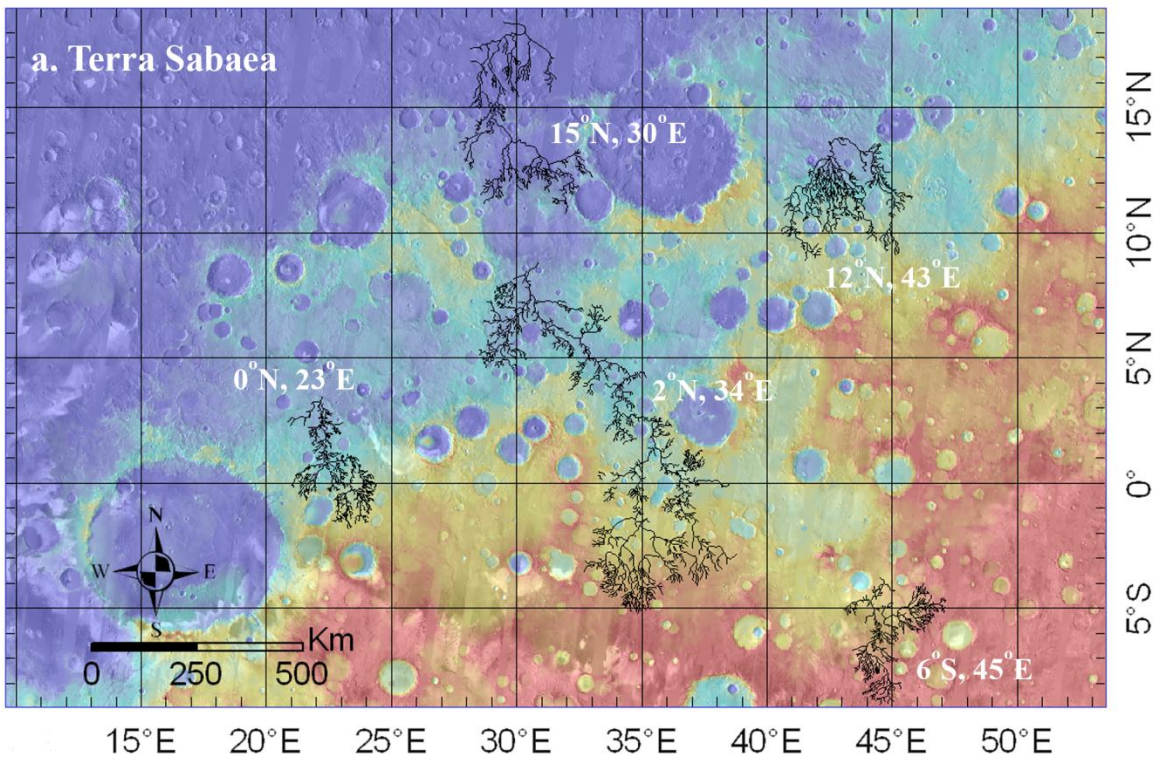
Figure 1. The ten martian valley networks in a) Terra Sabaea and b) Arabia Terra and Meridiani Planum that were analyzed in this study are shown with coregistered THEMIS daytime IR and MOLA topography data.

area is defined, but they show an overall difference in age between pristine and degraded valleys, with degraded valleys having an older age in all three methods. Both Pieri [1980] and Baker and Partridge [1986], while limited by image resolution, were able to describe a complex history for the Martian valley networks from analysis of their crater densities.

With the global THEMIS daytime IR dataset and MOLA topography, craters down to a few hundred meters across that overlap the valley networks can be accurately identified, allowing a more precise crater age dating of the valley networks themselves that is independent of the surrounding surface on which they lie [Fassett and Head, 2008b; Hoke and Hynek, 2008; following sections]. Since valley networks have limited surface areas, their crater densities can be better determined with a method tailored for counting craters on narrow linear features [Tanaka, 1982] (see Section 2.2). Due to the limited number of craters that can be counted on smaller valley networks, only the largest or most extensive valley networks were analyzed in this work. Here, we apply these techniques in Terra Sabaea, Arabia Terra, and Meridiani Planum because these ancient regions contain some of the most extensive and densest valley networks on Mars. While there is evidence that valley network formation occurred in isolated locations across the planet on much younger surfaces [e.g. Carr and Clow, 1981; Gulick and Baker, 1990; Baker et al., 1991; Gulick, 2001; Mangold et al., 2004; Quantin et al., 2005; Fassett and Head, 2008b; Hynek et al., 2008], the focus of this paper is on the highland valley networks that appear to have formed during the period of significant fluvial erosion that is associated with the Noachian and Early Hesperian.

2.2 Methods

The ten largest valley networks in Terra Sabaea, Arabia Terra, and Meridiani Planum were chosen for this study and were primarily mapped using visual inspection of coregistered

THEMIS daytime IR images and MOLA gridded topography in ArcGIS®, a Geographic

Information System (GIS) software that allows multiple datasets to be analyzed at the same time.

These valley networks, as shown in Figure 1, are hereafter referred to by their approximate

center coordinates. The smaller valley networks that were present between these ten large valley

networks were excluded from this study. The stream order, total stream length, drainage density,

and crater size-frequency distribution of these valley networks were determined to better

characterize the timing and variability of valley network formation in this ancient, fluvially

modified region of Mars.

2.2.1   Stream order and drainage density

To characterize the maturity of these valley networks, their stream orders were

determined by visual inspection of their branching behavior after they were fully mapped.

Several methods of ordering streams have been developed, though the Strahler [1958] method is

the most commonly used. This method is shown schematically in Figure 2a. This technique

assigns an order of one to the stream segments with no tributaries in a network (the smallest and

uppermost valleys in a drainage basin). As two first-order segments join, they form a

downstream segment of order two. Each merging of two streams of the same order forms a

downstream segment with an order of one greater, whereas merging two unequal streams forms a

downstream segment with an order equal to that of the higher of the two merging streams. The

overall network has the order of the trunk, the highest order stream in the network. Per unit

watershed area, higher stream order implies a much greater complexity and maturity in the

network.

Drainage density is the ratio of total stream length within a network to the area of the

drainage basin and essentially reflects the average spacing of the valleys within the drainage
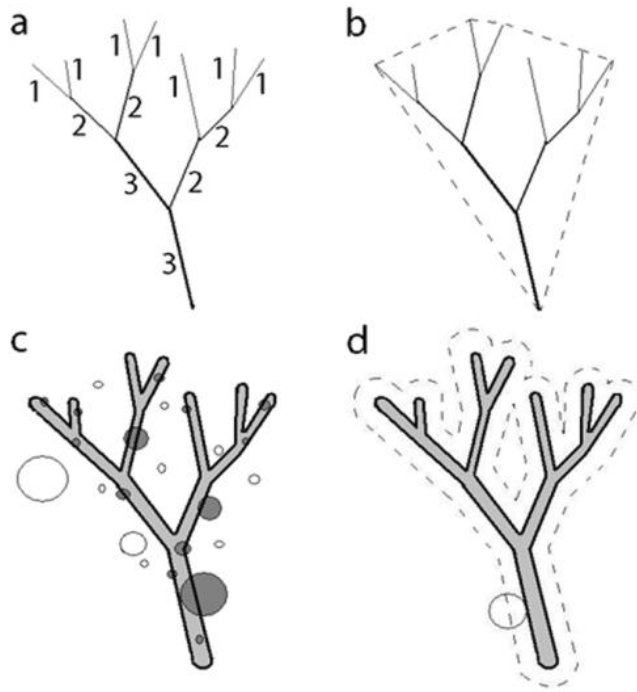
Figure 2. A schematic valley network is used to illustrate a) the Strahler [1958] method for ordering networks; b) the convex hull method for calculating drainage area for use in determining drainage density; c) tracing along the edges of the valley walls (heavy solid line) to provide the boundary on which to count craters whose rims superposed or were enclosed by the valley network (filled-in circles) and excluded those that did not (empty circles); and d) the area from Equation 1 used to convert crater counts to crater densities, which included the area of the valleys (gray shading) and the area of an envelope surrounding the valley network (dashed line) that is a function of crater radius and valley perimeter.

basin. The total stream length was determined by summing the lengths of all the mapped stream segments within the network using ArcGIS®. Determining the area of the drainage basin is more complicated, particularly for older networks, as impacts and geologic processes subsequent to the end of valley network formation may have severed valley segments and/or altered the location of drainage divides over the last ~3.5 billion years [Craddock and Howard, 2002]. Furthermore, the surface of Mars has experienced sufficient modification over this time to cause possible erasure of the shallower valley segments, and the full extent of the valley networks may not be

represented by the valleys visible today [Carr and Malin, 2000; Irwin and Howard, 2002]. To define the drainage area in this research, a convex hull method was used in which the visible exterior tributaries were connected with straight lines to form a polygon in which none of the internal angles exceeded 180° (Figure 2b). Since a significant number of tributaries in these networks reach up to drainage divides, the convex hull method is assumed to provide a reasonable approximation of the drainage area for these individual valley networks as they are visible today, given that their original extent has quite possibly been altered and is no longer visible.

2.2.2 Valley network age determination

Valley network age determinations have always posed a problem, given that they are narrow linear features that comprise little area and therefore provide poor crater-counting statistics. Using THEMIS daytime IR and MOLA topography data in ArcGIS®, and following the method outlined by Tanaka [1982] for counting craters along narrow linear features of limited surface area, we counted superposed (overlapping) craters for each valley network. This method ensured accurate crater counting that represented the cratering population since the end of valley formation. All craters on the surrounding surface that did not overlap the networks or were stratigraphically below the networks were excluded in the count. To improve the statistical validity of our results, we used the largest valley networks in Terra Sabaea, Arabia Terra, and Meridiani Planum to maximize the surface area and therefore increase the number of craters available to count.

First, the edges of the valleys along the top of valley walls were traced using ArcGIS®. This step was important for two reasons: 1) to define the boundary of the valley network for counting craters, and 2) to calculate the area and perimeter enclosed by the valley walls through

ArcGIS$^®$ for use in determining the crater density (see Figure 2c). Craters >1 km in diameter

that overlapped a valley network were counted using bin sizes that incremented by a factor of $\sqrt{2}$,

as is commonly used in crater density analyses [Melosh, 1989]. Craters smaller than 1 km were

not counted to limit the number of secondary craters included in the count [e.g. McEwen and

Bierhaus, 2006].

Because of the variability of ejecta blanket preservation, only craters whose rims

overlapped the valley network were counted. While ejecta blankets create a clear stratigraphic

relationship between their corresponding crater and the surface over which they lie, they have the

adverse effect of covering the surface surrounding the crater. With large craters, this blanketing

of ejecta material makes the proximity of the crater to narrow features, such as valley networks,

ambiguous. Since we only count craters that physically overlap the networks and exclude all

other nearby craters, we need to be able to see the crater rim/valley network wall relationship. If

the preserved ejecta blanket is small enough to allow a clear relationship between the superposed

crater rim and the underlying valley network, the crater is included in our count. Many of the

preserved ejecta blankets, however, belong to larger craters and are extensive and thick enough

to bury small valleys completely, making the proximity relationship between the crater rim and

valley walls unclear. Moreover, the preservation state of ejecta blankets varies greatly, with

some pristine and others entirely gone. Therefore, including ejecta blankets in crater counting on

valley networks adds a level of subjectivity that results in greater uncertainty in crater densities.

Tanaka's [1982] method is based on the observation that a linear feature of limited area

has a crater density that depends on the area defined by the crater diameters. Therefore, the area

used to determine crater densities includes the area within the valleys (on which craters were

counted) and an envelope circumscribing the valley network by one crater radius (Figure 2d). This area can be written as:

$$A = A_{v.n.} + R_{crater} \times P_{v.n.} + A_{crater} \tag{1}$$

where $A_{v.n.}$, R_{crater}, $P_{v.n.}$, and A_{crater} are the valley network area, crater radius, valley network perimeter, and crater area, respectively. To clarify, the area A includes the summation of the horizontal area of each individual valley within a network and the area of an envelope extending one crater radius around the perimeter of the valley network, whereas the drainage area described above includes an area surrounding and including the valley network as defined by a convex hull (compare the dashed lines in Figures 2b and 2d). The valley network perimeter, $P_{v.n.}$, is the total length of the valley network boundary as determined by tracing the valley walls, whereas the total stream length described above is measured along the approximate centerline of the valley network (compare solid lines in Figures 2b and 2d). The weighted mean crater diameter for each crater diameter bin was used instead of median crater diameter in determining R_{crater} and A_{crater} to account for the power law distribution of craters in which smaller craters are more abundant than larger craters for any given size range. The weighted mean crater diameter, $\overline{D}$, [Tanaka, 1982] was calculated by:

$$\overline{D} = \frac{\int_{D_a}^{D_b} D \, dN_c}{\int_{D_a}^{D_b} dN_c} = \frac{3}{2} \frac{D_a^{-2} - D_b^{-2}}{D_a^{-3} - D_b^{-3}} \tag{2}$$

where D_a and D_b are the crater diameters corresponding to a given bin, with $D_b > D_a$.

The number of craters counted in each bin was converted to a crater density, N, by dividing the count, n, in that bin by the corresponding valley network area, A, from Equation 1.

The cumulative crater density, N_c, was determined by summing the crater density in a given bin with the crater densities in all larger bin sizes [Arvidson et al., 1979]:

$$N_c = \sum_{j=1}^{k} N_j \qquad (3)$$

The cumulative crater densities of the valley networks were plotted vs. the corresponding weighted mean crater diameters on logarithmic plots and were compared to Martian epoch boundaries as defined by Tanaka [1986] and/or Neukum's production functions [Ivanov, 2001]. Error was determined by assuming a Poisson distribution and using a one-σ interval of $\pm N_c / \sqrt{n_c}$, where N_c is the cumulative crater density (Equation 3) and n_c is the cumulative crater count and is determined by summing the crater counts, n, in a given bin with the crater counts in all larger bin sizes [Arvidson et al., 1979; Tanaka, 1982].

$$n_c = \sum_{j=1}^{k} n_j \qquad (4)$$

The crater size-frequency distribution for each valley network was analyzed, and production and resurfacing regimes, if applicable, were identified for each. The production regime for the range of crater diameters used in this work (1 km to ~23 km) has a slope of approximately −1.8 on a log-log cumulative crater density vs. crater diameter plot [Melosh, 1989; Hartmann and Neukum, 2001]. A shallower crater density slope suggests that a period of erosion or burial occurred sometime in the valley network's past that preferentially obliterated smaller craters, as described by Melosh [1989]. The range of crater diameters in this shallower-sloped regime depends on the magnitude of the resurfacing event, reducing crater densities up to a given crater diameter. After the resurfacing event, the cratering rate will continue as before, allowing craters to accumulate on the surface with the same production-regime size frequency

distribution (i.e. a slope of −1.8 on a log-log plot) but with a lower cumulative number of small craters [Melosh, 1989]. The return to production regime will occur first for smaller craters, which have a higher probability of forming than larger craters, and will eventually grow toward larger crater diameters [Melosh, 1989]. Therefore the amount of time that has passed since the resurfacing event is represented by the range of smaller crater diameters that have returned to the steeper-sloped production regime. Because of the cumulative effect of cratering on planetary surfaces, the oldest valley networks are interpreted as those with greater cumulative crater densities.

One of the many difficulties in using crater densities for age-dating planetary surfaces is the presence of secondary craters that may inadvertently be included in the count. Secondary craters, which are typically small in diameter and numerous, are often seen surrounding large craters in clusters or rays. However, secondaries are not confined to a local area surrounding the primary; they may be distributed globally. McEwen and Bierhaus [2006] hypothesize that distant secondaries dominate the global distribution of craters smaller than 1 km in diameter on the Moon, and likewise play an important role in small crater populations on other planetary surfaces such as Mars and Europa.

Counting small craters for age-dating is complicated by the presence of secondary craters, as including secondaries increases the crater density at those diameters and may result in the interpretation of an older age. For crater populations affected by secondary craters, one should expect an upturn in the crater size-frequency distribution to slopes of approximately −3.5 to −5, which is much greater than that for the primary crater production function of approximately −1.8 to −2 [Shoemaker, 1965; Wilhelms et al., 1978; Bierhaus et al., 2001; McEwen et al., 2005].

31

Generally speaking, secondaries become statistically significant in crater counts at sizes less than ~0.4% the diameter of the primary [Shoemaker, 1965; Bierhaus et al, 2001; Dundas and McEwen, 2005; McEwen et al., 2005]. McEwen and Bierhaus [2006] show that for the Moon, the crossover from primary-dominated to secondary-dominated crater populations occurs at ~1 km, as hypothesized by Shoemaker [1965]. For Mars, where resurfacing continued for billions of years longer than on the Moon, this cross-over depends on the age of the surface; older surfaces have more large impacts and therefore will be affected by larger secondaries than will younger surfaces. For Martian surfaces with ages near the Noachian/Hesperian boundary, secondaries should become statistically significant at diameters of ~600 m (from craters ~150 km in diameter) [Skinner et al., 2006]. By excluding obvious secondary craters (oblong shape, clustered, rayed) and craters smaller than 1 km in our counting, our results provide crater ages that are not significantly affected by the presence of secondary craters.

Isochrons were plotted with our data to mark the boundaries between the Early, Middle, and Late Noachian; Early and Late Hesperian; and Early, Middle, and Late Amazonian epochs as defined by Tanaka [1986] and Neukum's production functions [Ivanov, 2001]. The crater diameter size range primarily used in this work based on the limited size of the valley networks, 1 km to ~16 km, is the same diameter range that gives the greatest disagreement between Neukum's [Ivanov, 2001] and Hartmann's [2005] production functions, leading to an uncertainty in isochron age of approximately a factor of 2 [Hartmann and Neukum, 2001]. Since Hartmann has developed his isochrons for incremental crater counts, we compare our results with Neukum's and Tanaka's production functions, which both apply to cumulative crater counts.

Because of the crossover from primary-dominated to secondary-dominated craters populations at 1 km for the Moon, and because the Martian production functions are based on

lunar production functions, there has been much debate about the validity of Martian production functions for crater populations smaller than 1 km [e.g. Hartmann, 2005; McEwen and Bierhaus, 2006]. The Hartmann and Neukum production functions both show an upturn in slope at smaller diameter craters [Hartmann and Neukum, 2001]. Unfortunately, this occurs at just above 1 km for Neukum Martian production functions, making it difficult to compare absolute ages for cumulative crater densities at 1 km with other published absolute ages based on cumulative crater densities at larger diameters, such as those by Fassett and Head [2008b]. Therefore, we use absolute ages solely as a means of quantifying the relative ages between valley networks within this study, and rely on the crater number (or density) at 2 km, N(2), to place the timing of the end of valley network formation in the context of Martian history.

An absolute age for each valley network (T) was assigned based on its cumulative crater density at 1 km diameter, or the 1 km crater number N(1), per 10^6 km^2 and the equation from Ivanov [2001] that follows the Neukum production function:

$$N(1) = 2.68*10^{-14} * [\exp(6.93*T) - 1] + 4.13*10^{-4} *T \qquad (5)$$

Due to the large uncertainties in applying absolute ages to Martian surfaces [Hartmann and Neukum, 2001], these ages should be taken loosely and used only as a means of quantifying the relative ages between valley networks within this study.

Fassett and Head [2008b] have similarly counted superposed craters on 30 Martian valley networks or valley network regions across the southern highlands and on volcanic constructs, primarily between $\pm 30°$ latitude. They use a different method to define the area for calculating the crater density, one that extends the envelope, or buffered area, far enough to allow craters with ejecta blankets that superpose the valleys to be included in their crater counts. This
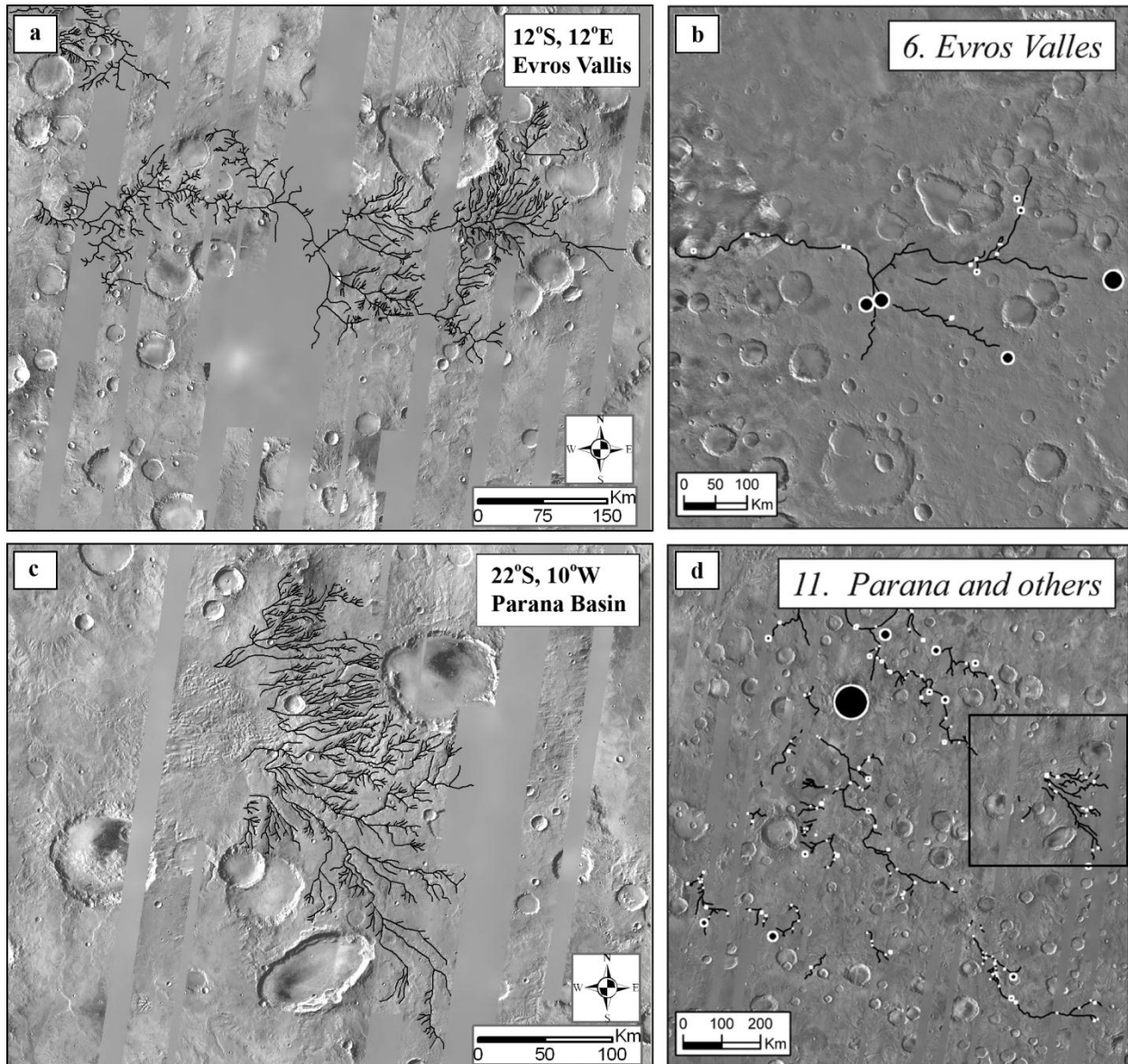
Figure 3. Differences in mapping the same Martian valley networks between Hoke and Hynek [this paper] (panels a and c) and Fassett and Head [2008b] (panels b and d) are shown here. Our mapped area in panel c is indicated by the box in Fassett and Head's [2008b] mapped area in panel d. Dissimilar methods led to different populations of craters counted (Table 1), which contributed to the different age estimates between the two studies.

buffered area is a function of the average valley width for the valley system rather than the actual

network dimensions. Our approach, while more tedious, is likely more accurate as it includes

only craters whose rims overlap the actual valley network, and an area that is a function of the

actual valley dimensions rather than an average width for the whole system. The additional

craters that Fassett and Head [2008b] include in their count by using crater ejecta blankets when identifying superposed craters would lead to an older age; however, the larger area afforded by the buffered area that includes the ejecta blankets would somewhat counter that effect.

Table 1. Comparison of some of the valley network ages based on the Neukum production function [Ivanov, 2001] from (a) this study and (b) Fassett and Head [2008b].

Location		Crater Counts and Age			
		Hoke and Hynek (a)		Fassett and Head (b)	
Reference in Hoke and Hynek (a)	Reference in Fassett and Head (b)	Number of craters used to determine age	Age (Gyr), based on N(1)	Number of craters used to determine age	Age (Gyr), based on N(5)
2°N, 34°E	Naktong and others, 4°N, 34°E	278 (west: 71) (east: 207)	3.72 ±0.01 (west: 3.79 ±0.02) (east: 3.70 ±0.01)	76	3.69 +0.03 -0.03
22°S, 10°W	Parana and others	82	3.68 +0.02 -0.03	84	3.73 +0.03 -0.03
7°S, 3°E	Meridiani: 5°S, 0°E	178	3.65 +0.02 -0.02	15	3.71 +0.08 -0.08
12°S, 12°E	Evros Vallis	130	3.63 +0.02 -0.02	16	3.76 +0.07 -0.07
10°S, 14°W	7°S, 13°W	119	3.58 +0.02 -0.03	16	3.79 +0.07 -0.06

Fassett and Head's [2008b] crater size-frequency distributions were fitted to Hartmann and Neukum production functions using a weighted least-squares technique that minimizes the misfit between their data and an expected distribution. The fitted data were then used to determine valley ages based on crater densities at 5 km, N(5). By fitting their data to production

functions, they were able to determine crater ages from fewer data points, allowing them to count craters on smaller valley networks.

By limiting our study to crater counting only on large valley networks, we are able to avoid fitting our data to the Hartmann or Neukum production functions, which have large uncertainties in the 1 km to 16 km crater diameter range [Hartmann and Neukum, 2001]. Our crater counts are large enough that we have sufficient data points to create crater size-frequency distributions that not only display the expected production regimes, but also show resurfacing regimes characterized by a downturn in crater density at intermediate crater diameters. Our methods allow us to analyze variations in the crater size-frequency distributions, which tell us something about the history of the valley networks during and after their formation.

The number of craters used to determine the ages of any given valley network can differ significantly between our work and that of Fassett and Head [2008b]. For example, we used 73 craters and 130 craters to determine N(2) and N(1) ages, respectively, for the valley network at 12°S, 12°E (Evros Vallis), whereas Fassett and Head [2008b] used 16 craters down to 2 km in diameter for their age determination. The difference in the number of craters counted for any given valley network is partially due to differences in the mapping of the network between different researchers. This difference can be seen in Figure 3 by comparing the mapping of the valley networks at 12°S, 12°E (Evros Vallis) and 22°S, 10°W (Parana Basin) by Hoke and Hynek [this paper] and Fassett and Head [2008b]. So while we often determine ages for the same valley network, the surfaces that are actually being crater-age dated are not entirely the same.

With different methods and assumptions in crater counting on the same Martian valley networks, it should be expected that our results will differ somewhat from those of Fassett and

Head [2008b] and other researchers. Using craters to determine surface age is in itself a very inexact science, especially with the added uncertainties of extrapolating impactor size-frequency populations, impact velocity, resulting crater size, and absolute age relationships from the Moon to Mars [i.e., Hartmann 2005]. Added to that are the difficulties of counting craters on features of limited surface area such as with valley networks, where deciding which craters should be included is at times very subjective. Indeed, both approaches [Fassett and Head, 2008b; this paper] have resulted in different ages for several valley networks. Overall, however, both place the end of Martian valley network formation in the Terra Sabaea, Arabia Terra, and Meridiani Planum regions near the Noachian-Hesperian boundary.

2.3 Results

The valley networks analyzed in this research (Table 2, Figure 1) each consist of one continuous network with the exception of two valleys: 22°S, 10°W (Parana Basin) and 2°N, 34°E (Naktong Vallis). The valley network at 22°S, 10°W (Parana Basin, Figure 3c) is actually a group of closely spaced valleys with similar morphology that flow into the putative paleolake of Parana Basin [Goldspiel and Squyres, 1991] from the east side. Because of their close spacing and similar morphology (and likely similar formation mechanism and age), they were treated as one network to allow greater surface area for crater-age dating. These networks were similarly grouped by Grant [2000] and Hynek and Phillips [2001], both of whom computed crater ages that place valley incision in the Parana basin at the Late Noachian and into the earliest

Table 2. Morphometric parameters and crater-age dating results for large valley networks in the Terra Sabaea, Arabia Terra, and Meridiani Planum regions of Mars are listed in order of decreasing N(1). Note that the results for 2°N, 34°E (Naktong) are listed separately for its west branch, east branch, and overall network.

Valley network location	Label for Figures	Strahler Stream Order	Stream Length (km)	Drainage Area (km^2)	Drainage Density (km^{-1})	Approx. Range of Elevation (m)	Degraded (D) or Pristine (P) State	Crater Number at 2 km, N(2)	Crater Number at 1 km, N(1)	Approx. Absolute Age (Gyr)	Reactivated Valley Networks (Sect 4.4)
2°N, 34°E west Naktong	1	5	2,563	22,183	0.12	+370 to -320	D	2579 ±563	8254 ±1057	3.79 +0.02 -0.02	
12°N, 43°E	2	6	6,463	69,672	0.093	+1050 to -150	P	1522 ±304	6177 ±651	3.73 +0.02 -0.02	
15°N, 30°E Scamander	3	5	5,794	103,310	0.056	+400 to -1500	D	1699 ±279	5847 ±576	3.72 +0.02 -0.02	X
2°N, 34°E Naktong	4	6	15,265	286,824	0.053	+2150 to -320	P, D	1634 ±170	5602 ±342	3.72 +0.01 -0.01	X
6°S, 45°E	5	6	4,851	48,775	0.10	+2520 to +1300	P	-	5148 ±576	3.70 +0.02 -0.02	
2°N, 34°E east Naktong	6	6	12,702	220,293	0.058	+2150 to -320	P	1369 ±175	5124 ±356	3.70 +0.01 -0.01	
0°N, 23°E	2.3.1.1	5	5,389	43,444	0.12	+1250 to -110	P	-	4758 ±599	3.68 +0.02 -0.03	
22°S, 10°W Parana	8	6	6,117	42,745	0.14	+870 to -1350	P	1491 ±282	4694 ±518	3.68 +0.02 -0.03	
7°S, 3°E	9	6	11,710	148,318	0.079	+100 to -1500	D	(841 ±128)	4157 ±312	3.65 +0.02 -0.02	X
12°S, 12°E Evros	10	5	9,050	149,693	0.060	+2700 to -150	D	1060 ±168	3790 ±333	3.63 +0.02 -0.02	
3°S, 5°E	11	5	5,617	44,298	0.13	-250 to -1400	D	(633 ±142)	3658 ±386	3.62 +0.02 -0.03	X
10°S, 14°W	12	6	6,134	115,827	0.053	-780 to -1750	D	844 ±139	3083 ±293	3.58 +0.02 -0.03	

Hesperian. In this work, this group of valley networks was given a stream order equal to that of the valley network with the highest order within the group, and the drainage density was determined for the group as a whole. The valley network at 2°N, 34°E (Naktong Vallis, Figure 4) shows clear evidence of multiple periods of formation along two separate branches that meet at 7°N, 31°E [Hoke and Hynek, 2007, 2008]. Therefore the east and west branches of this network have been analyzed separately.
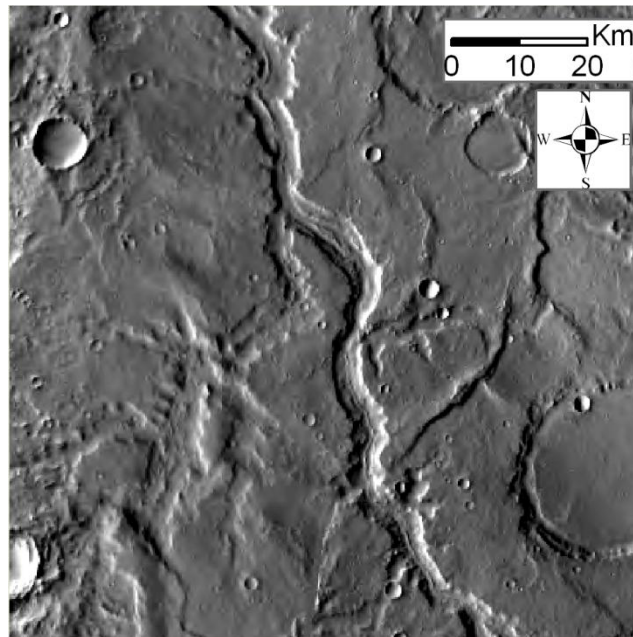
Figure 4. The east and west branches of the valley network centered on 2°N, 34°E (Naktong Vallis) have different degradation states and crater densities, indicating multiple periods of formation.

All of the valley networks studied in this work demonstrate characteristics consistent with formation by precipitation, including densely spaced dendritic form with interiors that increase in width and depth downstream; sinuous main trunks and major tributaries that occasionally also exhibit multiple interior channels, braiding, and terracing; and tributaries that often reach right up to drainage divides. The valley networks at 12°S, 12°E; and 0°N, 23°E follow a curving, meandering path along a surface of low slope, whereas the networks at 22°S, 10°W; 6°S, 45°E;

and 12°N, 43°E have mostly long, parallel, densely spaced tributaries that likely reflect the steeper slopes on which they formed (Table 2). The valley networks at 2°N, 34°E; 0°N, 23°E; and 10°S, 14°W contain some evidence of interior channels, braiding, and terracing in their main trunks and/or major tributaries. These characteristics all point to formation by a widespread, abundant source of water that eroded the Martian surface primarily through overland flow rather than through subsurface erosion. However, the major tributaries or main trunk of some valley
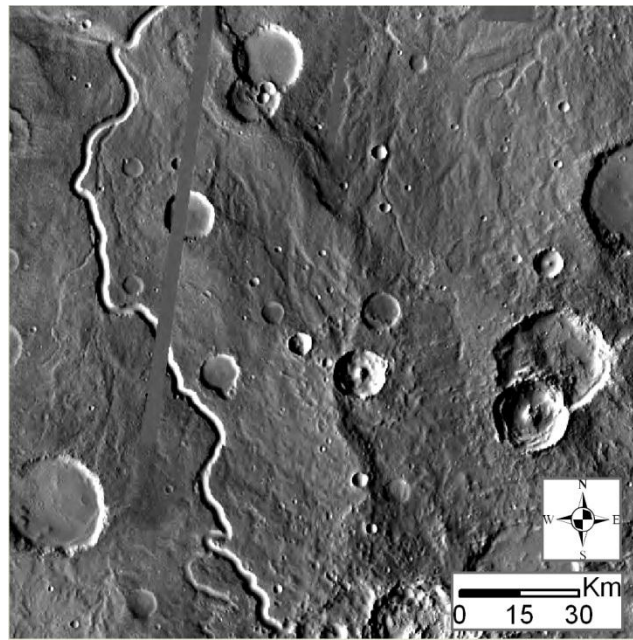
Figure 5. The valley network centered approximately at 15°N, 30°E (Scamander Vallis) has markedly differing morphologies, including many faint, filled-in tributaries and one very pristine main trunk that suggests it was modified by some late-stage reactivation of valley network formation, likely from a localized source, such as from a paleolake [Irwin et al., 2005a].

networks (i.e. 15°N, 30°E, shown in Figure 5) have morphologies that indicate they have experienced late-stage reactivation consistent with erosion from a very localized source of water, such as from a paleolake [Irwin et al., 2005a; Fassett and Head, 2008b] or groundwater sapping [Baker and Partridge, 1986; Williams and Phillips, 2001]. Both pristine and degraded preservation states are seen in the Terra Sabaea, Arabia Terra, and Meridiani Planum valley

networks (Figure 6, Table 2). Similar to Baker and Partridge [1986], we define pristine valleys (Figure 6a–6c) as being characterized by smooth walls with sharp boundaries between the valley and surrounding terrain. The degraded valleys (Figure 6d–6f) are characterized by jagged, irregular walls, indicating they have experienced more slumping and erosion, and often have a filled-in appearance with wide, flat floors.

Often both U- and V-shaped interiors are observed within a single valley network system. Historically, Martian valleys with U-shaped interiors have been interpreted as having formed primarily by groundwater sapping and mass wasting, while V-shaped interiors were associated with formation by precipitation and surface runoff [e.g. Carr, 1996]. Therefore, a valley with both U- and V-shaped interiors may indicate a progression from precipitation-driven surface runoff that creates the V-shaped profiles and dendritic form to reactivation of the network by groundwater sapping in downstream reaches that widens the valley and creates the U-shaped profiles [Baker and Partridge, 1986; Williams and Phillips, 2001; Harrison and Grimm, 2005]. Alternatively, the presence of both U- and V-shaped profiles could be caused by different degrees of erosion and/or infilling within a single network, with a progression from V- to U-shape as valley segments are modified [Carr and Malin, 2000; Irwin and Howard, 2002; Irwin et al., 2005a]. Additionally U- and V- shaped profiles may indicate erosion and downcutting into different hardnesses of surface material, in which V-shape indicates downcutting with little modification of the valley walls whereas U-shape indicates retreat of the walls with little downcutting [Williams and Phillips, 2001; Irwin et al., 2005a, 2008]. The latter may be a result of both groundwater sapping and surface runoff from precipitation, with seepage weathering controlling wall steepness and flooding removing the debris [Irwin et al., 2008].

All of the valley networks in this study that have degraded valleys (including 2°N, 34°E

41
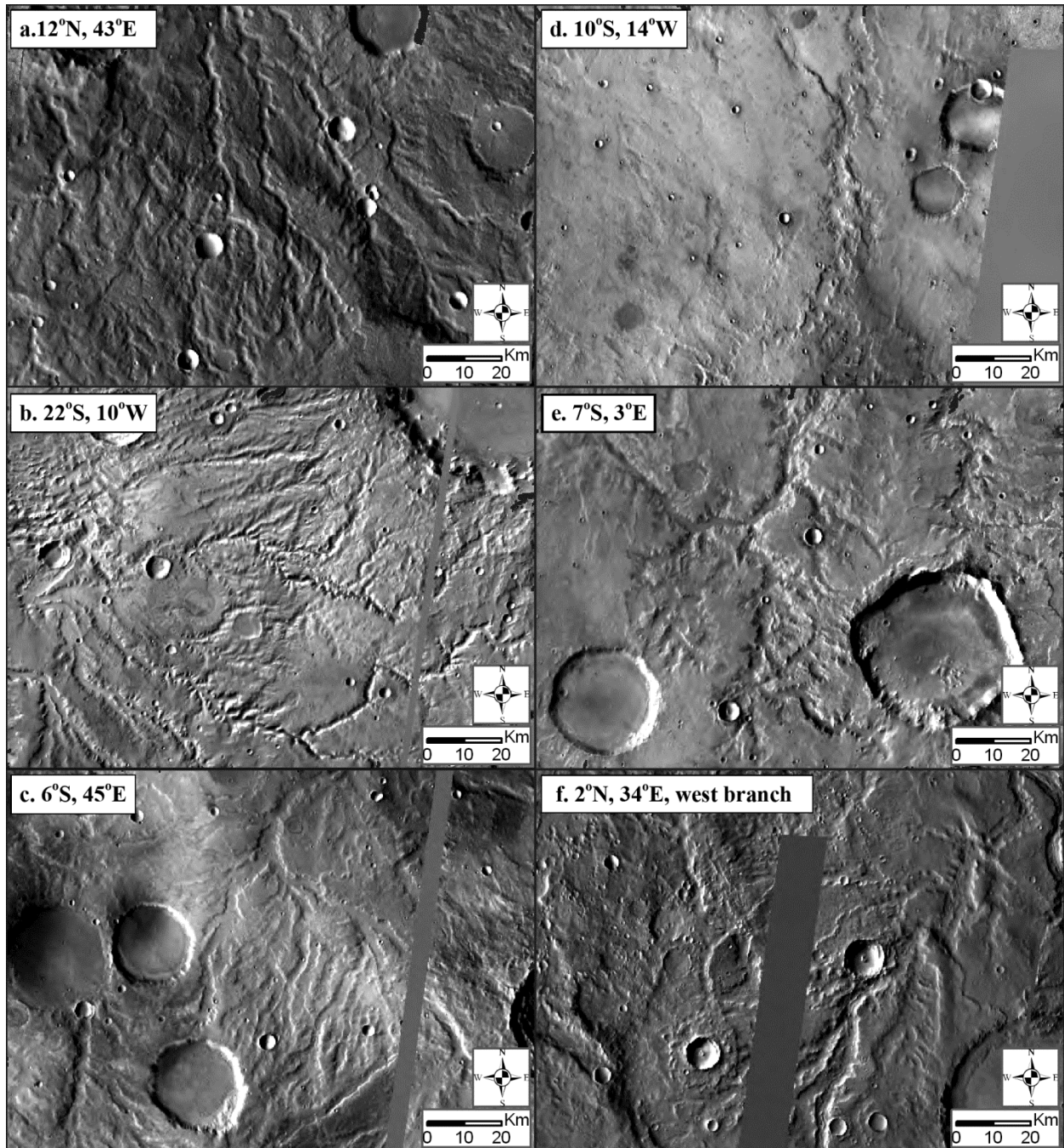
Figure 6. Several examples of both pristine (a, b, c) and degraded (d, e, f) preservation states are shown here. The pristine morphologies include primarily smooth walls with a sharply defined transition between valley and surrounding terrain and overall narrower valleys than their more degraded counterparts. The degraded morphologies include jagged, irregular walls with evidence for slumping and erosion and shallow, flat, wide floors that give a filled-in appearance. All of these images are THEMIS daytime IR [Christensen et al., 2004].

(Naktong Vallis); 15°N, 30°E (Scamander Vallis); 7°S, 3°E; 12°S, 12°E (Evros Vallis); 3°S, 5°E; and 10°S, 14°W) exhibit both U- and V-shaped interiors, whereas the more pristine valley networks (including 12°N, 43°E; 6°S, 45°E; 0°N, 23°E; and 22°S, 10°W (Parana Basin)) either had primarily V-shaped interiors or had both U- and V-shapes. These observations support the hypothesis that interior shape is affected by the preservation state of the valley, and that preservation state may play a bigger role than formation mechanism in determining the interior shape of the valley. Interestingly, and in support of this hypothesis, is the observation that the pristine valley in the network at 15°N, 30°E (Scamander Vallis, Figure 5) that has been attributed to late-stage reactivation by groundwater sapping [e.g. Baker and Partridge, 1986] or paleolake overflow [Irwin et al., 2005a] has a V-shaped interior, while the surrounding less pristine tributaries exhibited both U- and V-shapes.

2.3.2 Stream order and drainage density

The Strahler stream order and drainage density for each valley network are given in Table 2 along with the corresponding total stream length, drainage area, range of elevation of each basin, degraded or pristine preservation state, crater numbers at 1-km and 2-km diameters, and approximate absolute age. All of the valley networks analyzed in this research have Strahler stream orders of 5 or 6. Sixth-order networks are among the highest identified so far on an updated map of Martian valley networks [Hynek et al., 2008]. For comparison, the largest terrestrial river system, the Amazon, has a Strahler stream order of 12, the Mississippi river system has a Strahler stream order of 10, and the Ohio river system has a stream order of 8. Since only large, extensive Martian networks were chosen for this study, it is not surprising that they all have high stream orders, by Martian standards. These values therefore do not represent

43

the average Martian valley network, but rather the upper range of what is visible today in these regions.

The drainage densities of these valley networks range from 0.053 km^{-1} to 0.14 km^{-1} (mapped at ~1:500,000 scale). These are comparable to, albeit on the low end of, the Carr and Chuang [1997] terrestrial drainage densities that were mapped using a similar method with Landsat 4 images and which range in value from 0.065 km^{-1} to 0.174 km^{-1} (at 1:2,000,000 scale) and 0.079 km^{-1} to 0.209 km^{-1} (at 1:1,000,000 scale). The terrestrial valleys in the Carr and Chuang study were located in five different regions in the United States, each having different climate, relief, rock types, and, in cases, vegetation that served to aid in their identification. The smaller scale at which the Martian valley networks were mapped in this study likely produced larger drainage densities than if they were mapped at larger scales, which should be kept in mind when comparing the Martian and terrestrial drainage densities described above. Due to the many differences between the two planets, and the observation that these Martian valley networks are billions of years old while those measured by Carr and Chuang [1997] are still active, the similarity in drainage densities is not necessarily directly comparable. So while it is interesting that our Martian drainage density values are near in value to those similarly determined for Earth, drainage density remains best-used as a tool for comparing valley networks within a given data set.

Many of the valley networks that are characterized by moderate to high degrees of erosion and infilling have low drainage densities relative to the other valley networks (Figures 5, 6, and 7). Two of these networks (15°N, 30°E (Scamander Vallis) and 7°S, 3°E) have low drainage densities (0.056 km^{-1} and 0.079 km^{-1}, respectively). However, both of these networks drain large areas, suggesting there was enough widespread water available and sufficient time to

have formed denser networks. Some of the tributaries of the valley network at 12°S, 12°E

appear faint, indicating that they may have experienced significant infilling, resulting in a lower

drainage density (0.060 km^{-1}) seen today. The craters surrounding the valley network at 10°S,

14°W have an eroded appearance similar to that of the network walls, suggesting similar erosive

processes throughout this area during and/or after valley network formation. This valley network

has evidence of infilling and/or resurfacing, particularly in low-lying areas, that likely

contributes to its low drainage density (0.053 km^{-1}). Alternatively, several valley networks

(22°S, 10°W (Parana Basin); 12°N, 43°E; 6°S, 45°E; and 0°N, 23°E) have main trunks and

major tributaries that are well-defined and comparatively pristine with correspondingly higher

drainage densities. The valley network at 6°S, 45°E has well-developed, smooth, pristine

tributaries at higher elevations and a more degraded appearance at lower elevations. This

network is characterized by slumping walls and jagged boundaries between the valley wall and

the surrounding surface along the lower reaches of its major tributaries. Since it appears that

most of the tributaries in this network have remained in a pristine state, it is probably reasonable

to say that the drainage density (0.10 km^{-1}) of this valley network was only moderately affected

by the erosion/infilling that affected its lower reaches. Two exceptions to this discussion lie with

the valley networks centered at 3°S, 5°E and 2°N, 34°E. The valley network at 3°S, 5°E has an

overall degraded morphology and a high drainage density (0.13 km^{-1}) while the valley network at

2°N, 34°E has both pristine and degraded morphologies and a low drainage density (0.053 km^{-1}).

The Martian drainage densities do not appear to correlate with latitude, longitude,

elevation, or age (Table 2, Figure 7). The lack of a strong correlation indicates that other

variables, such as the resistance of the surface layer to erosion, the infiltration capacity of the

soil, the frequency and/or duration of rainfall events, and the preservation state of the valleys,
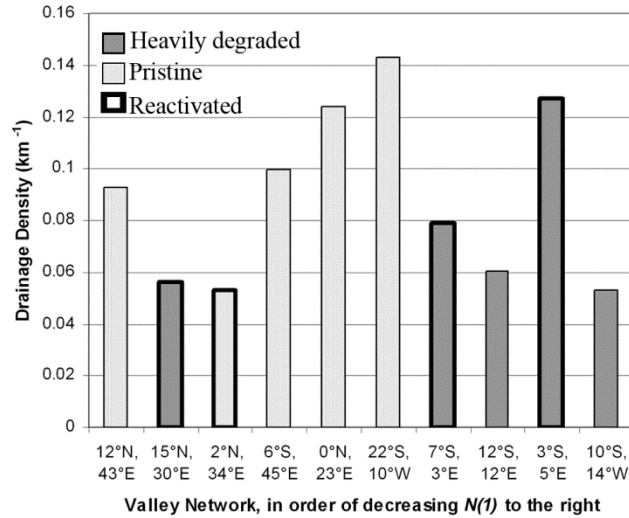
Figure 7. The drainage densities of each valley network are shown here in approximate chronological order according to the corresponding N(1) value, with youngest on the right. Preservation state of the valley networks are indicated by solid gray fill (degraded) or dotted fill (pristine), and reactivated valley networks are indicated by the heavy outline. The lack of a clear trend in this figure suggests drainage density is a function of many variables. Drainage density does appear to be affected by preservation state, with the more pristine networks having an overall higher drainage density than the more degraded networks.

played a bigger role in determining the density of the drainage systems. Drainage density is further discussed in Section 4.1.

2.3.3 Crater counting

Crater counting was performed separately for each valley network, including the east and west branches of the network at 2°N, 34°E. Craters 1 km in diameter and larger were counted in bins that incremented as √2D. Crater counts per bin ranged from 1 to 91, depending on valley network and crater size (see Table A1 in Appendix A). To improve the crater density statistics, the crater counts for each valley network were adjusted by limiting the largest crater bin size to that which had two or more craters; all larger bin sizes that had one or fewer counts were set to zero so as to not affect the cumulative count. The power law distribution of crater sizes places most of the data used for crater counting at the smallest size bins, so truncating the data range at

46

the large-diameter end removes only one to a few craters from the total count and therefore does not affect the determination of N(1) or N(2) significantly. See Appendix B for further discussion on the effect of removing the unpopulated large-crater size bins from our data. This cutoff occurred at different diameters for different valley networks and limited two valley networks (6°S, 45°E and 0°N, 23°E) to only four bins of crater counts.

Log-log cumulative crater size-frequency distributions for all the valley networks studied in this work are plotted in Figure 8. Isochron lines (gray) representing the boundaries between the Martian epochs as defined by Neukum's [Ivanov, 2001] and Tanaka's [1986] production functions are included. Individual cumulative crater size-frequency distribution plots for each valley network are provided along with their mapping in subsequent plots or in Appendix C. Error bars have been left off the plot in Figure 8 for clarity, though they are included in all other plots.

Four of the valley networks examined, 15°N, 30°E and 2°N, 34°E in Terra Sabaea and 7°S, 3°E and 3°S, 5°E in Meridiani Planum, have crater size-frequency distributions that include a resurfacing regime (Figure 9). These networks have greater crater densities at large crater diameters than the other networks, and they have a turndown in slope at intermediate crater diameters that the other networks do not. This turndown indicates that they have experienced some erosion and/or infilling at some point after their primary valley-forming event that has preferentially removed smaller craters up to a given crater diameter. The crater size-frequency distribution slopes that define the production and resurfacing regimes are given in Appendix A, Table A2. For most of the valley networks, the slope values are approximately −1.74 to −2.34, which correspond to production regimes [Melosh, 1989; Hartmann and Neukum, 2001]. Whereas, the resurfacing regimes have much shallower slopes at approximately −0.89 to −1.37.

47
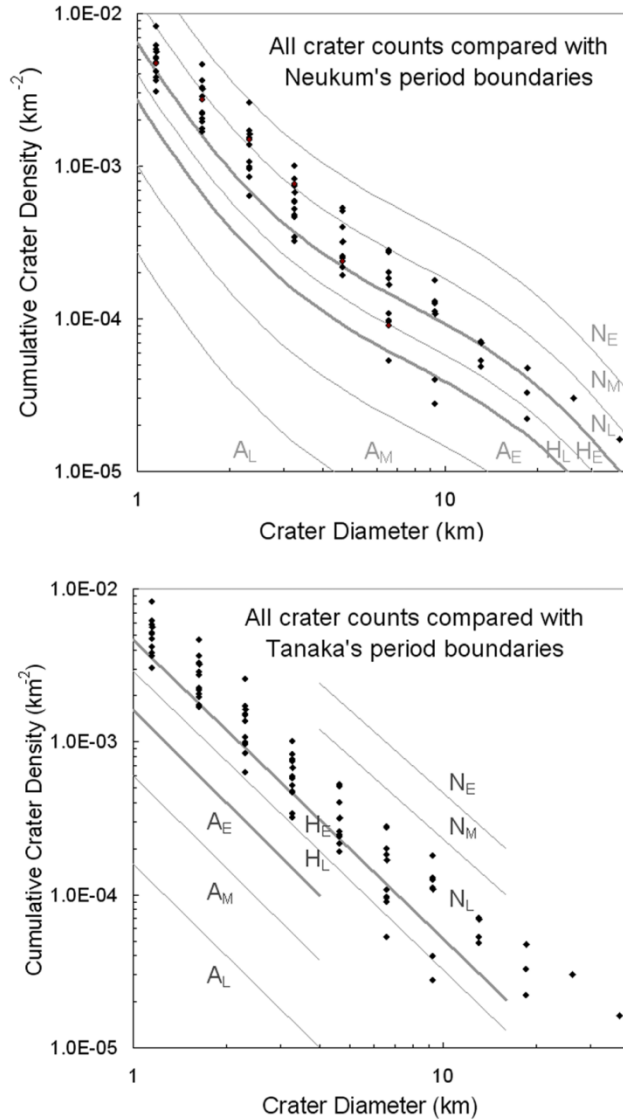
Figure 8. Cumulative crater densities for all Terra Sabaea, Arabia Terra, and Meridiani Planum valley networks analyzed in this study place the end of valley incision primarily within the Late Noachian and Early Hesperian. Error bars were not included in this particular plot for clarity, but they appear in subsequent plots. Isochrons for a) Neukum and b) Tanaka production functions are shown in gray and represent the boundaries between (from the top) the Early, Middle, and Late Noachian (N_E, N_M, and N_L, respectively); Early and Late Hesperian (H_E, and H_L, respectively); and Early, Middle, and Late Amazonian (A_E, A_M, and A_L, respectively).

All of these reactivated networks have crater densities at smaller crater diameters that indicate

the modification events are coincident with the formation of the other valley networks.

Therefore, these four valley networks are interpreted as having initially formed prior to the

a. 15°N, 30°E
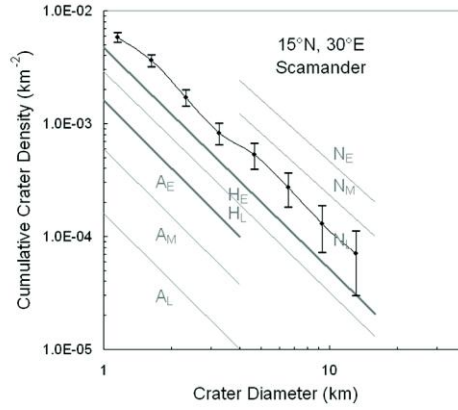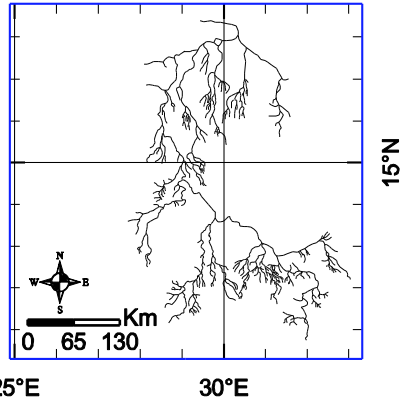
b. 2°N, 34°E

c. 3°S, 5°E

d. 7°S, 3°E

49
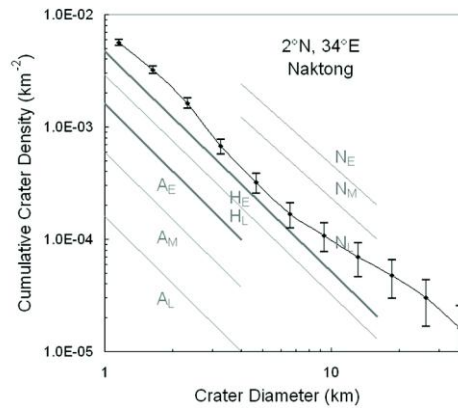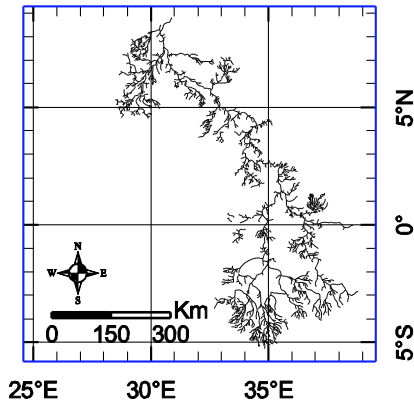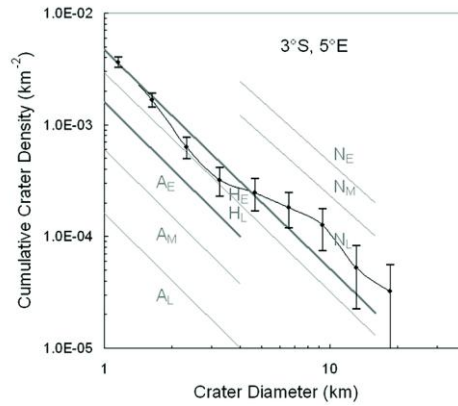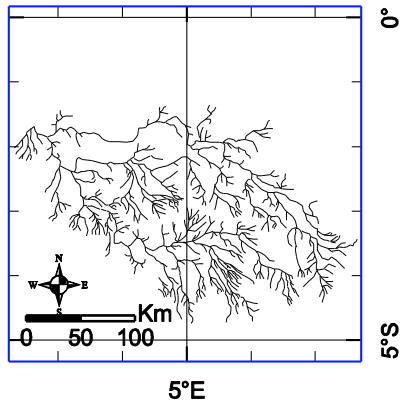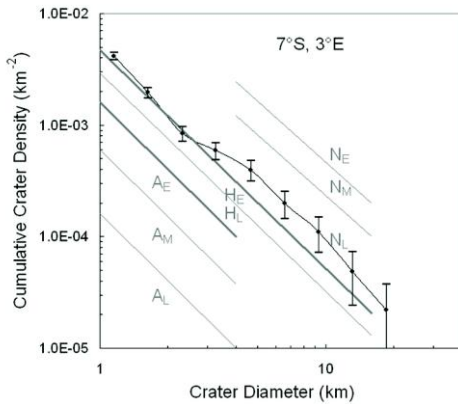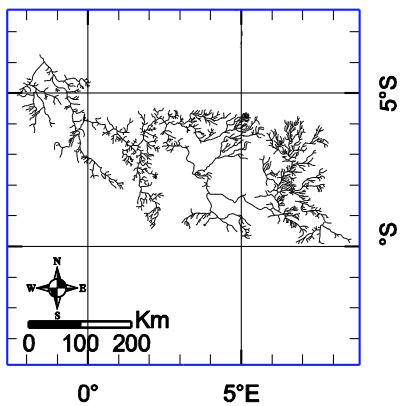
others and then experienced reactivation as the younger valley networks formed. For example, the valley network at 15°N, 30°E (Scamander Vallis) was modified sufficiently to affect its crater density up to 4 km, possibly at the same time the valley network at 12°N, 43°E formed (Figures 1 and 11). The reactivated valley networks at 7°S, 3°E and 3°S, 5°E were similarly modified when the neighboring valley network at 12°S, 12°E (Evros Vallis) formed (Figures 1, 11, and 13).

To allow comparison with the Hartmann and Neukum isochrons, our N(2) crater numbers are also given in Table 2. Due to the limited extent of some valley networks, not all of our networks (0°N, 23°E and 6°S, 45°E) have enough superposed craters to give statistically relevant N(2) values. Additionally, several of these valley networks have lower crater densities at 2 km and other intermediate crater diameters due to apparent resurfacing, making those networks (3°S, 5°E and 7°S, 3°E) non-ideal for determining age based on their N(2) values. Therefore, valley networks with low N(2) values due to resurfacing or other processes are provided in parentheses in Table 2 and are indicated as open diamonds in Figure 10. Our N(2) crater numbers range from 633–1731 per 10^6 km^2 (or 844–1731 per 10^6 km^2 without the low N(2) from resurfacing regime). The N(2) values that mark the Middle/Late Noachian boundary according to the Hartmann and Neukum production function (4334 per 10^6 km^2, 1862 per 10^6 km^2, respectively), the Noachian/Hesperian boundary (996 per 10^6 km^2, 954 per 10^6 km^2), and the Early/Late

---

Figure 9 (previous page). The cumulative crater density plots for the reactivated valley networks, a) 15°N, 30°E; b) 2°N, 34°E; c) 3°S, 5°E; and d) 7°S, 3°E, are plotted vs. weighted mean crater diameter on log-log plots. These valley networks generally have crater size-frequency distributions that are characterized by greater crater densities at large crater diameters and downturns at intermediate crater diameters that suggest multiple periods of formation. Error bars represent a one-σ interval of $\pm$ N$_c$/√n$_c$. Tanaka's isochrons are shown in gray and represent the boundaries between epochs as in the previous figure.
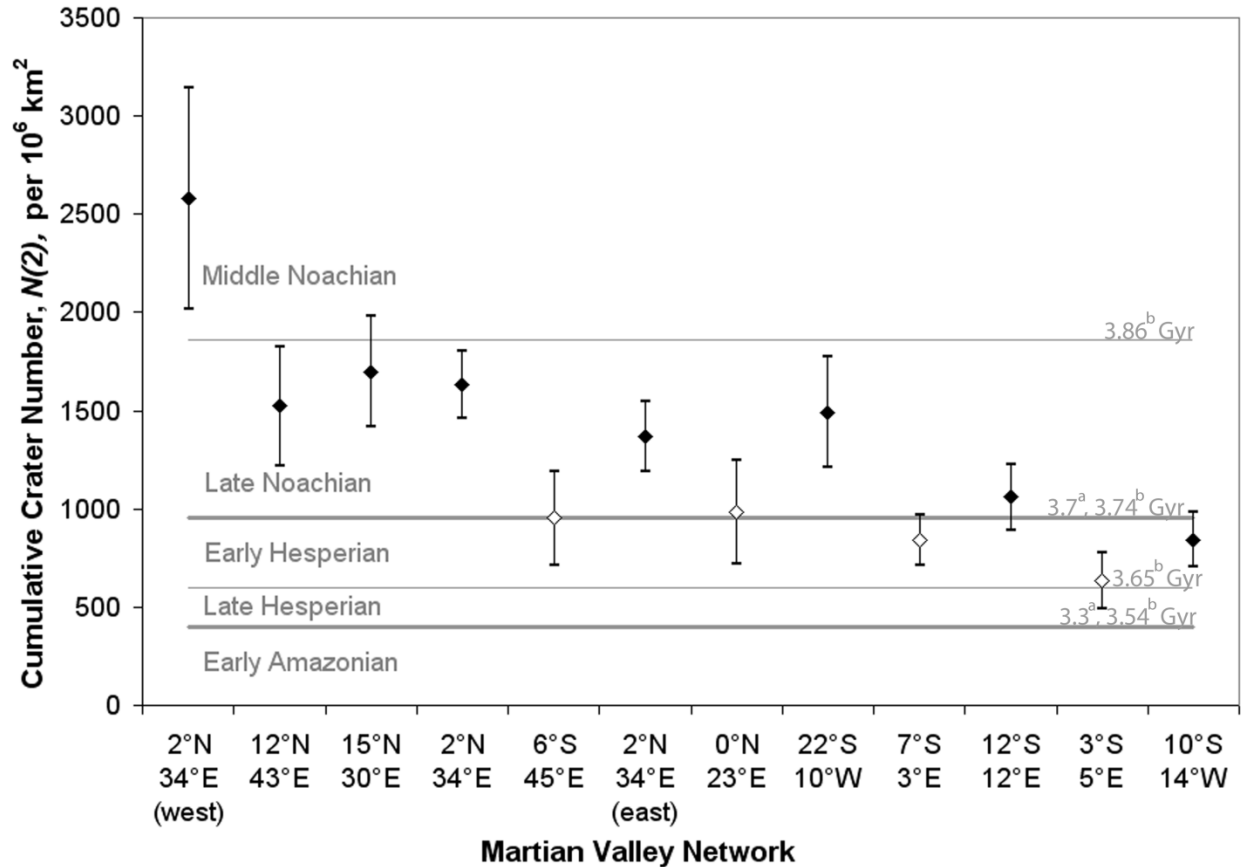
Figure 10. The 2-km crater numbers, N(2), for the valley networks in this study show that the timing of the end of valley network formation clustered in the Late Noachian with some values extending into the Early Hesperian and one value (west branch of Naktong Vallis) occurring in the Middle Noachian. The valley networks with reduced crater density at 2 km due to reactivation or other processes are represented by open diamonds. Isochrons, as defined by the Neukum production function [Ivanov, 1986], are shown in gray and correspond to the approximate absolute ages by a) Hartmann and Neukum [2001] and b) Fassett and Head [2008b], as indicated on the right.

Hesperian boundary (623 per 10^6 km^2, 596 per 10^6 km^2) [Fassett and Head, 2008b] all place our

N(2) values for the end of valley network formation within the Late Noachian and Early

Hesperian. A majority of these valley networks have N(2) values that place the end of their

formation in the Late Noachian, with only the youngest valley network falling in the Early

Hesperian. This result does not include the two networks (3°S, 5°E and 7°S, 3°E) with low N(2)

values due to a downturn at intermediate crater diameters. While their N(2) values (633 and 841

per 10^6 km^2, respectively) would place the end of their formation in the Early Hesperian, analysis

of their full crater size-frequency distribution and comparison of their N(1) values with those of

other valley networks that do not contain a downturn at intermediate crater diameters place the

end of their formation in the Late Noachian. The two networks with insufficient data for N(2)

analysis (0°N, 23°E and 6°S, 45°E), incidentally, have N(2) values (985 and 954 per 10^6 km^2,

respectively), which places their formation at the Noachian-Hesperian boundary. However this

is probably a slight underestimate of their actual age as their N(1) values place the end of their

formation before several of the other Late-Noachian-age networks (i.e. 22°S, 10°W (Parana

Basin) and 12°S, 12°E (Evros Vallis)).
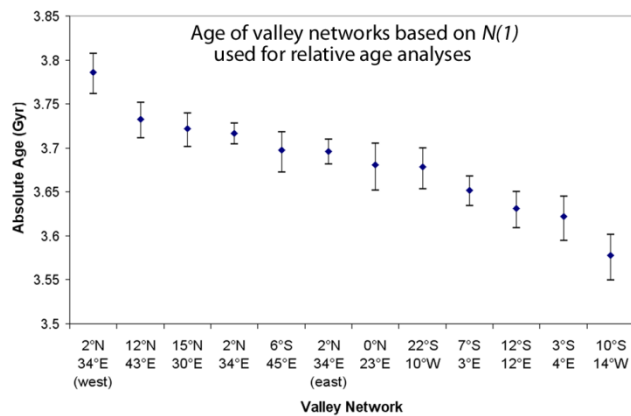
Figure 11. The absolute ages for each valley network based on their N(1) values are shown here
in sequential order. While Figure 10 shows that these valley networks have crater populations
that indicate they formed in the Late Noachian and Early Hesperian, the spread in ages in this
figure indicates that there were punctuated episodes of valley network formation that
independently affected localized regions within Terra Sabaea, Arabia Terra, and Meridiani
Planum. As described in Section 2.2, these absolute ages should be used only as a means for
comparing ages between the valley networks, and not used to place the timing of valley network
formation within the context of Martian history. These ages show a difference of 210 ± 50 Myr
between the oldest and youngest valley networks in this study, with some networks having
distinctly different ages and others being coeval.

To aid in comparing the relative ages of these valley networks, the crater number at 1 km, N(1), values are given in Table 2 along with their corresponding absolute ages (see also Figure 11). Our results, which range from ~3051-8213 per 10^6 km^2, are similar to those of Baker and Partridge [1986], who found that their pristine network segments had N(1) values of ~5112–6699 per 10^6 km^2 and their degraded segments had N(1) values of ~7081–9184 per 10^6 km^2, depending on the counting method used. Our corresponding absolute ages differ by as much as ~210 ± 50 Myr between our oldest (the west branch of 2°N, 34°E) and youngest (10°S, 14°W) valley networks, with ~ 90 ± 30 Myr difference between the east and west branches of 2°N, 34°E (Naktong) (Table 2 and Figure 11).

It is important to note that the crater-age dating in this study provides information on the timing of the end of a feature's formation as well as significant modification events that affected crater densities down to 1 km, but says nothing about the rate or duration of formation, or smaller precipitation events. Figure 10 shows that all of these valley networks ceased formation toward the end of the Late Noachian or at the beginning of the Early Hesperian, consistent with results from Hynek and Phillips [2001] and Fassett and Head [2008b]. Our ages do not extend into earlier Martian history, nor significantly into the Hesperian, and the spread in these ages (Figure 11) indicates they did not all form, or cease formation, at the same time.

2.4 Discussion

The results from this research place precipitation-driven formation of the Martian valley networks in Terra Sabaea, Arabia Terra, and Meridiani Planum in the Late Noachian and earliest Hesperian. Some of these networks appear to have experienced multiple periods of formation, both from precipitation-dominated valley formation and from erosion originating at localized sources of water such as paleolakes and groundwater sapping at springs. These valley networks

also appear to be in different stages of preservation, with some networks being highly eroded and/or infilled while others appear pristine. These variations in valley network morphology can be seen in their drainage densities and crater densities, as discussed below.

2.4.1 Drainage density

The balance between valley-forming and valley-filling processes over long periods of time affects drainage density, both during formation and after the valley-forming phase has stopped. Variations in Martian drainage density reflect different interactions of geology, climate, surface topography, and preservation state. For example, a Martian valley network with high drainage density (i.e. closely spaced valleys) may indicate a greater frequency and/or duration of rainfall events, a surface composition with a reduced resistance to erosion, a reduced infiltration capacity of the soil, and/or an increase in initial soil water content (assuming no vegetation) [Ritter, 1978; Baker and Partridge, 1986; Tucker and Slingerland, 1997; Tucker and Bras, 1998; Solyom and Tucker, 2004]. Or with all those factors being equal, a higher Martian drainage density may be the result of less infilling and therefore a greater number of small tributaries identified and included in the calculations.

The drainage density values we calculated for these valley networks are similar in value to terrestrial drainage densities determined by Carr and Chuang [1997], though comparing drainage densities between the two planets is complicated. Many factors can affect the determination of drainage density on Earth and Mars differently, and they do not include the factors that affect the formation of different drainage densities. Since the determination of drainage density is strongly influenced by the identification of small tributaries, Mars will be prone to smaller densities due to the limits of image resolution and 3.5 Gyr of surface modification, whereas Earth will be prone to higher densities due to their younger, active state

54

and the presence of water and vegetation that aids in identification of small tributaries [e.g. Craddock and Howard, 2002; Irwin and Howard, 2002]. While it is highly probable that the Martian valley networks formed under conditions and on surfaces very different than river systems actively forming on Earth today, it is interesting that the drainage densities determined in this work for Martian valley networks and the drainage densities calculated for terrestrial river systems [Carr and Chuang, 1997] are so similar after accounting for the inequality in detection/measurement biases for Earth and Mars. The similarity in drainage density between Martian and terrestrial drainage systems supports the hypothesis that the Martian valleys were formed, at least in part, by precipitation [e.g. Hynek and Phillips, 2003], and the somewhat lower Martian values likely reflect not only differences in the conditions of their formation but also the greater difficulty in their identification and measurement.

Resolution and detail of the dataset affects the mapping and quantitative analysis of the Martian valley networks, as described by Irwin and Howard [2002]. This effect can be seen in Table 3 in which stream order and drainage density for three valley networks are compared when determined by THEMIS and MOLA (this study), MOC WA and MOLA [Hynek and Phillips, 2003], and Viking images [Carr, 1995]. The mapping of valley networks with Viking data [Carr, 1996] did not produce networks with stream orders as high as those in this study, though the MOC data was detailed enough to give the same stream orders as this work. In two of the three cases, drainage densities for each valley network increased as the detail of the dataset increased.

Further increase in resolution of the images may result in further increase in the calculated drainage densities due to the ability to identify and map the smallest tributaries that may not be visible in comparatively lower resolution images. This increase will happen until the valley has been mapped at resolution better than the narrowest valley segment, such as is likely

Table 3. Comparing Martian valley network stream order and drainage density as determined with (a) THEMIS and MOLA [this paper], (b) MOC and MOLA [Hynek and Phillips, 2003], and (c) Viking [Carr, 1995] datasets. An overall drainage density is given here for 2°N, 34°E that includes both the east and west branches.

Valley Network Location (lat., long.)	Strahler Stream Order			Drainage Density (km^{-1})		
	THEMIS and MOLA (a)	MOC and MOLA (b)	Viking (c)	THEMIS and MOLA (a)	MOC and MOLA (b)	Viking (c)
3°S, 5°E	5	5	3	1.3×10^{-1}	9.5×10^{-2}	2.2×10^{-2}
0°N, 23°E	5	5	2	1.2×10^{-1}	8.2×10^{-2}	1.1×10^{-2}

the case with the more degraded/filled-in valleys that we mapped with THEMIS daytime IR. The valley networks that we mapped in THEMIS daytime IR that are pristine and/or narrow will likely increase in drainage density if mapped with higher resolution images. To illustrate the increase in drainage density with increased resolution, we mapped the relatively pristine valley system at 22°S, 10°W (Parana Basin) with the higher resolution THEMIS Visible images (18 m/pixel) that we manually coregistered with MOLA topography using ArcGIS$^{©}$ software. Drainage density for this valley network system increased from 0.14 km^{-1} in THEMIS daytime IR (230 m/pixel) to 0.17 km^{-1} in THEMIS Visible (18 m/pixel) due to an increase in valley length from 6,117 km to 8,029 km and an increase in area from 42,745 km^{2} to 45,984 km^{2}. While the calculated drainage density increased, it did not increase dramatically, suggesting the values determined with THEMIS daytime IR may slightly underestimate the drainage densities for some valley networks, particularly for those with pristine or narrow valleys that are at the limit of resolution in this data set. The moderate increase in drainage density with an approximate 12× increase in image resolution is likely due to the obliteration of the smallest tributaries since their emplacement, as described by others [e.g. Irwin and Howard, 2002; Craddock and Howard, 2002; Hynek and Phillips, 2003]. Interestingly, Carr and Malin [2000] did not identify any valleys smaller than a few hundred meters wide in high-resolution (1.5

m/pixel) MOC images, which may be a result of infilling of the small valleys or erosion of the valley walls, or may indicate insufficient time for valleys of that size to form in those locations.

Since drainage density is strongly dependent on the ability to identify even the smallest tributaries, it is expected that there should be a bias toward higher drainage densities for more pristine networks within a set of calculations using the same resolution and techniques. Figure 7 shows a rough correlation between preservation state and drainage density. Four of the five more pristine networks have high drainage densities relative to the others, whereas the more degraded networks have overall lower drainage densities.

With the expectation that the determination of drainage density is affected by the amount of erosion and/or infill a network has experienced, it is possible that the more degraded valley networks once had greater drainage densities than are visible today. Further, the drainage densities of the more pristine networks may be nearer to their original value, though their values may be limited by the resolution of the THEMIS daytime IR data set we used for mapping.

Figure 7 shows a general lack of correlation between drainage density and age, as the networks are arranged in order of decreasing crater number, N(1), from left to right. The lack of a clear trend emphasizes that drainage density is a function of many variables and cannot be described by age and preservation state alone.

2.4.2 Crater densities

The crater densities of all the valley networks analyzed in the Terra Sabaea, Arabia Terra, and Meridiani Planum regions of Mars correspond to values that cluster in the Late Noachian and Early Hesperian epochs, consistent with their formation during the hypothesized final stage of fluvial erosion [e.g. Hynek and Phillips, 2001, 2003; Howard et al., 2005; Irwin et al., 2005a; Hynek et al., 2008]. Although their crater densities suggest that they all formed by the end of the

57

Late Noachian or earliest Hesperian (Figure 10), the spread in ages suggests that they did not all form or cease formation simultaneously (Figure 11). Using the equation of Ivanov [2001] that relates crater number, N(1), with absolute age, the difference in age between the oldest and youngest valley networks in Terra Sabaea, Arabia Terra, and Meridiani Planum analyzed in this work is ~210 ± 50 Myr. Within this range are valley networks that have distinctly separate ages, and those that appear to be coeval.

One striking example of this variability in the timing of precipitation is seen in the crater size-frequency distributions of the east and west branches of the valley network at 2°N, 34°E (Naktong Vallis) in Terra Sabaea (Figure 12). The crater size-frequency distribution of the entire valley network at 2°N, 34°E (Naktong Vallis, Figure 9b) has the characteristic downturn at intermediate crater diameters that suggests this network experienced multiple periods of valley formation. This interpretation of multiple periods of incision is supported by the different ages between the two branches (Figures 11 and 12, Table 2); the west branch has a higher crater density at all crater diameters than its neighboring east branch, giving it an older age. The absolute age of the west branch is an estimated 90 ± 30 Myr older than that of the east branch. These valleys have clear signs of formation by surface runoff of water including braided channels and terraces; therefore these ages correspond to the timing of precipitation in this area. Our interpretation is that precipitation fell for a period of time near 7°N, 31°E, incising the valleys in the west branch of what becomes the valley network today centered at 2°N, 34°E (Naktong Vallis), as well as likely incising some valleys in the nearby east branch. Rainfall and valley incision in this area eventually stopped for a time, possibly moving north and east as it reactivated the valley network at 15°N, 30°E (Scamander Vallis) while forming the nearby valley network at 12°N, 43°E (Figures 1 and 11, Table 2). Eventually rain returned in an
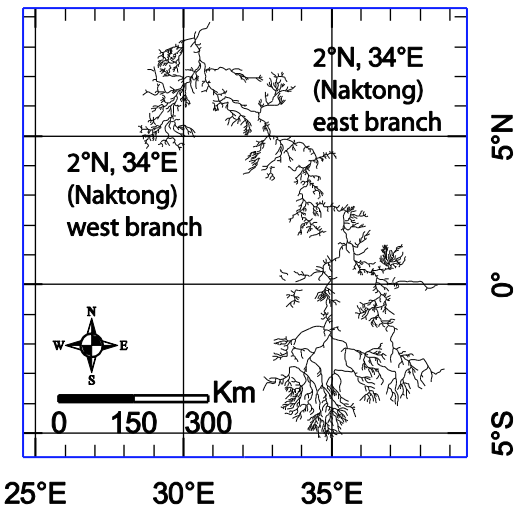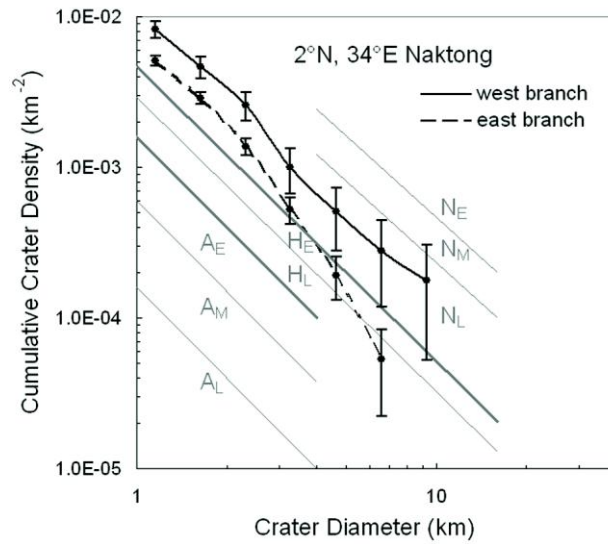
Figure 12. Comparison of the crater densities for the east and west branches of the 2°N 34°E valley network (Figure 4) shows two distinct ages. Error bars represent a one-σ interval of ± $N_c/\sqrt{n_c}$. Isochrons, as defined by Tanaka [1986], are shown in gray and represent the boundaries between epochs as in Figure 8.

upslope region to the south and east of the west branch of 2°N, 34°E (Naktong Vallis), forming

new valleys. As the network grew, it eventually took over the eastern branch of the older

network at 7°N, 31°E, re-incising its main branch and forming what is seen today. The period of

precipitation that formed the current east branch of 2°N, 34°E (Naktong Vallis) also appears to

have formed the valley network at 6°S, 45°E as they have similar crater-determined ages

59

(Figures 1 and 11, Table 2). This similarity in valley network age suggests that this region experiencing precipitation spanned 15° in longitude and 10° in latitude and possibly much more.

This is not to say that precipitation was not occurring elsewhere on the ancient Martian surface at the same time. Crater-age dating of valley networks found in other regions on the ancient highlands of Mars, as determined by Hoke and Hynek [2009] and Fassett and Head [2008b], show similar crater-age dating as those that we discuss in this work and suggest that the period of precipitation seen in the regions covered herein extended globally. Additionally, these results apply to major valley-forming precipitation episodes and do not exclude the possibility that precipitation and surface runoff were occurring to a lesser extent on these valleys at times other than what their crater densities above about 1 km in diameter indicate.

Another interesting sequence of events deduced from the crater size-frequency distributions of several valley networks lies near Meridiani Planum. Three closely spaced valley networks were analyzed, 7°S, 3°E; 12°S, 12°E (Evros Vallis); and 3°S, 5°E (Figures 1 and 13). Two of these, 7°S, 3°E and 3°S, 5°E, have crater densities that indicate they formed prior to their neighbor 12°S, 12°E (Evros Vallis), which lies at a higher elevation (Figure 13, Table 2). It is possible that the precipitation that fell as 7°S, 3°E and 3°S, 5°E were forming did not reach high enough in elevation or extend far enough south or east so as to include 12°S, 12°E (Evros Vallis). However, tens of millions of years later while 12°S, 12°E (Evros Vallis) was forming, its two neighbors were also being modified as indicated by their similar crater numbers (Figures 9 and 13, Table 2), suggesting that this region spanning 20° in longitude and 15° in latitude experienced a period of rainfall that ended approximately 80 million years after the incision of Naktong Vallis and its neighbors ceased. The valley networks at 7°S, 3°E and 3°S, 5°E have degraded morphologies with primarily U-shaped interiors and a turndown in crater density that
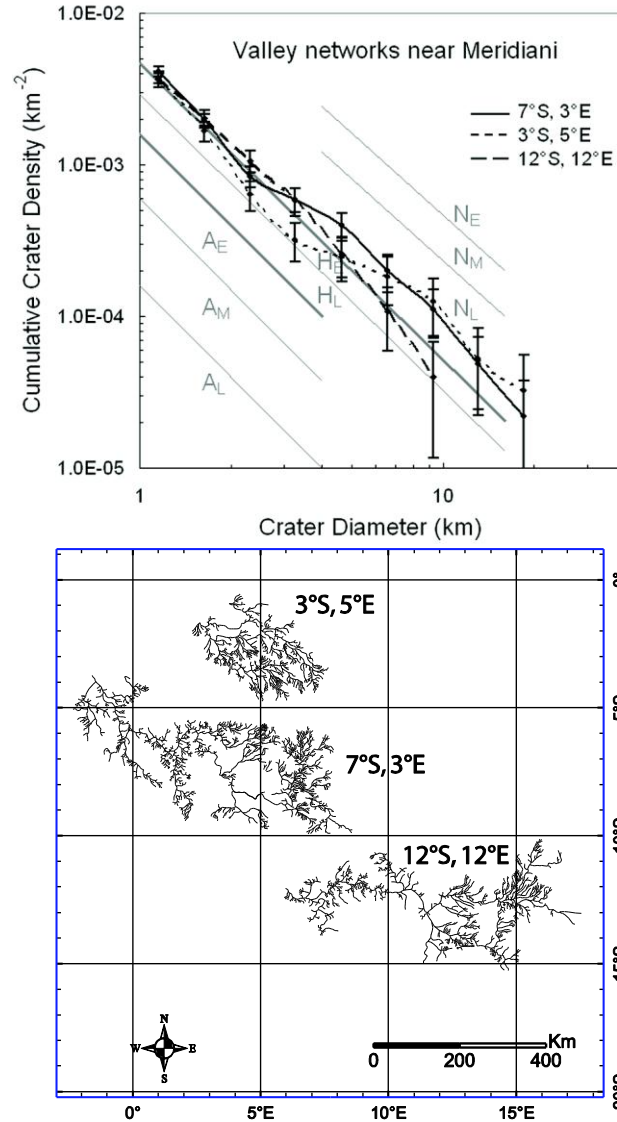
Figure 13. Crater densities for three adjacent valley networks near Meridiani Planum (3°S, 5°E; 7°S, 3°E; and 12°S, 12°E) are shown here. Their crater size-frequency distributions suggest 3°S, 5°E and 7°S, 3°E were reactivated with the formation of 12°S, 12°E. Error bars represent a one-σ interval of ± $N_c/\sqrt{n_c}$. Isochrons, as defined by Tanaka [1986], are shown in gray and represent the boundaries between epochs as in Figure 8.

indicates a loss of craters up to 4 km and 8 km in diameter, respectively. Numerous factors may have been responsible for the loss of craters up to these diameters in their crater size-frequency distributions, including reactivation of these fluvial systems. The valley network at 12°S, 12°E

(Evros Vallis), which has no downturn in crater density at intermediate crater diameters, also has a degraded morphology, but to a lesser extent, and both U- and V-shaped valleys exist. The valley network at 3°S, 5°E is at the lowest elevation and has the highest drainage density of these three networks (Table 2). Being at a lower elevation may have increased the frequency or duration of rainfall events or increased the amount of water in the soil and thereby increased the amount of runoff, either of which could have led to the higher drainage density of this valley network. Interestingly, the valley networks at 7°S, 3°E and 3°S, 5°E are buried by the layered materials on which the Mars Exploration Rover Opportunity rests, implying that these deposits post-date much of the fluvial activity in the region and that they were emplaced toward the very end of the Noachian or in the Hesperian.

2.4.3   Implications for the Late Noachian Climate

The spread in ages combined with the apparent lack of correlation of drainage density with latitude, longitude, elevation, or region (i.e. Terra Sabaea, Arabia Terra, or Meridiani Planum) suggests that local variations in climate and geology were more important than regional differences in affecting the formation of the valley networks. For most of these crater-ages, the error bars overlap with those of the nearest temporal neighbor(s), either indicating that precipitation moved gradually and allowed many valley networks to form coevally or that the precipitation moved over shorter timescales than our data can distinguish.

It is important to remember that precipitation on Earth does not occur to the same degree in all regions across the planet, even though our atmosphere supports precipitation. A geographic region may experience changing levels of precipitation over time, driven by changes in topography and relative locations of source bodies of water, changes in atmospheric circulation patterns, and/or changes in orbit and obliquity. An example of this can be seen in the

Basin and Range province within Nevada. At present, conditions are extremely arid and desert-like, whereas the Pleistocene climate permitted vigorous hydrological activity and long-lived lakes covering much of north and west Nevada [e.g. Hostetler and Benson, 1990]. Likewise, precipitation is not expected to have occurred everywhere simultaneously on Mars. Colaprete et al. [2004] showed that regional variations in rainfall would be expected during periods of warmer/wetter climate. This variability in precipitation is especially important for a hypothetical early Mars without a large ocean to constantly supply water to the same region. Both the morphologies and crater ages of these valley networks indicate precipitation did not extend everywhere simultaneously on Mars, and regions of precipitation moved around during the Late Noachian and Early Hesperian.

It is beyond the resolution of our data to say whether the atmosphere was continuously warmer and thicker during the end of the Noachian, and the location of rainfall changed over the ~210 million years that these networks span; or if instead the global climate was changing on short timescales, producing shorter, perhaps more intense episodes of temporarily warm/wet conditions that allowed valley network formation to occur in localized regions.

The lack of valley networks in this large region older than the Late Noachian is surprising. This observation could indicate that valley network formation in Terra Sabaea, Arabia Terra, and Meridiani Planum did not occur earlier in the Noachian, or that any traces of valleys whose formation ceased earlier in the Noachian have been erased. If valley formation had occurred earlier in the Noachian, it would be expected that these valleys would have experienced greater infilling and erosion with increased age, resulting in valleys with morphologies that gradually degraded to the point of non-detection. None of the valleys we analyzed exhibited this degree of modification, supporting the corresponding crater-age dating

that places their formation to within a few hundred million years of each other. However, it could be that valleys from older episodes of formation have been so modified by erosion, infilling, impact craters, and subsequent valley network formation episodes that they are no longer represented by individual, large, connected networks and were therefore excluded from this study. While our selection of valley networks may have excluded the smaller remains of older valley networks, Fassett and Head [2008b] were less limited by valley network size and still found that most of the ancient valley networks in their study had Late Noachian crater ages. When they applied their data to Hartmann [2005] production functions, it resulted in no networks older than Late Noachian, with the oldest valley network (Naro Vallis) having an age of 3.81 Gyr [Fassett and Head, 2008b]. Using the Neukum production function [Ivanov, 2001], however, placed a few valley networks in the Middle Noachian, with a maximum age of 3.93 Gyr (123°E, 0°N) [Fassett and Head, 2008b]. This discrepancy is due to differences between the Hartmann and Neukum production functions [Hartmann and Neukum, 2001], and therefore is inconclusive as to whether valley network formation extended into earlier Martian history.

Several factors toward the end of the Noachian likely created a climate conducive to valley formation that may or may not have been present earlier in Martian history and only intermittently in more recent Martian history. Segura et al. [2002, 2008] hypothesized that large impacts may have created the temporary climate change necessary for valley formation. This model favors the hypothesis that valley network formation extended into earlier Martian history and would suggest significant valley formation earlier in the Noachian, corresponding to the early large impacts and valley formation dying off with the declining impact rate in the Late Noachian. There are, however, several issues with invoking impactors to produce the degree of climate change necessary for valley network formation. The size and frequency of impactors is

thought to have greatly decreased during the Noachian [Hartmann and Neukum, 2001]. Thus, putative intense episodes of climate change from larger and more frequent impacts would have mostly occurred several hundred million years earlier in the Noachian than when these large valley networks, some of the largest on the planet, formed. Further, one would expect valley network formation to have waned over time as impacts diminished in size and frequency, producing a relationship between age and size, stream order, drainage density, etc; none of which is evident in our results (Table 2, Figure 7). Additionally, studies done on the morphology of fluvially-modified craters that date to the Late Noachian and Early Hesperian [e.g. Craddock and Howard, 2002; Barnhart et al., 2009] also do not favor the impact-induced climate change models. The low occurrence of exit breaches in crater rims in the southern highlands suggests there were moderate, episodic periods of precipitation and evaporation that lasted $10^5 - 10^6$ years [Barnhart et al., 2009]. This observation requires that valley formation did not occur under deluge-like conditions [Barnhart et al., 2009] that would be present in intense, brief periods of precipitation lasting up to 10^3 or 10^4 years, as modeled by Segura et al. [2002, 2008]. The interpretations of our data and others suggest that the impact model is less plausible, or provides only part of the story, for explaining the timing of climate change that corresponds to valley network formation.

An alternative hypothesis for the primary cause of climate change that allowed valley network formation during the Late Noachian is outgassing from the Tharsis rise. Analysis of tectonic, magnetic, gravity, topographic, relative stratigraphic, and crater density data place the formation of most of the Tharsis load prior to the Late Noachian [Anderson et al., 2001; Hartmann and Neukum, 2001; Phillips et al., 2001; Johnson and Phillips, 2005]. Valley network formation followed a majority of the Tharsis formation since the drainage pattern of the valley

networks on the ancient surfaces on Mars follows the long-wavelength topography created by the Tharsis load [Jakosky and Phillips, 2001; Phillips et al., 2001]. The constraint that most of the ancient valley networks we see today on the Martian surface formed after most of Tharsis formed is further supported by our valley network crater ages that place valley formation at the end of the Noachian.

Many researchers have determined that the quantities of CO_2 and H_2O released during Tharsis formation may have been sufficient to warm the atmosphere during the Late Noachian to the point that liquid water was stable at the surface [e.g. Forget and Pierrehumbert, 1997; Phillips et al., 2001]. So the Tharsis model conceivably fits with the timing of valley network activity in Terra Sabaea, Arabia Terra, and Meridiani Planum. Further, the Tharsis model does not exclude the possibility of valley network formation earlier in the Noachian, but it does not require it either. Precipitation and valley incision may have coincided with a balance between episodes of volcanic outgassing and the steady loss of atmospheric constituents to the surface and space. Alternatively the atmosphere may have been sufficiently stable to allow a more continuous period of clement weather while the location of precipitation moved in time with changes in global circulation patterns, local atmospheric pressure, surface topography, insolation, and other variables [Craddock and Howard, 2002].

Additionally, as Tian et al. [2009] describe, the early Martian climate may have been significantly affected by the strong solar EUV flux from the young sun during the first several hundred million years of solar system history. This strong EUV flux would have led to increased thermal escape of carbon from early Mars, keeping the early Martian climate relatively cold and dry [Tian et al., 2009]. Eventually, the decrease in solar EUV flux as the sun matured may have allowed a build-up of atmospheric carbon that, combined with a possible release of volatiles

trapped in ices on the surface of Mars, could have led to a warm, wet period lasting a few hundred Myr in the mid to late Noachian [Tian et al., 2009].

Regardless of the trigger (i.e. impact, volcanic, solar, or a combination) for climate change, valley network formation in this part of the ancient highlands of Mars ceased near the Noachian/Hesperian boundary. While atmospheric concentrations of CO_2 and H_2O would have been lost to space throughout the Noachian through solar wind stripping, impact ejection, and thermal escape, the loss rate would have increased as the internal magnetic field disappeared [Jakosky and Phillips, 2001]. While the timing of this event is largely debated [Acuna et al., 1999; Schubert et al., 2000; Stevenson, 2001; Nimmo and Tanaka, 2005], it is generally placed sometime in the Pre-Noachian before the formation of the large impact basins, and it therefore predates all crater-age dated valley networks. Additionally, the formation of carbonates and hydrated minerals and the growth of the polar caps and sub-surface ice reservoirs would have further reduced atmospheric concentrations of CO_2, H_2O, and other greenhouse gases [Brain and Jakosky, 1998; Carr, 1999; Jakosky and Phillips, 2001; Phillips et al., 2001; Bibring et al., 2006]. Together with a decreasing impact rate and a decline in Tharsis volcanic activity, these factors would have led to the loss of enough atmosphere to end precipitation-related valley network formation within a timespan of less than a few hundred million years [Phillips et al., 2001].

2.5   Conclusions

The ten large valley networks in this study are characterized by morphologies and drainage densities that suggest they formed primarily by precipitation. Some of these networks appear to have experienced multiple periods of formation, predominantly from precipitation-dominated valley formation and also from a few localized sources of water including paleolakes and groundwater sapping at springs. The valley networks also appear to be in different stages of

preservation, with some networks highly eroded and/or infilled while others appear pristine. This preservation state affects the calculation of drainage density so that the more degraded networks have an overall lower density. Exceptions lie with the reactivated networks, which are interpreted as having experienced multiple periods of formation that likely contributed to their greater drainage densities.

Determining the ages of actual valley formation through crater counting on the valley networks themselves provides much more precise constraints on the timing and duration of warmer, thicker atmospheric conditions than does analysis of stratigraphic and cross-cutting relationships. Using a method tailored for counting craters on narrow linear features and performing crater counting only on large valley networks, we were able to improve the crater counting statistics and estimate ages for these valley networks. The results show that in Terra Sabaea, Arabia Terra, and Meridiani Planum the Late Noachian and Early Hesperian were at least periodically warm enough to support an active hydrological cycle. Our ages do not extend into earlier Martian history, nor later than the Early Hesperian, and the spread in these ages indicates they did not all form, or cease formation, at the same time. A span of ~210 ± 50 Myr passed between formation of the oldest and youngest valley networks that were analyzed in Terra Sabaea, Arabia Terra, and Meridiani Planum. Within this range of ages are valley networks that appear to be coeval and those that have distinctly separate ages, including two branches of the same network that formed ~90 ± 30 Myr apart.

These results support two possible climate scenarios. The ancient Martian atmosphere may have been continuously warm and thick during the end of the Noachian, while the location of rainfall changed in response to other parameters. Alternatively, the ancient global climate may have been changing on small timescales, producing shorter, more intense episodes of

68

temporarily warm/wet conditions that allowed valley network formation to occur in localized regions. Regardless, it is apparent that precipitation was not continuous in space or time in all equatorial regions of the ancient Martian surface. Rather, zones of precipitation appear to have roamed throughout Terra Sabaea, Arabia Terra, and Meridiani Planum, sometimes returning to previously rainy regions.

This observation has important implications for any life that may have existed on early Mars. Although the surface was evidently warmer, wetter, and more habitable for some period of time during the Late Noachian and Early Hesperian, the variability in the location and amount of water at the surface would have made it difficult for life to evolve if it required a stable environment to do so. Alternatively, the variable climate may have forced life, if it ever existed, to adapt to extreme conditions or seek refuge within the Martian crust in order to survive the implied dry spells [Sleep and Zahnle, 1998].

The lack of valley networks in this large region older than the Late Noachian could indicate that valley network formation in Terra Sabaea, Arabia Terra, and Meridiani Planum did not occur earlier in Martian history, or that any traces of valleys whose formation ceased earlier in the Noachian have been erased. The timing of valley network formation on ancient Mars appears to coincide well with the accumulation of CO_2 and H_2O from Tharsis outgassing, providing a possible explanation for the climate change necessary for liquid water to be stable on the surface of Mars and the formation of dense valley networks. However, this environment was not constant; the areas of the surface receiving rainfall changed over the timescales of tens to hundreds of millions of years. As Tharsis activity waned and atmospheric constituents continued to be lost to space, the surface, and the subsurface, precipitation waned and valley incision on these ancient highlands of Mars stopped at roughly the Noachian/Hesperian boundary.

3 Formation Timescales of Large Martian Valley Networks

ABSTRACT: Assessing timescales for formation of the ancient Martian valley networks is key to interpreting the early climate on Mars. We determined the likely formation times for seven of the largest ancient valley networks on Mars using the Darcy-Weisbach equation for average flow velocity, three different sediment transport models, and a range of input parameters to encompass possible formation conditions. With runoff rates similar to intense storms in arid regions on Earth, the minimum formation timescales of these Martian valley networks range from 10^5 to 10^7 years, depending on the specific valley network. Shorter formation timescales require hurricane-scale flows that, if minimized with assumptions of continuous formation unlike even terrestrial rates, could complete large valley network formation in as little as 200 to 5000 years, though this is not the preferred interpretation. While these results do not support impact-induced climate change as the sole mechanism for creating precipitation sufficient to incise the large valley networks, neither do they extend the amount of time required to form the networks beyond their range in age, consistent with hypotheses that valley incision was constrained to a relatively short period of Martian history near the Noachian-Hesperian boundary, approximately 3.6 to 3.8 Ga.

3.1 <u>Introduction</u>

The presence of valley networks across much of the ancient surface of Mars (e.g. Hynek et al., 2010), together with the locations and morphologies of the Martian deltas (e.g. Di Achille and Hynek, 2010b) and ancient paleolakes (e.g. Fassett and Head, 2008a; Irwin et al., 2005a), provides strong evidence that the Martian surface environment was once capable of sustaining liquid water at the surface. Many of the largest Martian valley networks, with their meandering trunks, densely dendritic form, and tributaries that reach up to drainage divides, appear to have formed primarily from surface runoff of precipitated water (e.g. Craddock and Howard, 2002; Hoke and Hynek, 2009; Howard et al., 2005; Hynek and Phillips, 2003; Hynek et al., 2010). These same valley networks have crater densities that place their formation in the Late Noachian and Early Hesperian (~3.5-3.8 Ga) (Fassett and Head, 2008b; Hoke and Hynek, 2009), consistent with their formation during a period of enhanced fluvial erosion and incision on Mars (e.g.

Craddock and Howard, 2002; Howard et al., 2005; Hynek and Phillips, 2001, 2003; Hynek et al., 2010). Sustained liquid water on the Martian surface requires a thicker and warmer atmosphere than exists there today, though it has remained unclear how long such conditions were needed to produce the valley networks.

The large Martian valley networks likely formed by similar processes as terrestrial river valleys (e.g. Craddock and Howard, 2002; Howard et al., 2005; Hynek and Phillips, 2001, 2003; Irwin et al., 2005b), typically by the gradual erosion of sediment through bed load, suspended load, and wash load processes (e.g. Komar, 1980; Milton, 1973). Numerous sediment transport equations and friction functions have been derived from first-order physical laws and calibrated with terrestrial data to incorporate the influence of particle size and density, surface roughness, flow turbulence, and gravitational acceleration (e.g. Meyer-Peter and Mueller, 1948; Ribberink, 1998; van Rijn, 1984a, 1984b), and some of these have been applied to Mars (e.g. Kleinhans, 2005; Komar, 1979, 1980; Wilson et al., 2004).

Often the Manning (1891) equation for depth- and width-averaged flow velocity is applied to Martian conditions by adjusting the empirical Manning coefficient with the difference in equatorial surface gravity between Earth and Mars (e.g. Goldspiel and Squyres, 1991; Irwin et al., 2005b; Komar, 1979), and, in some cases, by incorporating the differences in roughness predictors between different flow systems (e.g. Gioia and Bombardelli, 2002; Wilson et al., 2004). The modified Manning coefficients, however, are weakly dependent on flow depth, do not explicitly include gravity or bed roughness, assume bankfull flow, and produce flow velocities that can vary by over a factor of two (e.g. Kleinhans, 2005; Wilson et al., 2004). This results in sediment transport rates that vary significantly, thus creating large error in discharge

71

rates and calculated volumes of water required to carve Martian outflow channels and valley networks (e.g. Wilson et al., 2004).

An alternative to the Manning equation that is often overlooked in the planetary science community is the Darcy-Weisbach (D-W) equation (Silberman et al., 1963), which, unlike the Manning equation, maintains an explicit dependence on the acceleration due to gravity (g). In addition, whereas the Manning equation includes an implicit power-law scaling relationship between roughness and flow depth, the D-W equation allows greater flexibility in calculating roughness directly from flow depth (h) and median grain size (D_{50}) (e.g. Silberman et al., 1963). Both flow depth and grain size are important variables in determining flow velocity and can have significantly different values for various terrestrial systems and, likewise, Martian flows. Therefore the D-W equation and the included friction function are better suited for modeling flows associated with sediment transport on Mars (e.g. Kleinhans, 2005; Komar, 1979; Wilson et al., 2004).

Additionally, some planetary researchers rely on empirical relationships between flood discharge (Q) and width (w) (e.g. Osterkamp and Hedman, 1982) to estimate the amount of water that carved the Martian valley networks (e.g. Irwin et al., 2005b). However, many of the Martian valley networks do not likely follow the empirical scaling relationships between width, slope, and area that are used for perennial channels on Earth (Som et al., 2009). With the improved topographic data now available for measuring volume, slope, and depth, Martian sediment transport can be better estimated with the less-empirical, more physically-based equations by van Rijn (1984a), Ribberink (1998), Meyer-Peter and Mueller (Wong and Parker, 2006), and others.
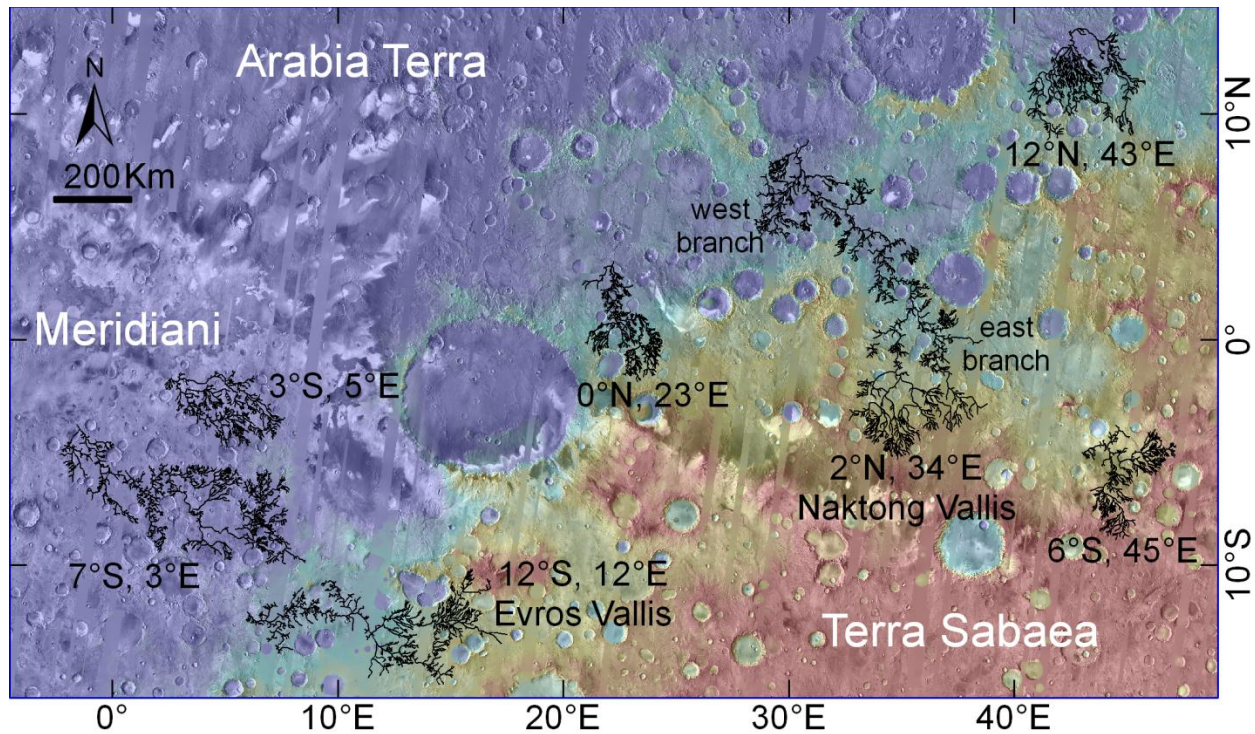
Figure 1. The seven valley networks analyzed in this study (black lines) are shown with coregistered THEMIS daytime IR and MOLA topographic data.

In this work, we investigate the formation timescales of the Martian valley networks through the use of three different sediment transport models, the D-W equation, and a variety of parameters to encompass a range of possible formation conditions. This is done specific to each of seven of the largest valley networks in the Terra Sabaea, Arabia Terra, and Meridiani regions of Mars (Figure 1, Table 1). With total valley lengths that range from about 5000 km to 15,000 km, these valley networks represent some of the largest and most mature valley network systems on Mars. All of the valley networks in this study have dendritic branching patterns with drainage densities comparable to terrestrial values (e.g. Carr and Chuang, 1997; Hoke and Hynek, 2009; Hynek and Phillips, 2003). First-order tributaries within these networks reach up to drainage divides and interior valley dimensions increase downstream, consistent with their formation by precipitation (e.g. Hoke and Hynek, 2009). Crater-density analyses using techniques specific for

Table 1. Valley Network Characteristics and Ages (Hoke and Hynek, 2009)

Valley Network	Stream Length (km)	Drainage Area (km^2)	Drainage Density (km^{-1})	Approximate Absolute Age (Ga)
12°S,12°E Evros	9050	149,700	0.060	3.63 ± 0.02
7°S, 3°E	11,710	148,300	0.079	3.65 ± 0.02
3°S, 5°E	5617	44,300	0.13	3.62 ± 0.03
0°N, 23°E	5389	43,400	0.12	3.68 ± 0.03
2°N,34°E Naktong	15,265	286,800	0.053	3.72 ± 0.01
west branch	2563	22,200	0.12	3.79 ± 0.02
east branch	12,702	220,300	0.058	3.70 ± 0.01
12°N, 43°E	6463	69,700	0.093	3.73 ± 0.02
6°S, 45°E	4851	48,800	0.10	3.70 ± 0.02

narrow, linear features with limited surface area placed the end of formation for these valley networks at approximately 3.62 to 3.73 Ga (Hoke and Hynek, 2009) or 3.69 to 3.76 Ga (Fassett and Head, 2008b), all during the Late Noachian and Early Hesperian. Within this range of ages are valley networks that have distinctly separate ages and those that appear to be coeval (Hoke and Hynek, 2009). In some cases, the valley network morphologies and crater age dating indicate multiple periods of formation, including one network (Naktong Vallis) that has two branches (east and west) of distinctly different morphology and age (Hoke and Hynek, 2009).

To better represent past Martian conditions, we minimize the use of terrestrial empirical relationships, when possible. As well, we complete an analysis of an analogous terrestrial river system with the same methods. Finally, the valley network-specific sediment transport rates and formation timescales are compared with prior age-dating of the valley networks through crater

density analysis (Hoke and Hynek, 2009) to understand the state of the climate at this time in Martian history.

3.2 <u>Methods</u>

To determine the formation timescales of the Martian valley networks using sediment transport models, three major variables are needed: the volume of sediment (V_s) removed during valley network formation; some measure of the distribution of grain sizes (D) that were presumably transported away during valley network formation; and the dimensions of the ancient river channels within the valleys that contained the flow. Many of these variables can be measured specific to the valley network and, when combined with a host of other minor variables (Table 2), provide valley network-specific paleo-discharges, sediment transport rates, and formation timescales.

Table 2. Values of constants in Mars sediment transport equations.

Acceleration due to gravity (g)	3.71 m/s^2
Bed porosity (λ)	0.3
Sediment density (ρ_s)	3400 kg/m^3
Water density (ρ_w)	1000 kg/m^3
Kinematic viscosity (ν)	1.6x10^{-6} Pa•s
Von Karman constant (κ)	0.4
Critical Shields parameter (θ_{cr})	0.03

3.2.1 Sediment Volume

Volumes within the valleys were measured using ArcGIS software and Mars Global Surveyor (MGS) Mars Global Laser Altimeter (MOLA) topographic data (~463 m/pix) (Smith et al., 2001) and, where available, Mars Express High Resolution Stereo Camera (HRSC) topographic data (~75 m/pix) (Jaumann et al., 2007; Neukum et al., 2004). Valley topography was extracted using a mask that was manually drawn along the outer walls of the visible valleys from co-registered topographic data and Mars Odyssey (MO) Thermal Emission Imaging System (THEMIS) daytime infrared (IR) images (256 m/pix) (Christensen et al., 2004), and accounting for the local slope of the surrounding surface. It is assumed that infill of material since the end of valley network formation is negligible compared to the total volume of the valleys. The infill that undoubtedly has occurred has the effect of reducing the measured sediment volumes (V_s) from what actually may have been removed. Therefore, these volume estimates are minimum values that in turn correspond to minimum formation timescales.

3.2.2 Grain Size

The distribution of rock sizes present during valley network formation is a very important variable in sediment transport calculations, but it also provides some of the greatest uncertainty in our results. For Mars, determining what grain size to use in calculating sediment transport is made especially difficult by the lack of direct measurements of the rock size distribution within the valleys during their formation due to their current inactive state and the accumulation of dust and sand (e.g. Carr and Malin, 2000) within the valleys over the last 3.6 to 3.8 Ga since the end of their formation (Hoke and Hynek, 2009). Using MGS Thermal Emission Spectrometer (TES) thermal inertia data (Putzig and Mellon, 2007) to determine grain size (e.g. Pelkey et al., 2001; Presley and Christensen, 1997) within these valleys produced median grain sizes of up to a few

hundred micrometers in diameter, typical of sand. However, Christensen (1986) showed that the fine particle component of a surface dominates the thermal inertia values and thus thermal inertia values are unreliable for predicting particle size distributions on Mars, particularly for ancient features.

Rock size distributions from lander measurements provide an alternative to thermal inertia-derived grain sizes. Viking landers 1 and 2, the Pathfinder lander, and the Mars Exploration Rovers (MER) found rock size distributions to consist mostly of gravel and cobbles, 10 mm to 1 m in diameter, and sand, 0.1 mm to 2 mm in diameter (Fenton et al., 2003; Golombek et al., 2003, 2005, 2006; Herkenoff et al., 2004; Squyres et al., 2004). Converting the compiled rock size data (Wilson et al., 2004) from the Viking 1 and 2 landers and Pathfinder missions (Golombek and Rapp, 1997; Golombek et al., 2003) to a size-frequency distribution by mass rather than by number and accounting for kinematic sieving, Kleinhans (2005) determined a median grain size (D_{50}) value of 0.1 m. Although none of the lander-data compiled and analyzed by Wilson et al. (2004) and Kleinhans (2005) are from locations in or near valley networks, it is assumed this rock distribution is typical of low latitude regions of Mars where these valley networks are found since all these surfaces have been similarly affected by impact gardening, aeolian processes, and other events that produced the rock size distribution we see today. Indeed, the MER rock size measurements (Golombek et al., 2005, 2006) produced similar distributions as other landers, though with fewer rocks and more sand at the Opportunity landing site in Meridiani Planum (Golombek et al., 2005; Squyres et al., 2004).

It should be noted that the 0.1 m median rock size determined by Kleinhans (2005) and used in this work has a large associated uncertainty since many processes may have modified the rocks since they were first emplaced (e.g. Carr, 1996; Fenton et al., 2003; Kleinhans, 2005). As

well, limitations of the lander measurements, such as camera resolution, kinematic sieving, and shielding of smaller grains by larger cobbles, may result in inaccurate measurements that favor larger grain sizes (e.g. Kleinhans, 2005). Further, any differences in rock sizes between the southern highlands where most of the valley networks formed and the northern lowlands where most of the Martian landers are located may make the median grain sizes assumed in this work less applicable. Since the sediment transport calculations depend strongly on grain size, as discussed in following sections, the order of magnitude uncertainty in the 0.1 m median grain size is an important consideration. However, this is the best estimate at present and further refined estimates of surface rock size distributions will lead to more accurate formation timescales.

3.2.3 Channel Dimensions

Measurements of the channel dimensions within the valleys nearest to the network outlet were preferred as they represent the space through which all upstream flow and sediment traveled. Channel slopes (s) were calculated with MOLA data along the lower 10% of the longest length profile of each valley network. This assumes the channel slope is the same as the valley slope, which is a reasonable assumption given the uncertainty in these calculations.

Channel widths (w) were measured using 6 m/pixel resolution Mars Reconnaissance Orbiter (MRO) Context Camera (CTX) data (Malin et al., 2007), taking the width as being the distance across the channel perpendicular to the presumed direction of flow. Figure 2 shows representative width measurements (in white) of the interior channel near the outlet of Naktong Vallis, along with corresponding cross-valley HRSC elevation profiles (in black). Channel width measurements for each valley network (Table 3) are averages of all channel measurements made near the outlet. Where no inner channels at the valley network outlet were visible, the average

78
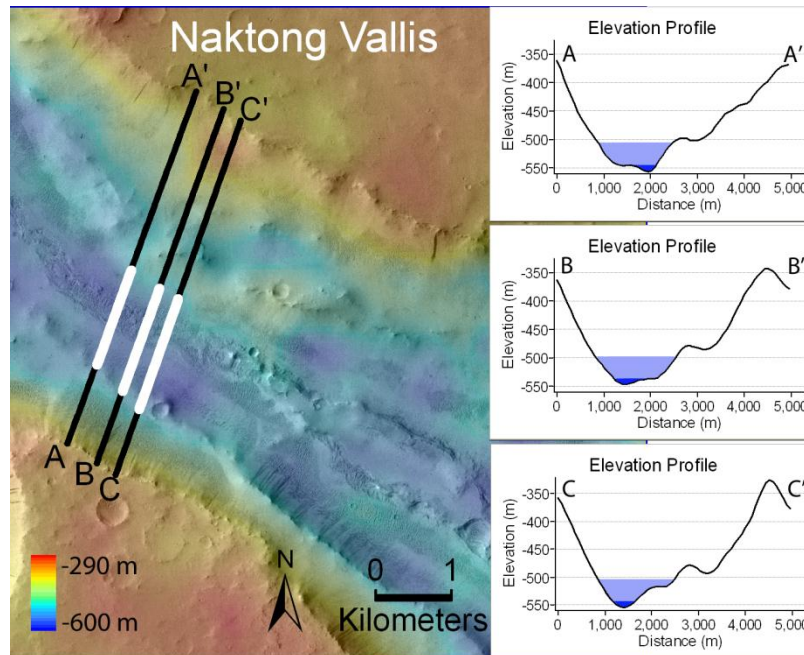
Figure 2. Representative channel width measurements (white lines) and corresponding cross-valley elevation profiles (black lines and graphs) within Naktong Vallis near the outlet of the east branch. Width measurements across A, B, and C are 1.33 km, 1.55 km, and 1.34 km, respectively. Final width values in calculations for each valley network were averages of all measurements made within the network outlet area. Hypothetical depths of 10 m (dark blue fill) and 50 m (light blue fill) are shown in each elevation profile on the right. Image is co-registered CTX (P04_002758_1880_XI_08N329W) and HRSC data, centered at 7.5ºN, 30.7°E.

widths of the channels in other valley networks were used since the overall valley widths were similar. The measured channel widths interior to the valleys in this work are large compared to interior channel width measurements in other studies (e.g. Irwin et al., 2005b; Jaumann et al., 2005). However, the valley networks in this work are among the largest on Mars, and all measurements were made near the outlet where widths are expected to be greatest. Whereas, for example, the channel width measurements of ~450 +/- 50 m made by Jaumann et al. (2005) were from a valley network having a total length of 400 km, much smaller than the valley networks in this study (Table 1). Likewise, Irwin et al. (2005b) took interior channel measurements of 90 m to 1000 m from small valleys that were not necessarily located near the outlet of the respective network.

Table 3. Input variables and results for formation timescales of the Martian valley networks

Valley Network	Volume V (m³)	Channel width, w (m)	Slope, s (m/m)	Flow depth,[a] h (m) calc. deep	Flow velocity, u (m/s) calc. deep	Flow discharge, Q_f (m³/s) calc. deep	Sediment discharge, Q_s (m³/s) calc. deep	Runoff rate, Q_f/A (cm/day) calc. deep	Intermittent formation timescales,[b] T_i (yr) calc. deep Rib.	MPM	van Rijn
12°S,12°E Evros;	9.6x10¹²	2330	0.0031	3 / 40	1 / 8	7x10³ / 7x10⁵	0.6 / 500	0.4 / 42	9x10⁶ / 1x10⁴	1x10⁷ / 3x10⁴	9x10⁷ / 2x10⁴
7°S, 3°E	7.2x10¹¹	1460	0.0009	10 / 25	1 / 3	2x10⁴ / 1x10⁵	0.3 / 10	4 / 6	1x10⁶ / 4x10⁴	2x10⁶ / 7x10⁴	1x10⁷ / 2x10⁵
3°S, 5°E	2.8x10¹¹	1950	0.0015	6 / 34	1 / 5	1x10⁴ / 3x10⁵	0.4 / 76	3 / 63	4x10⁵ / 2x10³	5x10⁵ / 4x10³	4x10⁶ / 5x10³
0°N, 23°E	1.5x10¹²	1820	0.0009	10 / 31	1 / 4	3x10⁴ / 2x10⁵	4 / 20	5 / 40	2x10⁶ / 4x10⁴	3x10⁶ / 8x10⁴	2x10⁷ / 1x10⁵
2°N,34°E Naktong west;	4.8x10¹¹	1400	0.0017	5 / 24	1 / 4	8x10³ / 1x10⁵	0.2 / 35	3 / 53	2x10⁶ / 8x10³	2x10⁶ / 2x10⁴	2x10⁷ / 2x10⁴
2°N,34°E Naktong east;	8.0x10¹²	1400	0.0012	7 / 24	1 / 3	1x10⁴ / 1x10⁵	0.1 / 16	0.5 / 4	3x10⁷ / 3x10⁵	4x10⁷ / 5x10⁵	4x10⁸ / 9x10⁵
12°N, 43°E	1.7x10¹²	1820	0.0022	4 / 31	1 / 5	8x10³ / 3x10⁵	0.3 / 130	0.9 / 38	3x10⁶ / 8x10³	4x10⁶ / 2x10⁴	4x10⁷ / 2x10⁴
6°S, 45°E	2.1x10¹²	1820	0.0011	8 / 31	1 / 4	2x10⁴ / 2x10⁵	0.3 / 31	3 / 39	4x10⁶ / 4x10⁴	5x10⁶ / 7x10⁴	4x10⁷ / 1x10⁵
Batha River, Africa	6.5x10¹²	1480	0.0004	7	4	4x10⁴	4	6	1x10⁶	4x10⁶	1x10⁶

[a] Calculated flow depths were determined using Equation (4). Deep flow depths were determined from the widths of channels interior to the valleys and a width-to-depth ratio of 58.
[b] Intermittent formation timescale results for each of the three models: Rib (Ribberink, 1998), MPM (Wong and Parker, 2006), and van Rijn (1984a). The Martian results assume valley-incising storms were occurring 5% of the time, as is typical for Earth (Wolman and Miller, 1960). However, the Batha River experiences bankfull discharge for approximately four days out of the year (Schick, 1988), so the Batha results reflect an intermittency of 1%. Continuous formation timescales can be determined by dividing the Martian intermittent formation timescale by 20 or the Batha River intermittent formation timescales by 100.

The depth of the flow (h) is a particularly important variable in sediment transport. Since the valley-incising flow depths of ancient rivers cannot be directly measured, they must be inferred from analysis of the interior channel morphology. The presence of terraces in MOLA and HRSC topographic data can provide a measure of bankfull depth, but this is made more difficult given the scarcity of identifiable channels where high-resolution topographic data (such as HRSC) exists and the obvious infilling by sand and dust as seen in high resolution images (such as CTX). Previously, researchers such as Goldspiel and Squyres (1991) used depths of 1 m, 5 m, 10 m, and 50 m in Martian discharge calculations. Others have measured depths of 25-55 m in Martian channels interior to other smaller valleys (Hauber et al., 2008; Jaumann et al., 2005). Measurements with HRSC data over Naktong Vallis based on identifying terraces within the ancient river channel provided depths of 31 +/- 12 m. Due to the uncertainty in depth estimates, we maintain a range of depths between 1 m and 50 m in all calculations.

In an effort to more tightly constrain probable flow depths specific to each valley network, we also calculated flow depth using two methods. A width-to-depth ratio of 58 based on terrestrial river dimensions for gravel river beds (Finnegan et al., 2005) and averaged parameters from satellite data (Bjerklie et al., 2003) resulted in Martian flow depths between 24-40 m, depending on the valley network. The applicability of this empirical relationship to ancient Martian rivers, however, is highly uncertain, and so it is used here simply as a guide for identifying possible flow depths.

Alternatively, flow depth was also estimated by setting the mean shear stress of the flow (τ) equal to 120% of the critical shear stress (τ_{cr}) required for sediment transport. This can be assumed for rivers with equilibrium banks and mobile gravel beds (e.g. Paola and Mohrig, 1996;

Parker, 1978), which are likely applicable to the unconsolidated regolith of Mars. The shear

stress is a function of flow density (ρ), gravity (g), flow depth (h), and bed slope (s):

$$\tau = \rho ghs \tag{1}$$

Non-dimensionalizing this relationship sets the Shields parameter (θ) equal to 1.2 times the

critical Shields number (θ_{cr}), in which the Shields parameter (θ) is defined as:

$$\theta = \frac{\tau}{(\rho_s - \rho)gD_{50}} \tag{2}$$

where ρ_s is sediment density. Using a critical Shields (θ_{cr}) value of 0.03, which is applicable for

gravel bed rivers (e.g. Kleinhans and Van den Berg, 2011), and the relative submerged density

(R)

$$R = \frac{\rho_s - \rho}{\rho} \tag{3}$$

with a sediment density (ρ_s) value of 3400 kg/m³ for Martian basaltic rock and a flow density (ρ)

value of 1000 kg/m³, the following depth equation is derived

$$h = 1.2 \frac{0.03 D_{50} R}{s} \tag{4}$$

Flow depths of 3-10 m resulted from Equation (4). The range in probable flow depths that

resulted from both methods agrees well with the few measured values of interior channel depths

described above (Hauber et al., 2008; Jaumann et al., 2005).

3.2.4   Flow Velocity and Sediment Transport Models

The Darcy-Weisbach (D-W) equation for depth- and width-averaged flow velocity (u)

maintains a dependence on the acceleration due to gravity (g) and uses a friction factor (f) to

describe the effect of bed roughness on the flow. The D-W equation (Silberman et al., 1963),

used herein to calculate average flow velocity (u), is given by:

$$u = \sqrt{\frac{8ghs}{f}} \tag{5}$$

Since the Martian interior channels are much wider than they are deep, as is typical of terrestrial rivers, the flow depth (h) is used in Equation (5) as a simplification of the hydraulic radius, hw/(w+2h).

The friction factor (f) is often expressed as a function of the relative roughness of the bed (h/D) and incorporates the effect of turbulence, bed forms, and sediment-flow interactions on flow velocity. There is a wide range of D-W friction factors that have been developed for terrestrial flows and applied to Martian conditions (e.g. Kleinhans, 2005; Komar, 1979; Wilson et al., 2004), and their predicted roughness varies considerably (Kleinhans, 2005). However, for the relative roughness typical of these Martian flows ($\sim10^2$), the various friction factors (as described in Wilson et al., 2004 and Kleinhans, 2005) produce very similar results with differences well below the level of uncertainty in the calculations. For this work, we use the White-Colebrook function (Silberman et al., 1963).

$$\sqrt{\frac{8}{f}} = 5.74 \log_{10}\left(\frac{h}{k_s}\right) + 1.0864 \tag{6}$$

Here, the Nikuradse roughness length (k_s) is taken as being equal to D_{90}, or 0.6 m (Kleinhans, 2005).

The equations that describe sediment transport only deal with the transport of material where grains of sand and rock are sitting on the river bed ready to be moved downstream (transport-limited); they do not reflect the time and energy needed to break up the surface into transportable pieces (erosion-limited). Since these valley networks formed on a substrate that had recently experienced heavy bombardment by impactors, the surface is expected to have had a kilometer or more of unconsolidated, poorly sorted regolith (e.g. Baker and Partridge, 1986; Hartmann and Neukum, 2001), suggesting they formed in transport-limited conditions. Further, when bedrock was exposed, the material transported through bedload processes (i.e. saltating)

would act to break up the surface into additional transportable pieces, depending on sediment supply and transport capacity (Sklar and Dietrich, 2004). To account for variations between sediment transport models, which often produce results that are orders of magnitude apart (e.g. Gomez and Church, 1989; Kleinhans, 2005), we compare the results from three models to provide likely timescales of formation. These include models by van Rijn (1984a), Ribberink (1998), and Meyer-Peter and Mueller (Wong and Parker, 2006), which were chosen for their applicability to larger grain bed rivers, their independence on the choice of roughness length (k_s), and their physics-based formulation that minimizes empirical approximations. The sediment transport rates for bed load (q_b) and suspended load (q_s) are often given in non-dimensional form by

$$\phi_{b,s} = \frac{q_{b,s}}{(Rg)^{1/2} D_{50}^{3/2}}$$

(7)

To determine the rate of sediment transport through bedload processes, van Rijn (1984a) solved equations of motion for individual particles within a flow and used experiments of gravel-sized particles to calibrate the model. The van Rijn (1984a) equation for bed load (ϕ_b) transport is a function of the Shields parameter (θ) and non-dimensionalized grain size (D^*):

$$\phi_b = 0.053 \left(\frac{\theta - \theta_{cr}}{\theta_{cr}} \right)^{2.1} D_*^{-0.3}$$

(8)

for which the median grain size is non-dimensionalized with the relative submerged density (R), gravity (g), and kinematic viscosity (ν):

$$D_* = D_{50} \left(\frac{Rg}{\nu^2} \right)^{1/3}$$

(9)

Using the bed shear stress in equation (1) to determine the Shields parameter rather than a grain-related shear stress can be done if the river bed had no dunes or other bed forms present. Equation (1) is preferred over calculating a grain-related shear stress as the latter requires additional use of empirical approximations. The assumption of a plane bed can be supported by conditions at or near those for incipient motion, which is particularly true for the shallower flow depths in each model. All of our model scenarios, however, have Froude numbers less than that for plane bed conditions, placing them in the subcritical flow regime, similar to many terrestrial rivers. Use of the shear stress in equation (1) may therefore overestimate the rate of sediment transport, leading to minimum formation timescale results.

The Ribberink (1998) equation for bed load sediment transport was calibrated using a large amount of terrestrial data from a variety of flow regimes, flow velocities, and grain diameters, making it a good choice for modeling sediment transport on Mars (Kleinhans, 2005). The Ribberink (1998) equation is given as:

$$\phi_b = 11(\theta - \theta_{cr})^{1.65} \tag{10}$$

The Meyer-Peter and Mueller (1948) equation for bedload transport, which is commonly used in terrestrial applications, was re-analyzed by Wong and Parker (2006). They found that by removing an unnecessary bed roughness correction and improving the treatment of boundary shear stress due to side wall effects, the revised Meyer-Peter and Mueller equation better represents bedload transport (Wong and Parker, 2006). This equation is given as

$$\phi_b = 3.97(\theta - \theta_{cr})^{1.5} \tag{11}$$

The equations for sediment transport are strongly dependent on flow depth and grain size, both of which have large uncertainties with application to ancient Martian flows. With median grain sizes of 0.1 m and flow depths of 1-50 m, sediment transport within these Martian valley

networks occurred primarily through bedload processes rather than suspended by turbulence within the flow. This is similar to sediment transport modeling of Martian delta formation (e.g. Kleinhans et al., 2010). Even for the deepest flows (50 m), which correspond to the fastest flow velocities, we calculate that bed load transport contributes at least one order of magnitude more to the total flux of sediment than suspended load transport. This is confirmed with the high Rouse numbers (greater than 3.2 in all cases) that indicate the settling velocities are many times greater than the shear velocities for all flow depths within each valley network, and therefore that the 0.1 m grains would not have been suspended by these flows. Therefore, suspended load calculations (e.g. van Rijn, 1984b) have not been included in the formation timescales described below.

3.2.5   Valley Network Formation Timescales

Calculating the sediment discharge (Q_s) as a function of the bed load transport rate (q_b) across the width (w) of the channel can be done by:

$$Q_s = q_b w \tag{12}$$

whereas flow discharge (Q_f) is calculated by:

$$Q_f = hwu \tag{13}$$

To estimate the duration of time (T) for a valley network to form, the total volume of sediment (V_s) is compared with the rate of sediment transport across the channel (Equation 13) through the equation (Kleinhans, 2005):

$$T = \frac{V_s}{(1-\lambda)Q_s} \tag{14}$$

A value of 0.3 (Kleinhans, 2005) is used for the average porosity (λ) of the transported material. This method assumes no additional sediment sources or sinks than what is represented by the current measurable volume within the valleys. If additional sediment was added to the system
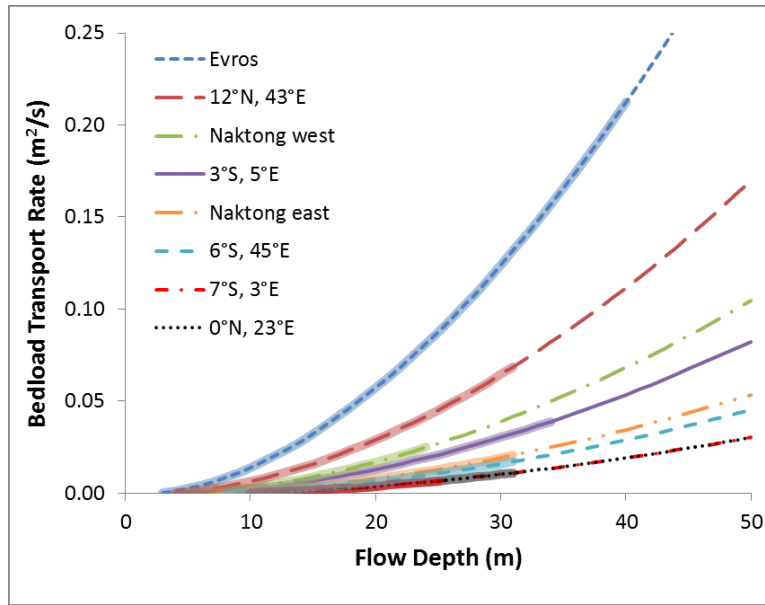
Figure 3. Bed load sediment transport rates (q_b) for each valley network show a range in values that are a reflection of differences in slope between these valley networks and that are strongly dependent on flow depth. The average values of the three transport models (Section 2.4) are used here. Highlighted ranges in each curve correspond to probable flow depths, as discussed in Section 2.3.

through aeolian transport or upslope supply (and not visible as an incised valley either due to a resistant surface layer or subsequent infilling), the formation timescales would be longer. Additionally, if these systems were at times erosion-limited, or if their beds experienced armoring as smaller grains were carried downstream leaving a resistive layer of larger grains behind, the transportability of the sediment would be decreased and the formation timescales would be increased. Therefore, these results reflect the minimum amount of flow needed to form the valley networks and, accordingly, the minimum formation timescales.

3.3 Results and Discussion

The valley network specific depth- and width-averaged flow velocities vary between 1-8 m/s, depending on flow depth and valley network (Table 3). These velocities are comparable to flow velocities in many terrestrial rivers, including many natural rivers with average velocities

between 0.5 and 1.5 m/s (Kleinhans and Van den Berg, 2011), and faster rivers that, depending on the depth of flow, which is often controlled by dam releases, can vary between a few m/s to ten or more m/s (e.g. Graf, 1995; Konieczki et al., 1997). The sediment transport rates on Mars (Figure 3) increase with flow velocity and result in formation timescales for the eight valley networks in this study that range from about 10^3 years to 10^8 years, depending on the valley network and the combination of parameters used (Figure 4, Table 3).

Exploring the parameter space in these models helps to illustrate the effect many of the variables have on our results, as is shown in Figure 5 with formation timescale results for Evros Vallis averaged from the three sediment transport models. Grain size (Figure 5a), which provides some of the greatest uncertainty in these calculations (Kleinhans, 2005), has a significant effect in the resulting formation timescales. If the median grain sizes were smaller than the 0.1 m rocks used in this work that are based on analyses of lander rock size measurements (Kleinhans, 2005), formation timescales would be shorter. Additionally, bedload transport would occur at smaller flow depths and suspended load transport would contribute to an increased transport rate until the system was no longer transport-limited, further decreasing formation timescales. Slope (Figure 3 and 5b) also has a strong influence on formation timescales, with the steeper slopes facilitating the transport of material downstream and carving out the valleys in shorter time. Changes in flow width (Figure 5c) have a linear effect on formation timescales (combining equations 12 and 14). Varying width by one or two standard deviations affects the formation timescales by the same factor, which is relatively small compared to the larger uncertainty in grain size and flow depth. Nonetheless, its use in estimating flow depths and runoff rates for these networks makes it an important variable. Bed porosity (Figure 5d) has only a minor effect on formation timescales. Increasing the flow density
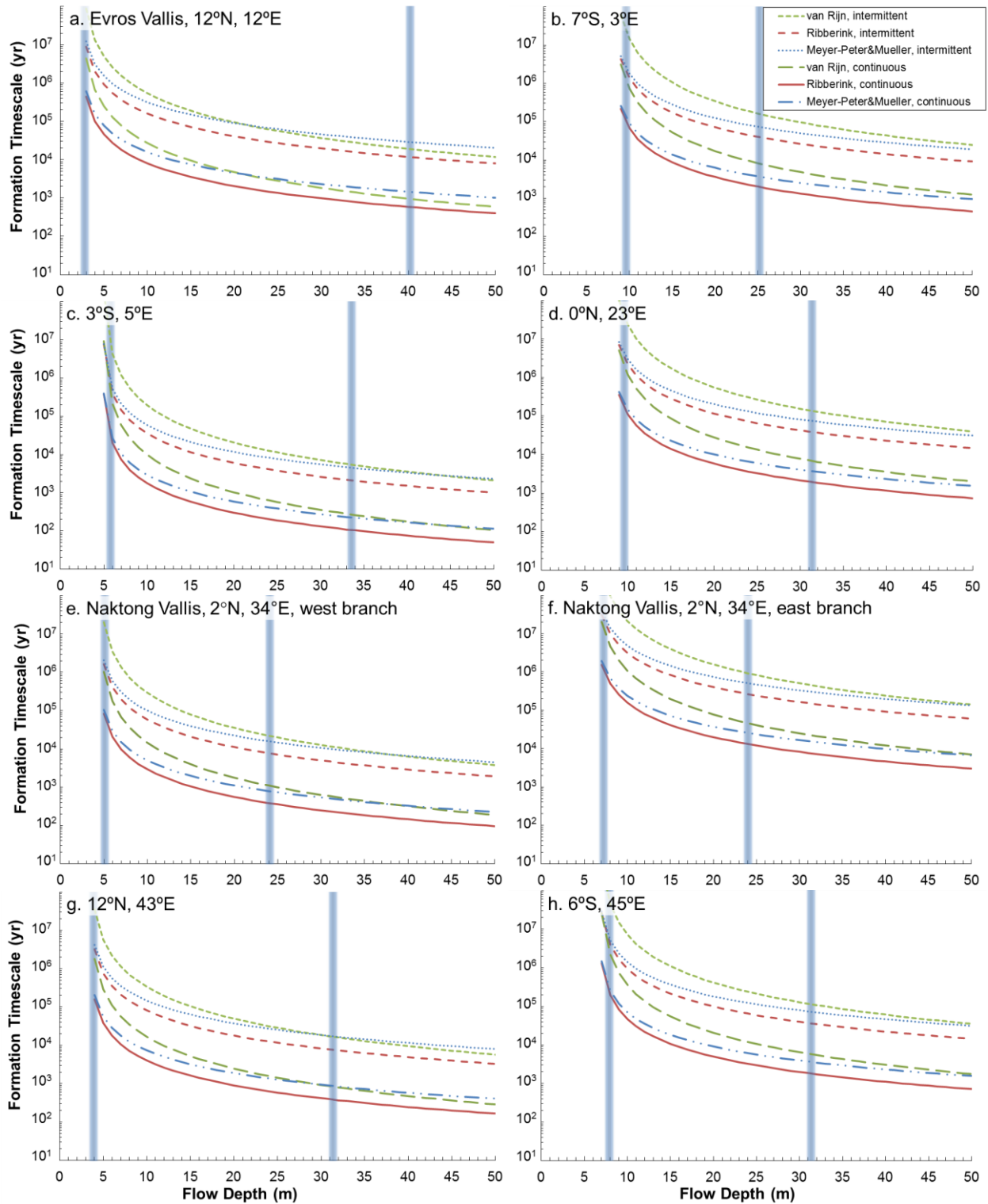
Figure 4. Formation timescale results for each valley network are given, including both continuous and intermittent results for the van Rijn (1984a), Ribberink (1998), and Meyer-Peter and Mueller (Wong and Parker, 2006) models. Shaded vertical lines correspond to estimated flow depths (Section 2.3, Table 3) that highlight probable formation conditions.

89

(Figure 5e) to account for salinity had a negligible impact on bed load sediment transport and formation timescales, though sediment density differences between granite (2700 kg/m^3) and Martian basalt (3400 kg/m^3) has as much of an effect on formation timescales as does differences in surface gravity (Figure 5f). Perhaps more importantly in the low flow depth scenarios where conditions are near that for the beginning of motion, the combination of grain density (Figure 5e), grain size (Figure 5a), bed slope (Figure 5b), and critical shields parameter (Figure 5g) all affect the minimum depth at which sediment is transported. Although differences in the acceleration due to gravity between Earth, Mars, or even Titan (Figure 5f) have an important effect on sediment transport, it is not by itself the most significant variable that changes when applying terrestrial sediment transport equations to flow on other planets.

These methods were also applied to terrestrial river valleys in arid environments to test the validity of the results and our underlying assumption that the Martian valley network formation timescale can be determined by the amount of time it took to transport the sediment out of the drainage basin (i.e. transport-limited). Since terrestrial rivers differ greatly from the ancient Martian valley networks (Carr and Chuang, 1997) due to the influences of vegetation and civilization on water supply, channel incision, and sediment transport, as well as their current active state, and presumably different climatic and tectonic conditions than what Martian valley networks experienced, we applied these same techniques to ephemeral terrestrial rivers so as to minimize these differences. Using Shuttle Radar Topography Mission topographic data (Farr et al., 2007) and Landsat GLS 2005 images (USGS and NASA, 2009) we calculated formation timescales for the African Batha River in the Sahara Desert, Chad. The Chad basin likely experienced alternating periods of aridity and heavy rainfall in response to changing global ice coverage since its formation when the surrounding region experienced uplift approximately 25

90
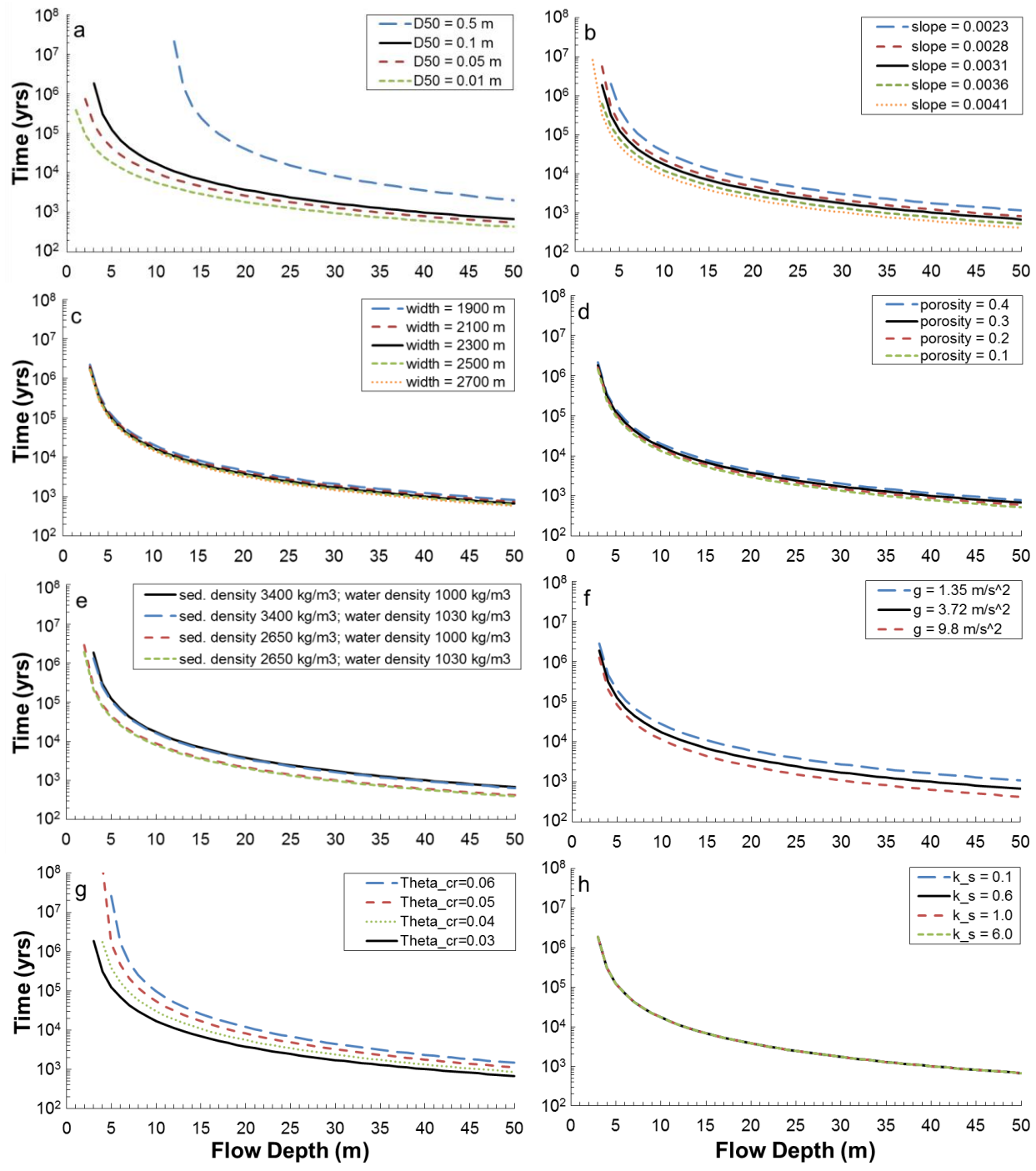
million years ago (Burke, 1976). Assuming median grain sizes of 1 mm (sand) with a density of

2650 kg/m^3; using measured volume (7x10^{12} m^3), slope (0.0004), width (1480 m), and terrace

height (7 m) values; treating the porosity (0.3) the same as for the Martian valley network cases;

and assuming intermittent formation with flows occurring 4 days out of the year (Schick, 1988),

formation timescales for the Batha River were calculated to be 5x10^6 to 2x10^7 years. With the

smaller grain sizes used in these calculations and suspended load transport rates comparable to

bedload transport rates, formation timescales that incorporate both bed load and suspended load

transport are reduced to approximately 4x10^6 years. Given the complexity in terrestrial climate

and tectonic histories and the simplifications we have assumed in this analysis so as to make

them applicable to Martian conditions, calculating a formation timescale for the Batha River that

is within an order of magnitude of the age of that basin (Burke, 1976) gives confidence to the

application of these methods to Martian valley networks.

Table 3 provides estimated runoff rates (Q_f/A) at the network outlet for shallow and deep

flow depths for all the Martian valley networks in this study. Any contribution from

---

Figure 5 (previous page). The effect of key variables on the formation timescale results are shown here. All plots use the average formation timescale results of the three models (Section 2.4) for continuous formation within Evros Vallis. The measured and/or preferred combination of variables (Tables 2 and 3) is indicated by the solid black line. a) Though median grain size (D_{50}) has an uncertainty of one order of magnitude, it is varied here from 0.01 m to 0.5 m due to the interpretation that this is more likely an over estimate than an underestimate of the median grain size at the time of valley formation. b) Slope and c) width values are incremented by +/- one and two standard deviations of their average measured values. d) Bed porosity (λ) varies between 0.1 and 0.4 in equation (14). e) Sediment density (ρ_s) is varied between that for sandstone (2650 kg/m^3) and Martian basalt (3400 kg/m^3), and water density (ρ) is varied from pure water (1000 kg/m^3) to increased salinity (1030 kg/m^3). f) Equatorial surface gravity values include those for Earth, Mars, and Titan. g) The critical Shields parameter (θ_{cr}), which determines the minimum shear stress required for sediment transport, usually varies between 0.03 and 0.06. h) The sediment transport models are all independent on choice of Nikuradse roughness length (k_s).

groundwater sapping or other sources is assumed to be minimal as these valley networks are all

interpreted to have formed primarily by precipitation (e.g. Craddock and Howard, 2002; Hoke

and Hynek, 2009; Howard et al., 2005; Hynek and Phillips, 2003), and therefore these runoff

rates can be used to approximate precipitation rates over the valley networks. The smaller runoff

rates of 0.4-6 cm/day are similar to intense rainfall events that quickly produce flooding in desert

regions on Earth (e.g. Coppus and Imeson, 2002; Schick, 1988) and correspond primarily to the

shallower flow depth scenarios for each valley network. Two exceptions are the relatively low

runoff rates of 6 cm/day and 4 cm/day that occur with the deeper flow depths of 7°S, 3ºE (25 m)

and the east branch of Naktong Vallis (24 m), respectively. The higher runoff rates of 38-63

cm/day, which approach hurricane conditions on Earth, all occur with deeper flows. If the valley

networks formed in arid environments (e.g. Barnhart et al., 2009; Irwin et al., 2011; Stepinski

and Stepinski, 2005) in which there were higher infiltration rates and significant evaporation

reducing the amount of runoff reaching the mouth of the valley network, the corresponding

precipitation rates would have needed to be even greater to produce the calculated runoff rates at

the network outlet. Due to the rareness of crater breaches (Barnhart et al., 2009) and the

morphology of the valleys and their surrounding terrain that identify precipitation and surface

runoff as the primary formation mechanism, it is not expected that the Late Noachian and Early

Hesperian were characterized by the extreme runoff rates many of our deeper flow depths

require. Therefore, these results suggest many of the shallower flow depths may be more

realistic than the deeper scenarios, and the corresponding longer formation timescales of 10^5 to

10^8 years (Table 3 and Figure 4) better represent the period(s) of climate conditions conducive to

precipitation during the Late Noachian and Early Hesperian.

This interpretation agrees with the results of landform evolution modeling by Howard (2007) and Barnhart et al. (2009), who found that runoff and evaporation rates in the Late Noachian and Early Hesperian resembled those in arid to semi-arid regions on Earth, characterized by numerous and repeated moderate floods separated by periods of evaporation. Barnhart et al. (2009), who modeled the formation of Parana Vallis, a valley network system that is similar in size and age to the valley networks analyzed in this work (Hoke and Hynek, 2009), found that repeated episodic flows with interim evaporation corresponded to formation timescales of 10^5-10^6 years for that valley network.

The formation timescales we have determined for these large valley networks are significantly longer than formation timescales that have been calculated for Martian deltas, which often range from days to hundreds of years depending on the delta and methods used (e.g. Hauber et al., 2008; Kleinhans et al., 2010; Kraal et al., 2008). This difference in formation timescale is not surprising due to the steep channel slopes, smaller delta volumes, and at times extremely large flow depths (up to 100 m) that produce delta formation on such short timescales (e.g. Hauber et al., 2008; Kleinhans et al., 2010; Kraal et al., 2008).

The hypothesis that the Martian valley networks formed during periods of climate change caused primarily by impact events early in Martian history (e.g. Segura et al., 2008) is not supported by the results of this nor other work (e.g. Fassett and Head, 2008b, 2011; Hynek et al., 2010). Contrary to the arguments in Toon et al. (2010) that the timing of the impact events (Werner, 2008) coincided with the timing of valley network formation (Fassett and Head, 2008b), hundreds of millions of years span the formation of most of the large impacts (3.9-4.1 Ga) and the formation of most of the large (by total valley length) valley networks (none older than 3.8 Ga), with the possible exception of a few younger, smaller impact basins (e.g.

94

Antoniadi, and Lowell) and some older, smaller valley networks. The greatest degree of valley incision, which presumably coincides with the greatest degree of precipitation and surface runoff (e.g. Irwin et al., 2011), occurred at least 100 to 200 million years after the impact-related climate change described by Segura et al. (2008). Since each impact event produced only a few centuries, at best, of active hydrological cycles and precipitation, the timing of valley incision and impact-related climate change cannot be considered contemporaneous.

Further, all of the valley networks in this study require several orders of magnitude longer durations of clement conditions to form than can be provided by the impact events, even considering unrealistic scenarios of continuously high runoff rates. So although a few impact basins may have formed during the time of large valley network formation, the few tens to hundreds of years of precipitation related to those events, whether continuous or intermittent, is insufficient to form these large valley networks.

Comparing the formation timescales of each valley network with their corresponding crater ages suggest the precipitation that produced flows of sufficient magnitude to allow bed load transport and incision of the large valley networks was 1) limited to the Late Noachian and Early Hesperian, as many others have suggested (e.g. Howard et al., 2005; Hynek and Phillips, 2001; Irwin et al, 2005a, 2011), 2) did not happen simultaneously across the planet, and 3) lasted intermittently for periods of 10^5 to 10^6 years. For example, the east and west branches of Naktong Vallis exhibit different preservation states and distinctly different crater populations, suggesting the east branch is overall younger than the west branch (Hoke and Hynek, 2009). Comparing their formation timescales shows that the west branch (and likely part of the east branch) formed about 3.79 Ga with possible runoff rates of >3cm/day lasting intermittently for 10^5-10^7 years (Figure 6). Then, 60-90 million years later when intense precipitation returned to

this region, it was focused to the south and east over the more densely dendritic part of the east branch and its neighbor at 6°S, 45°E (Figure 1). These valley networks share similar crater ages as their neighbors at 12°N, 45°E and 0°N, 23°E, placing their formation together at approximately 3.70-3.73 Ga (Hoke and Hynek, 2009). Assuming the duration of formation was about the same order of magnitude for these neighboring valley networks, precipitation likely occurred intermittently for 10^6-10^7 years, with runoff rates of 1-3 cm/day across Naktong Vallis, 1-2 cm/day at 12°N, 43°E, >4 cm/day at 6°S, 45°E, and >5 cm/day at 0°N, 23°E (Figure 6). Likewise, the three proximal valley networks located to the southeast of Meridiani Planum (Figure 1) all have crater ages that place their formation coevally around 3.63 to 3.65 Ga (Hoke and Hynek, 2009), approximately 60-80 million years after Naktong Vallis and its neighbors finished forming. Assuming these valley networks near Meridiani Planum experienced approximately the same duration of precipitation as each other, it is likely these valley networks formed with intermittent runoff rates of 1-9 cm/day, lasting 10^5-10^7 years (Figure 6).
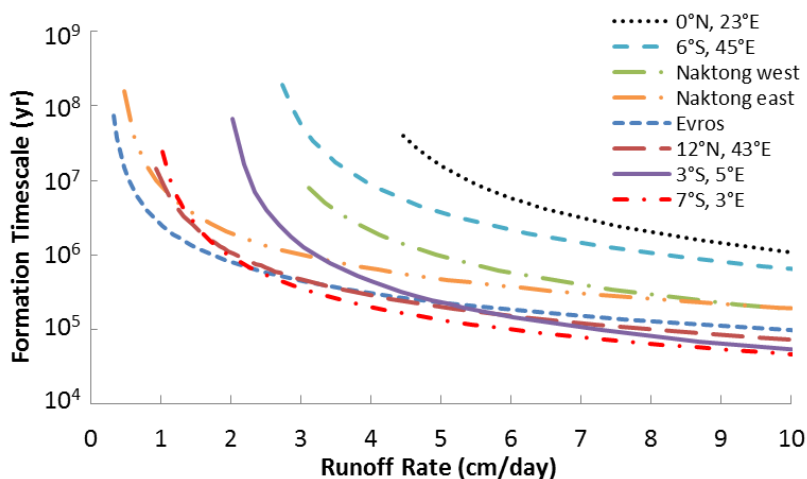
Figure 6. Comparing the runoff rates (cm/day) with the corresponding formation timescale (years) for each valley network helps constrain possible formation scenarios.

96

However, given the large uncertainty of these results and the choice of parameters that led to these timescales being minimum values, these results do not exclude the possibility that there may have been some overlap in formation episodes. Either way, regions not actively incising may have been extremely arid, or, more likely, may have experienced minor precipitation in amounts too low to support sediment transport and valley incision, as has been suggested for much of Martian history prior to the Noachian-Hesperian boundary and incision of most of the valley networks (Irwin et al., 2011). If this were the case, as Mars was becoming more arid toward the end of this final epoch of intense fluvial erosion in the Late Noachian, valley formation was also likely changing. On Earth, climate change toward increasing aridity can potentially increase erosion rates despite a decrease in the frequency of precipitation events and overall river discharge (e.g. Molnar, 2001; Tucker et al., 2006). We expect that valley networks that formed toward the end of this period of fluvial erosion may have been characterized by less frequent, more intense storms. This is supported by the relatively shorter formation timescales (factor of 10 less) for the valley networks that formed later (Meridiani group) than those that formed earlier (Naktong group).

3.4 Conclusions

Comparing the formation timescales of the valley networks analyzed in this work to their crater density-derived ages (Hoke and Hynek, 2009) reveals an early Martian climate characterized by many periods of increased precipitation and valley incision, each lasting 10^5-10^7 years, over the 10^8 years of valley formation. Though, considering the large uncertainty in these calculations and the combination of parameters that produced minimum timescales, it is possible the formation timescales approach durations similar to their span in ages. Valley networks often share similar ages and formation timescales as their neighboring networks, consistent with

regional weather patterns delivering precipitation of sufficient magnitude to form the valleys while other non-incising regions receive minor precipitation, if any. Regardless, the amount of time required to form these large valley networks does not extend valley formation to earlier than the Late Noachian and is consistent with hypotheses that valley incision was constrained to a relatively short period of Martian history near the Noachian-Hesperian boundary (e.g. Howard et al., 2005; Hynek and Phillips, 2001; Irwin et al, 2005a, 2011).

4 Modeling Martian delta formation with Sedflux 2.0: Effects of sediment supply and concentrations

ABSTRACT: We use a comprehensive morphodynamical model to explore the effects of changing hydrologic and sedimentary conditions on delta formation under Martian conditions. Sedflux 2.0 is a 2-D and 3-D basin-filling model that uses event-based time stepping (e.g. seasons) to determine the spatial and temporal deposition of sediment into a standing body of water. Sedflux creates a framework for individual processes to work, such as hypopycnal and hyperpycnal sediment plumes, river avulsion, sea level changes, subaqueous sediment diffusion, and seasonal changes in river discharge and sediment load. River and sediment discharge were calculated using the Darcy-Weisbach equation for width- and depth-averaged flow velocity and well known and tested terrestrial sediment transport predictors modified for application to Martian flows. A range in sediment grain sizes were determined from both landers and orbiting spacecraft data in order to include grain sizes typical of Mars and yet representative of the Martian deltas. Several different scenarios of seasonal river change were explored to encompass a range of possible formation conditions.

With the ability to track sediment as it is transported throughout the basin, it is apparent that non-negligible amounts of material are moved beyond the delta-forming region. This loss of sediment increased with greater river discharge, increasing the gap between the calculated and modeled formation timescales. These results have important implications for the formation timescales of the deltas and the lack of identifiable deltas on Mars today. Formation timescales that consider only the supply of sediment to the system and don't take into account factors affecting deposition and delta formation are underestimates of the actual amount of time needed to form the deposits. The lack of identifiable deltas in many paleolakes is likely a result of significant sediment transport beyond the coastal delta-forming region causing the boundaries of the delta to become unrecognizable.

4.1 <u>Introduction</u>

Many researchers have described the evidence for precipitation and surface runoff on

Mars during the Late Noachian (~3.7 to 3.8 Gyr) and Early Hesperian (~3.7 to 3.6 Gyr) when

the densest distribution of valley networks were incised (e.g. Craddock and Howard, 2002;

Hoke and Hynek, 2009; Hynek and Phillips, 2001; Irwin et al., 2005a). Many paleolakes

associated with the valley networks also formed at this time (e.g. Fassett and Head, 2008a).

Despite hundreds of potential paleolakes (Cabrol and Grin, 1999; Fassett and Head, 2008a),

delta deposits are relatively rare. This may be in part due to resurfacing by impact gardening

and eolian processes that limit the preservation of these features (e.g. Di Achille and Hynek,

2010b; Fassett and Head, 2008a; Howard, 2007). It may also be that many deltas did not form as a result of various conditions, such as short flow events that finish before a lake filled the basin (Kleinhans et al., 2010) and fluctuating lake levels and/or offshore sedimentation (Howard, 2007).

Deltas that are found across Mars express numerous morphologies and have volumes that range from approximately 1 km^3 to over 100 km^3, presumably reflecting a range of formation conditions and preservation states. The observed morphologies cover the spectrum from single debris flow to long-lasting subaqueous formation. A few of the 46 Martian deltas analyzed by Di Achille and Hynek (2010b) exhibit layering, avulsion and/or multilobate deposition, partial entrenchment of the delta surface, and at least partially integrated watersheds. These deltas exhibit characteristics similar to terrestrial river deltas and are often cited as evidence for long-lived flowing water on the surface of early Mars (e.g. Fassett and Head, 2008a; Moore et al., 2003).   The meandering channels (now inverted), layering, and multi-lobed shape of Eberswalde Delta (e.g. Malin and Edgett, 2003; Moore et al., 2003; Pondrelli et al., 2010; Wood, 2006) and the Jezero deltas (e.g. Ehlmann et al., 2008; Fassett and Head, 2005) suggest deposition of clay, sand, and gravel in a lacustrine environment with temporal variations in the composition of grain size of the supplied sediment, lake levels, and flow discharge rates. Interestingly, layers of gravel and boulders up to a few meters in diameter are also seen within the layers of Eberswalde and Jezero deltas (Ehlmann et al., 2008; Howard et al., 2007; Pondrelli et al., 2008; Schieber, 2007), suggesting at least some of the Martian deltas contain grain sizes that range from clay to boulders. These observations point to varied formation conditions that at times supported the slow deposition of the smaller grains and at other times were capable of transporting larger rocks.

100

Figure 1. Examples of three Martian deltas are shown in 25 cm/pixel HiRISE images (McEwen et al., 2007). a) Eberswalde (PSP_001336_1560) and b) Jezero (PSP_002387_1985) deltas show layering, lobate shape, and meandering channels that suggest deposition of a range of grain sizes in a lacustrine environment during varying river and sediment conditions. c) The Tyras (PSP_008602_1885) fan-delta deposit exhibits a more uniform shape and two scarps that may reflect wave-cut terraces (Di Achille et al., 2006). North is up in all images.

A majority of the deltas, however, have more uniform shape with little or no signs of avulsion or multilobate deposits and are associated with watersheds of limited length and distribution (Di Achille and Hynek, 2010b). The Nanedi delta deposit has meter-scale layering and steep 50-m high, well rounded distal edges that may indicate depositional lobes in a lacustrine environment (Hauber et al., 2008). Kleinhans et al. (2010) concluded that the Nanedi delta that nearly filled its small crater formed from a dilute bedload-dominated flow as a result of a single event, as evidenced by well-preserved shorelines. Some of these deltas show one or more intermediate steps that may indicate changing lake levels (e.g. Di Achille, 2006; Ori et al., 2000) or they may be a result of a rapid, single formation event (e.g. Kleinhans et al., 2010; Kraal et al., 2008). The Tyras deposit also appears to be composed of primarily fine-grained material and has two scarps that may have been carved by wind-generated waves, suggesting this fan-delta experienced a complicated formative history characterized by changing paleolake levels (Di Achille et al., 2006). Others, however, interpret the stair-step

topography similar to that of Tyras and other deposits as having formed by high discharges of both bedload and suspended load sediment over short periods of time during single outflow events (e.g. Kraal et al., 2008; Kleinhans et al., 2010).

Several researchers have estimated the timing and duration of formation through various approaches. Ori et al. (2000) described evidence for several Gilbert-type deltas in craters on Mars. This type of sedimentary deposit forms when a river enters into a body of water, slows, and deposits its load in a semi-circular fan-shaped body with relatively flat upper surfaces and steep distal fronts (Gilbert, 1885). Ori et al. (2000) argued that the Gilbert-type deltas on Mars cannot be formed by one or a few very high energy cataclysmic flooding events. Rather, due to the complex nature of some of the Martian deltas and the interpretation that terraces were formed by wave action, the lakes must have been present for several thousands of years, at a minimum. Likewise, if the Eberswalde and Jezero deltas formed intermittently by seasonal or ephemeral flows, their formation may have taken thousands to hundreds of thousands of years (e.g. Fassett and Head, 2005; Moore et al., 2003). For example, Fassett and Head (2005) estimate flow discharges for the 5 km^3 Jezero deltas, assume an intermittency of 1% for arid conditions, and calculate formation timescales on the order of 1000 years (or 11 to 18 years if continuously formed). Alternatively, Jerolmack et al. (2004) calculated continuous formation timescales for Eberswalde Delta of 50 years and 340 years based on the transport of sand and gravel, respectively, and assuming a reconstructed volume for Eberswalde Delta of 30 km^3 (or 10-70 years for the current volume of 6 km^3). Hauber et al. (2008) used the Ribberink (1998) bed load sediment transport equation and Kleinhans' (2005) median grain size of 0.1 m to calculate minimum, continuous formation timescales for the 1.15 km^3 Nanedi delta, the 9.4 km^3 Sabrina delta, and the 150 km^3 Hypanis deposit of 2 years, 20

years, and 183 years, respectively.   Likewise, Kleinhans et al. (2010) use similar input parameters for a conical deposition model that produced formation timescales for the Nanedi, Sabrina, Nepenthes, Tyras, and a stair-stepped delta of nearly 2 years, 41.7 years, 129 days, 4.25 days, and 133 days, respectively. These rapid formation timescales assume continuous formation of rapid flood discharges (~6 to 184 km^3/day) during single flood events (Kleinhans et al., 2010).

Most of the previous efforts to determine possible formation timescales of the Martian deltas relied on bulk flow and transport calculations of a single grain size, and assumed that all of the sediment supplied to the system was deposited in, and remained on, the delta. While these sediment transport calculations quantify a river's ability to supply sediment to a basin, they do not reflect the deposition processes affecting the sediment. Rather, often it is assumed that, since the river diverges upon entering the basin, the flow must slow sufficiently to drop the suspended material into a deposit at the mouth of the river. These assumptions become less applicable as river velocities increase and move the sediment further into the basin. Relative densities between the river water and basin water will affect how the incoming flow moves. Grain-specific settling rates distribute grains to different distances based on their size and density. The avulsing direction of the river as it flows into the basin will also affect where sediment is deposited. Slope failure, turbidity currents, compaction, and consolidation all affect how the deposited sediment moves before it becomes "fixed". Further, as the delta deposit grows, it changes the bathymetry of the basin, affecting movement and deposition of incoming material. Thus, the growth of a delta depends on more than just the rate of supplied sediment. Conclusions on the conditions of a delta's formation history are more robust if they

are based on a more detailed modeling of the deposition process (e.g. Hutton and Syvitski, 2008).

Here we use a comprehensive physics-based morphodynamical model used widely in the terrestrial community to explore delta formation Martian conditions. Several parameters have been adapted to Martian conditions, including reduced gravity, higher sediment densities typical of Martian basalt, reduced particle settling rates due to the lower Martian gravity, and river discharge estimates calculated for generalized Martian delta systems. The focus of this work is to 1) test the capability of Sedflux 2.0 for application to modeling Martian deltas and 2) investigate the effects of grain sizes and supply rates on Martian delta formation and associated timescales. For the latter, several questions were addressed in this work. What size of grains are deposited in the delta and what grains are transported beyond the delta-forming region? What are the effects of variability in flow discharge and sediment concentration in delta characteristics and formation timescales? And are these resulting formation timescales similar to what other researchers have determined with the use of a single D_{50} grain size?

4.2   <u>Methods</u>

For this work, we modeled the formation of Martian deltas using Sedflux 2.0, a 2-D and 3-D basin-filling model managed by the Community Surface Dynamics Modeling System (CSDMS) at the Institute for Alpine and Arctic Research (INSTAAR) of the University of Colorado (Hutton and Syvitski, 2004, 2008; Syvitski and Hutton, 2001). We explore the formation of generic Martian deltas rather than attempt to recreate specific delta morphologies seen on Mars today. This allowed some liberty in assuming river and bathymetric characteristics that are typical of many Martian deltas but not constrained to parameters corresponding to specific Martian deltas that are difficult to measure given their current inactive state and over 3.5 billion

years of modification since their formation. The Di Achille et al companion paper to this work explores the parameters specific to the formation of many deltas on Mars.

4.2.1 Sedflux 2.0 Modeling

Sedflux 2.0 uses event-based time stepping (e.g. seasons) to determine the spatial and temporal deposition of sediment into a standing body of water by creating a framework within which individual process-response models operate. These processes are used to distribute bedload material near the river mouth, transport the suspended sediment from the river mouth through hypopycnal or hyperpycnal plumes, redistribute seafloor sediments, and compact the sediment into a final deposit (Syvitski and Hutton, 2001). Additionally, the sediment transport and deposition processes are affected by sea level changes, river avulsion, seasonal changes in river discharge and sediment load, and other processes (Hutton and Syvitski, 2004, 2008).

The 3D version of Sedflux 2.0 tracks and records sediment in two lateral dimensions over a user-specified thickness (i.e. vertical resolution) within which the sediment characteristics are averaged. For the Martian delta modeling scenarios in this work, a vertical resolution of 0.5 m was used. Horizontal resolution corresponds to the distance in meters of the grid spacing in a user-created bathymetry file in which each grid value is a measure of elevation below the river. Horizontal resolutions of 25 m were used in this work.

Sediment is supplied into the basin by both bedload and suspended load processes from a river of specified velocity, width, and depth corresponding to an initial flow discharge (Q_0). Multiple grain types, each having independent user-specified characteristics, are tracked as they enter the basin and form the deposit. Sedflux distributes bedload material evenly across a wedge of pre-defined radius and angle from the river mouth. The bed load discharge (Q_b), which was determined for a mean bedload grain size using the methods described in Chapter 3

(Hoke et al., 2011), was in all scenarios distributed across a distance of 50 m from the river mouth and spread across 180 degrees. Suspended load concentrations (C_s) for each of six grain types were specified such that the initial mean suspended load discharge (Q_{s0}) determined by Sedflux (Syvitski and Hutton, 2001) is

$$Q_{s_0} = Q_0 \sum_{i=1}^{n} C_{s_i} \tag{1}$$

Densities of the river, lake, bulk sediment, and saturated sediment specified in the input files affect the movement of suspended sediment through either surface (hypopycnal) or subsurface (hyperpycnal) plumes. If the incoming sediment-laden river water is denser than the receiving basin water, the suspended load will be transported as a gravity-accelerated hyperpycnal flow suspended by fluid turbulence. Sedflux allows sea water and seafloor sediments to become entrained into the hyperpycnal flow, increasing the flow volume. As the hyperpycnal flows slows down due to seafloor friction, friction of the overlying water mass, and internal friction within the flow, sediment is deposited (Syvitski and Hutton, 2001). The rate of deposition is dependent on a pre-defined grain type-specific removal rate constant (λ) and the flow velocity relative to a critical value determined by the settling velocity and a drag coefficient (Syvitski and Hutton, 2001). Alternatively, if the incoming sediment-laden river water is less dense than the water in the receiving basin, the suspended load is transported by a momentum-driven hypopycnal plume. Sedflux tracks the suspended sediment inventory (I) (kg/m^3) within the basin according to the longitudinal (x-direction) and lateral (y-direction) velocities of the river plume, turbulent diffusivity within the flow, and the removal rate constant (λ) (Hutton and Syvitski, 2008).

The removal rate constant is related to a settling velocity (V) that is a function of gravity (g), grain size (D), and fluid (ρ) and sediment (ρ_s) densities, through a shape factor (α_3) and the flow depth (h) (Bursik, 1995).

$$V = \alpha_3 h \lambda \tag{2}$$

The shape factor was assumed to be the same on Mars as on Earth, which is estimated to be 1.74 at 7.5 m flow depths (Syvitski et al., 1988). Martian removal rate constants were calculated for each grain size following Bursik (1995) and Syvitski et al. (1988), and are listed in Table 1. In all cases, the Martian settling rates are slower than corresponding terrestrial values, as would be expected with the lower gravity on Mars.

Table 1. Martian sediment grain characteristics for input into *Sedflux 2.0*

Grain diameter	Removal rate constant[a] (/day)	Consolidation coefficient (m^2/yr)	Compaction coefficient
0.1 m	40	10^5	8×10^{-9}
1 mm	40	10^5	8×10^{-9}
400 μm	40	10^5	8×10^{-9}
300 μm	39	10^5	3.68×10^{-8}
200 μm	19	10^5	3.68×10^{-8}
100 μm	6	10^4	5×10^{-8}
50 μm	6	10^3	6×10^{-8}

[a]The maximum removal rate allowed in Sedflux is 40 /day.

The direction of the river is allowed to change over time in order to distribute sediment laterally within the basin. Sedflux 2.0 incorporates the river avulsion by changing the angle of the river at every timestep by an increment determined by a probability distribution having a mean value of zero and a user-defined standard deviation. For this work, the river was allowed to shift direction over 180 degrees within the basin and was set to avulse rapidly so that sediment would be distributed in all directions. This was done so that changes in sediment

supply would be highlighted in the resulting delta and not be complicated by non-uniform deposits resulting from a slowly avulsing river.

Some of the deposited sediment is re-suspended and transported down-slope by a two-dimension diffusion process. The amount of re-suspended material is proportional to the bathymetric slope and a diffusion coefficient that is a function of time, grain size, and water depth (Hutton and Syvitski, 2008). The fraction of the re-suspended material that is transported through diffusion is determined by a user-specified index between 0 and 1 that is specific to each grain size. The remaining sediment is mixed and re-deposited. For this work, ¼ of the re-suspended material for all grain sizes was allowed to be re-distributed down-slope.

The Sedflux 2.0 2- and 3-D output files contain measurements of a large number of delta properties, including elevation, deposit thickness, slope, and grain size. The output file measurements were made at pre-specified time intervals throughout each model run, which allowed analysis of the sediment transport and delta growth over time.

4.2.2 Grain size

The size and amount of grains available for transport and deposition is significantly affected by the discharge rates of the hypothesized river, and together these parameters determine the sediment supply rates to the basin and the rate at which the delta forms. For Mars, the lack of direct measurements of the rock sizes carried by the hypothesized rivers during delta formation makes this parameter especially difficult to determine and results in some of the greatest uncertainty in delta modeling results (e.g. Kleinhans, 2005; Wilson et al., 2004).

Many recent delta and valley network formation studies have based their sediment transport calculations on grain sizes determined from Martian lander data (e.g. Hauber et al.,

2008; Hoke et al., 2011; Kleinhans et al., 2010). Studies of data from Viking landers 1 and 2, the Pathfinder lander, and the Mars Exploration Rovers (MER) found bimodal rock size distributions that included smaller sand- to gravel-sized grains (0.1 mm to 2 mm) and larger cobble- to boulder-sized rocks (10 mm to 1 m) (Fenton et al., 2003; Golombek et al., 2003, 2005, 2006; Herkenoff et al., 2004; Squyres et al., 2004). From this, a median grain size (D_{50}) of 0.1 m was calculated (Kleinhans, 2005). This grain size distribution has a large associated uncertainty since many processes may have modified the rocks since they were first emplaced (e.g. Carr, 1996; Fenton et al., 2003; Kleinhans, 2005). Further, the lander-derived grain sizes are limited by camera resolution, kinematic sieving, and shielding of smaller grains by larger cobbles, which may result in inaccurate measurements that favor larger grain sizes (e.g. Kleinhans, 2005).

Alternatively, thermal inertia measurements can be used to determine grain sizes of a surface (Kieffer et al., 1973). This was done using the 100 m/pixel THEMIS thermal inertia mosaic (Christensen et al., 2004) over Eberswalde delta that was derived from nighttime infrared data (Fergason et al., 2006). Thermal inertia (I) is a measure of a material's resistance to changes in temperature and is a function of the thermal conductivity (κ), bulk density (ρ), and specific heat capacity per unit mass (c) of the material.

$$I = \sqrt{\kappa \rho c} \tag{3}$$

The thermal conductivity (κ) can be related to grain diameter (d) (Kieffer et al., 1973) through the equation (Presley and Christensen, 1997):

$$\kappa = CP^{0.6}d^{-0.11\log(P/K)} \tag{4}$$

in which C and K are constants equal to 0.0015 and 8.1×10^4 torr for Mars, respectively. Eberswalde Delta has an elevation of -1.45 km relative to the datum, which corresponds to an

atmospheric pressure (P) of 5.26 torr. Thermal inertia data from Eberswalde Delta was

extracted with ArcGIS software by carefully outlining the delta and avoiding regions that

appeared to be partially buried or covered by potentially non-deltaic material (Figure 2). Using

8.79×10^5 J/m^{3}K for the product $\rho * c$ (Edgett and Christensen, 1991), the extracted thermal

inertia values of 82 to 235 Inertia Units (IU) were converted to thermal conductivity values of

0.0077 to 0.063 W/mK, respectively. Using equation 2, converting to probability by mass, and

adjusting for kinematic sieving (Kleinhans, 2005), a range of grain sizes between 4 μm to 399

μm were calculated (Figure 2). However, the probability of grain sizes less than 70 μm within

that distribution is less than 1%, indicating that the grain sizes that characterize Eberswalde

delta are primarily fine- to medium-sand with a median grain size (D_{50}) of 250 μm (Figure 2).

The thermal inertia-derived grain sizes agree well with previous analyses that indicate

primarily sand-sized grains make up Eberswalde delta (e.g. Jerolmack et al., 2004; Malin and

Edgett, 2003; Moore et al., 2003; Wood, 2006) as well as many other Martian deltas (e.g.

Ehlmann et al., 2008; Hauber et al., 2008), but it does not represent the coarser bed material

also observed (Howard et al., 2007; Pondrelli et al., 2008; Schieber, 2007). Grain sizes derived

from thermal inertia measurements are limited by the grain size and the degree of sorting and

compaction of the material being analyzed, dusty coatings on the surface, atmospheric

conditions at the time of measurement, the resolution of the infrared data, as well as

uncertainties in the conversion of infrared data to thermal inertia to grain size (e.g. Jakosky,

1986; Presley and Christensen, 1997). Therefore, using thermal inertia to derive grain sizes

works best for homogenous, unconsolidated material within the top few cm of a surface

(Presley and Christensen, 1997). Any heterogeneity or layering at or below the surface will be

lost within the 100 m/pixel data, and the larger grains seen in at least some deltas and on Mars

in general needs to be accounted for in the grain size distribution.
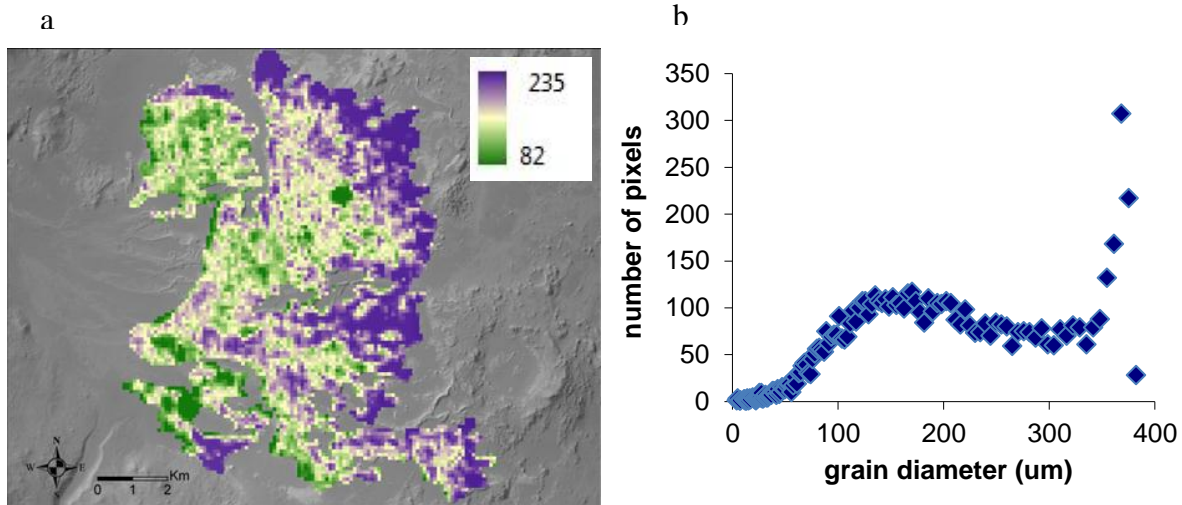
Figure 2. a) Derived thermal inertia over Eberswalde delta includes values from 82 (green) to 235 (purple) inertia units. The higher thermal inertia coincides with smaller grain sizes and the high albedo sedimentary material found along the distal edges. B) Thermal inertia-derived grain sizes range from 4 μm to nearly 400 μm, with a D_{50} of 250 μm.

In order to include grain sizes typical of Mars and yet representative of the Martian

deltas, we used a combination of grain sizes that incorporates data from both landers and

orbiting spacecraft. For the delta modeling in this work, the 0.1 m value was used as the

bedload grain size, and 1 mm, 0.4 mm, 0.3 mm, 0.2 mm, 0.1 mm, and 0.05 mm were used as

suspended load grain sizes. The results of other independent studies that identify grain sizes

within the Martian deltas that are similar to what we use here (e.g. Pondrelli et al., 2010) lends

confidence that our grain sizes, while not all-inclusive, are at least representative of conditions

present during delta formation.

4.2.3   River and Lake Characteristics

River discharge, receiving basin shape, and changes in paleolake levels are required

inputs for Sedflux modeling. To define the river discharge, valley slope, flow depth, and flow

width were determined. Profile measurements taken near the mouth of valleys feeding several

Martian deltas, including Eberswalde, Jezero, Sabrina, and Tyras were compared to get an

overall width-to-depth relationship that was used to approximate river conditions associated

with the formation of Martian deltas. Actual depths were not inferred from the valley profiles.

Rather, a range of possible river depths from 1 m to 40 m were used. The slope (s) at the

mouth of the river feeding the delta was set at 0.003, which is similar to what has been

observed in many Martian deltas (e.g. Hauber et al., 2008; Kleinhans et al., 2010). These

slopes, depths, and corresponding widths are summarized in Tables 2 and 3.

Table 2. Input parameters for modeling Martian delta formation with *Sedflux 2.0*

Bulk grain density (kg/m^3)	3400
Saturated grain density (kg/m^3)	2600
Water density (kg/m^3)	1000
Porosity	0.3
Martian gravity (m/s^2)	3.71
River slope	0.003

River discharge (Q_f) was calculated using the Darcy-Weisbach (D-W) equation for

width- and depth-averaged flow velocity (u) (Silberman et al., 1963), which maintains a

dependence on the acceleration due to gravity (g) and uses a friction factor (f) to describe the

effect of bed roughness on the flow.

$$Q_f = hwu \tag{5}$$

$$u = \sqrt{\frac{8ghs}{f}} \tag{6}$$

112

In all cases the hypothetical Martian rivers were assumed to be much wider than they are deep, as is typical of terrestrial rivers, and so the flow depth (h) was used in Equation (4) rather than the hydraulic radius, $hw/(w+2h)$.

The friction factor (f) is often expressed as a function of the relative roughness of the bed (h/D) and incorporates the effect of turbulence, bed forms, and sediment-flow interactions on flow velocity. There is a wide range of D-W friction factors that have been developed for terrestrial flows and applied to Martian conditions (e.g. Kleinhans, 2005; Komar, 1979; Wilson et al., 2004), and their predicted roughness varies considerably (Kleinhans, 2005). For this work, we used the White-Colebrook function (Silberman et al., 1963). The riverbed was assumed to have a grain size distribution typical of Mars, with a D_{50} of 0.1 m and D_{90} of 0.6 m (Kleinhans, 2005), and a Nikuradse roughness length (k_s) equal to the D_{90} value of the river bed grain size distribution was assumed.

$$\sqrt{\frac{8}{f}} = 5.74\log_{10}\left(\frac{h}{k_s}\right) + 1.0864 \tag{7}$$

The river was assumed to discharge into an initially-empty idealized impact crater 40 km in diameter (D). The depth (d) of the crater was estimated to be 1.5 km, based on the empirical depth-to-diameter relationship derived from Martian crater elevation data that applies to complex craters larger than 8 km in diameter (Garvin and Frawley, 1998; Kleinhans et al., 2010)

$$d = 0.25D^{0.49} \tag{8}$$

Elevation (km) of the crater surface (z) as a function of the distance (km) from the center of the crater (x) was calculated by

$$z = ax^n \tag{9}$$

for which the variables a and n for complex craters were calculated by (Garvin and Frawley, 1998; Kleinhans et al., 2010):

$$a = \frac{d}{(D/2)^n} \qquad (10)$$

$$n = 2.16D^{0.09} \qquad (11)$$

The resulting elevation profile was converted to meters below the crater rim and extended in the x- and y-directions to create a bathymetry file of elevation (Figure 3). The river was set to enter the crater halfway along the x-axis, 1 km above the crater floor; the 0.5 km above the river was removed such as from erosion and incision of the crater rim prior to delta forming conditions.
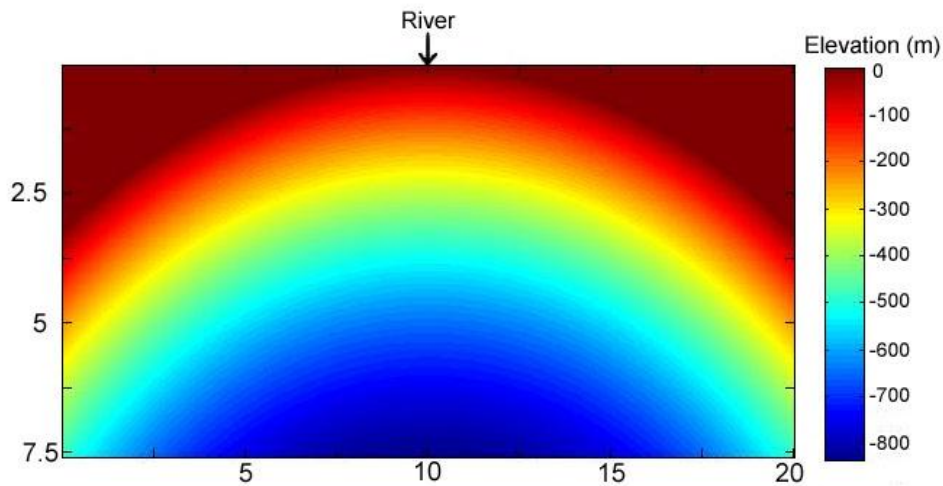
Figure 3. The elevation (m) below the rim within the initial bathymetry of the receiving basin is shown in 25 m/pixel vertical resolution. The final bathymetry file extended from the rim to the center of the crater and had spatial resolutions in the x- and y-axes of 25 m. The river entered the basin at the center of the x-axis, as indicated by the arrow. Distances along the x- and y-axes are given in km.

A lake was assumed to fill the crater at a rate determined by the river discharge (Table 3) until the lake was 1 km deep, or level with the river, at which point the water level was held steady for the remainder of the model run. This was calculated specifically for each river discharge scenario. In reality, evaporation, precipitation and surface runoff, ground

114

infiltration, groundwater sapping, changes in the water table, crater breaches, and other rivers (both in and out of the crater), may have affected the water level present during Martian delta formation, resulting in changes in water level during delta formation, as has been hypothesized by several researchers (e.g. Cabrol and Grin, 2001; Howard et al., 2007; Pondrelli et al., 2008; Wood, 2006). Future work that incorporates changes in water level will likely provide important information on Martian delta formation scenarios. This is particularly important in reproducing the topographic characteristics seen in many Martian deltas that are often attributed, at least in part, to water level changes (e.g. distinct lobes and terraces forming at different elevations within the delta). In this work, keeping the lake level constant after filling to the elevation of the river mouth allows us to focus on the effects of sediment grain size and supply on formation timescales.

Table 3. River characteristics and sediment load parameters for modeling Martian delta formation

River depth, h (m)	River width, w (m)	River velocity, u (m/s)	Flow discharge, Q_f (m^3/s)	Time to fill the crater paleolake (years)	Bedload discharge, Q_b (kg/s) (for 0.1 m grains)		Suspended load concentration, C_s (kg/m^3) (for 1 mm, 400 μm, 300 μm, 200 μm, 100 μm, and 50 μm grains)	
					Dilute	Dense	Dilute	Dense
1	175	0.3	44	415	0.0	0.0	0.01, 0.1, 0.2, 0.2, 0.02, 0.002	0.01, 0.1, 0.2, 0.2, 0.02, 0.002
5	272	1.5	2000	9	567	1530	0.02, 0.5, 1.4, 1.5, 0.2, 0.03	0.04, 1.3, 3.6, 3.8, 0.6, 0.07
10	403	2.7	11000	1.7	1770	9430	0.02, 0.5, 1.4, 1.5, 0.2, 0.03	0.08, 2.6, 7.4, 7.8, 1.1, 0.2
20	586	4.6	54000	0.33	3750	57100	0.02, 0.5, 1.4, 1.5, 0.2, 0.03	0.2, 7.7, 22, 23, 3.3, 0.4
40	872	7.7	270000	0.07	7180	317000	0.02, 0.5, 1.4, 1.5, 0.2, 0.03	0.8, 23.2, 64, 66, 9.5, 1.3

4.2.4 Sediment Supply

The concentration of sediment supplied by the river to the delta system was calculated using well known and tested terrestrial sediment transport predictors modified for application to Martian flows. These equations (described in Hoke et al., 2011) were chosen for their independence on the choice of roughness length (k_s) and their physics-based formulation that

minimizes terrestrial empirical approximations that might not be applicable to Mars.

Calculating the sediment discharge (Q_s) as a function of the bed load transport rate (q_b) and suspended load transport rate (q_s) across the width (w) of the channel can be done by:

$$Q_s = (q_b + q_s)w \hspace{4cm} (12)$$

The bed load (q_b) and suspended load (q_s) transport rates were calculated using the van Rijn (1984a, 1984b), Ribberink (1998), and Meyer-Peter and Mueller (Wong and Parker, 2006) equations. These equations assume transport-limited conditions, which can be expected for Late Noachian Mars given the heavy bombardment by impactors the surface had experienced not long before this time that likely created a kilometer or more of unconsolidated, poorly sorted regolith (e.g. Baker and Partridge, 1986; Hartmann and Neukum, 2001). These equations also assume dilute concentrations of sediment. With the river and sediment characteristics used in this work, these flows are capable of becoming densely concentrated. Dense flows on Earth are rare, and it is unclear whether rivers on Mars would have been dilute or dense, though that likely depends on many factors, including discharge rates and sediment supply (Kleinhans et al., 2010). Therefore, this work explores both dilute and dense sediment concentrations, though the default in most scenarios is dilute flow conditions. Dilute flows are assumed to have a total sediment flux (Q_s) that is 1000 times less than the flow discharge (Q_f), and the calculated values from equation 12 have been adjusted accordingly. Alternatively, dense flows are considered to be the full transport-limited sediment flux calculated with equation 12, which have sediment discharge to water discharge ratios of 3:1000 (for 5 m deep flows) to 64:1000 (for 40 m deep flows).

Each model was run until the delta volume (V) reached a target value consistent with observed volumes on Mars (i.e. 1 km^3, 5 km^3). This was done by identifying and integrating

the thickness of the grid coordinates that enclosed the modeled delta. This region often

included some adjacent distal deposits, though this was minimized as much as possible. The

time to reach the target volume is the formation timescale (T_m) of the delta, which are all given

in Table 4. Since the formation timescales of the deltas were significantly longer than the time

it took to fill the crater with water (by a factor of approximately 4 to approximately 40), the

final formation timescale (T_m) was not adjusted by subtracting the initial time it took to form

the lake.

These timescales were compared with the calculated minimum formation timescales

(T_c) that were determined by comparing the total volume (V) of the delta to the total sediment

flux (Q_s) and an assumed average porosity (λ) of the transported material of 0.3 (Kleinhans,

2005).

$$T_c = \frac{V}{(1-\lambda)Q_s} \qquad (13)$$

The calculated formation timescale (T_c) assumes no additional sediment sources or sinks and

reflects a minimum formation timescale for the delta. Whereas the model formation timescale

(T_m) incorporates deposition and erosion of the river channel and delta deposit, settling rates,

compaction and consolidation, loss of sediment beyond the delta region, etc, and produces

longer formation timescales overall.

4.2.5 Delta Formation Scenarios

The event-based timestepping that Sedflux uses allows different timesteps to be used

according to the desired temporal resolution of the seasonal event. This allows short duration,

high-energy events, such as river floods, to be incorporated into the model. Temporal

resolutions typically were a day for these simulations, though each process module within

Table 4. Model set-up and formation timescale results for each modeled scenario

Scenario	Horiz. res.	Vert. res.	Timestep (d=day, m=month)	Form Time, T_c (ref. vol.)	Form Time, T_m (ref. vol.)
1m-deep continuous river, dilute concentration	25 m	0.5 m	6 m	3780 y (1 km^3)	4750 y (1 km^3)
	50 m	0.5 m	12 m	3780 y (1 km^3)	4700 y (1 km^3)
5m-deep continuous river, dilute concentration	25 m	0.5 m	1 d	11 y (1 km^3)	45 y (1 km^3)
	50 m	0.5 m	1 d	11 y (1 km^3)	36 y (1 km^3)
	100 m	0.5 m	1 d	11 y (1 km^3)	22 y (1 km^3)
10m-deep continuous river, dilute concentration	25 m	0.5 m	1 d	10 y (5 km^3)	32 y (5 km^3)
	25 m	0.5 m	1 d	2 y (1 km^3)	12 y (1 km^3)
	50 m	0.5 m	1 d	2 y (1 km^3)	14 y (1 km^3)
	100 m	0.5 m	1 d	2 y (1 km^3)	11 y (1 km^3)
10m-deep continuous river, dense concentration	25 m	0.5 m	1 d	2 y (5 km^3)	6 y (5 km^3)
20m-deep continuous river, dilute concentration	25 m	0.5 m	1 d	2 y (5 km^3)	7 y (5 km^3)
	25 m	0.5 m	1 d	0.4 y (1 km^3)	3 y (1 km^3)
	50 m	0.5 m	1 d	0.4 y (1 km^3)	5 y (1 km^3)
40m-deep continuous river, dilute concentration	25 m	0.5 m	1 d	0.8 y (10 km^3)	3 y (10 km^3)
	25 m	0.5 m	1 d	0.4 y (5 km^3)	1.5 y (5 km^3)
	25 m	0.5 m	1 d	0.08 y (1 km^3)	0.8 y (1 km^3)
5m-deep continuous river, 95% dilute and 5% dense concentration	25 m	0.5 m	34x10d + 7x1d, 18x1d	52 y (5 km^3)	110 y (5 km^3)
	25 m	0.5 m	34x10d + 7x1d, 18x1d	10 y (1 km^3)	40 y (1 km^3)
	50 m	0.5 m	21x1m+5x1d, 33x1d	10 y (1 km^3)	36 y (1 km^3)
10m-deep continuous river, 95% dilute and 5% dense concentration	25 m	0.5 m	34x10d + 7x1d, 18x1d	2 y (1 km^3)	9 y (1 km^3)
5m-deep river for 5% of time (ephemeral), dilute concentation	25 m	0.5 m	18x1d, 34x10d + 7x1d	214 y (1 km^3)	840 y (1 km^3)
20m-deep river for 5% of time (ephemeral), dilute concentration	25 m	0.5 m	18x1d, 34x10d + 7x1d	40 y (5 km^3)	213 y (5 km^3)
	25 m	0.5 m	34x10d + 7x1d, 18x1d	8 y (1 km^3)	63 y (1 km^3)
5m-deep continuous river that floods to 10m for 5% of time, dilute concentrations	25 m	0.5 m	34x10d + 7x1d, 18x1d	51 y (5 km^3)	105 y (5 km^3)
	25 m	0.5 m	34x10d + 7x1d, 18x1d	10 y (1 km^3)	35 y (1 km^3)
5m-deep continuous river that floods to 20m for 5% of time, dilute concentrations	25 m	0.5 m	34x10d + 7x1d, 18x1d	102 y (10 km^3)	120 y (10 km^3)
	25 m	0.5 m	34x10d + 7x1d, 18x1d	51 y (5 km^3)	78 y (5 km^3)
	25 m	0.5 m	34x10d + 7x1d, 18x1d	10 y (1 km^3)	27 y (1 km^3)
	50 m	0.5 m	21x1m+5x1d, 33x1d	10 y (1 km^3)	33 y (1 km^3)
5m-deep continuous river that floods to 20m for 5% of time w/ 1/3 of flood having dense concentration	25 m	0.5 m	34x10d + 7x1d, 18x1d	103 y (10 km^3)	44 y (10 km^3)
	25 m	0.5 m	34x10d + 7x1d, 18x1d	51 y (5 km^3)	27 y (5 km^3)
	25 m	0.5 m	34x10d + 7x1d, 18x1d	10 y (1 km^3)	12 y (1 km^3)

118

Sedflux uses shorter time stepping as necessary. Some low-energy events were given a timestep of 10 days (Table 4).

Several different scenarios of seasonal river change were explored to encompass a range of possible formation conditions. First, we created a series of deltas formed by continuous dilute rivers with depths including 1 m, 5 m, 10 m, 20 m, and 40 m. The depths, their corresponding widths, flow velocities, discharge rates, and sediment concentrations are listed in Table 3. These continuous dilute river scenarios provide a baseline with which to compare varying sediment and river scenarios. They also allow some comparison with other recent work that describes evidence for continuous, single-event discharge events that formed some of the Martian deltas (e.g. Kleinhans et al., 2010; Kraal et al., 2008). Others have applied an intermittency of 1% or 5% by multiplying continuous formation by a factor of 100 or 20, respectively (e.g. Fassett and Head, 2005; Hoke et al., 2011; Moore et al, 2003;). To investigate how the deposits may be affected by re-suspension and transportation further into the basin during ephemeral flows, we modeled a series of deltas that were formed by dilute rivers that flowed for only 5% of the time; the remainder of the time no river or sediment was supplied to the system. Most deltas on Earth are formed at the mouth of rivers that vary in discharge throughout the year, with flood stages occurring less frequently but having a greater capacity to transport sediment. Therefore we modeled scenarios that incorporated fluctuating river discharge levels as from a flood event (i.e. 95% of the time at low discharge levels and 5% of the time at "flood" discharge levels). Since the valleys that fed the deltas formed on a substrate that had recently experienced heavy bombardment by impactors, the surface is expected to have had a kilometer or more of unconsolidated, poorly sorted regolith (e.g. Baker and Partridge, 1986; Hartmann and Neukum, 2001), suggesting they formed in transport-

limited conditions. To compare delta formation in dense and dilute scenarios, we added a continuous 10-m deep densely concentrated river scenario. And to incorporate alternating dilute and dense concentrations as from a sudden increase in sediment supply from a wall collapse in the valley upstream from the delta, we modeled a continuous 10-m deep river that was dilute for 95% of the time and dense for 5% of the time. Finally, combinations of these scenarios were also explored, including the delta that forms from a dilute low river that floods to a dense deep river that becomes a dilute deep river before dropping back to a dilute low river.

4.3   Results and Discussion

4.3.1   Morphometry of the modeled deltas

Deltas that have been observed on Mars have radii of a few km to 10's of km, thicknesses of 10's of m to 100's of m, and volumes of just over 1 km^3 to more than 100 km^3 (e.g. Di Achille et al., 2006; Di Achille and Hynek, 2010b); Fassett and Head, 2005; Hauber et al., 2008; Irwin et al., 2005a; Kleinhans et al., 2010; Malin and Edgett, 2003; Moore et al., 2003; Ori et al., 2000). The radius of modeled topset deposits range from about 2 km (for 1 km^3 delta-volumes) to nearly 7 km (for 10 km^3 delta-volumes) and thicknesses range from about 275 m (1 km^3) to 550 (10 km^3). These modeled volumes and radii are on the low end, but still inclusive, of what has been measured for actual deltas on Mars, and the results of this work can be expanded to larger deltas by increasing the total run time. The Di Achille et al companion paper has investigated formation timescales specific to individual Martian deltas.

Our model results include mostly Gilbert-type deltas characterized by flat upper surfaces, steep frontal scarps, and shallow-sloped thinner distal deposits (Gilbert, 1885). The overall shape of the modeled deltas is likely strongly influenced by the bathymetry of the

120

receiving basin, which in this case was a moderately-sized (40 km in diameter), shallow (1 km deep) crater with interior slopes of 2º to 4° near the rim. The Gilbert delta shape may also, at least in part, be due to the same density given to the river and lake water (1000 kg/m3), which has been attributed to the formation of Gilbert deltas (Gilbert, 1885). However, the increase in density in the river due to the suspended sediment, particularly in dense concentration scenarios, created hyperpycnal conditions that are characterized by the transport of finer sediments to greater distances (Bates, 1953). With our densely-concentrated 10 m-deep scenario, a clear delta deposit did not appear until deposits were greater than 1 km^3. This was due to thick, rough deposits extending from the river mouth to the center of the crater, blurring the distinction between coastal and offshore deposits.

Any deviation in the model runs from a continuous river and sediment discharge resulted in deltas with irregular outlines as the sediment was supplied and deposited non-uniformly over time. This is seen in the delta that formed from a continuous dilute river that experienced temporary increases to dense concentrations (Figure 4), as well as the delta that formed from a dilute shallow river that occasionally increased to deeper flood stages (Figure 5). Changes in sediment concentrations (i.e. dilute vs. dense) seem to have a greater impact on delta shape than river flood stage. These results are consistent with the interpretation that Martian deltas such as Eberswalde and Jezero, which are characterized by lobes of deposits, formed by flows of changing discharge and sediment concentrations. Analyses of distributary channel and deposit morphologies (e.g. Bhattacharya et al., 2005; Pondrelli et al., 2008; Wood, 2006), including sinuosity of meanders, point bars, chute channels, crevasse splays, etc, indicate sediment was transported under both bedload-dominated conditions as well as bedload
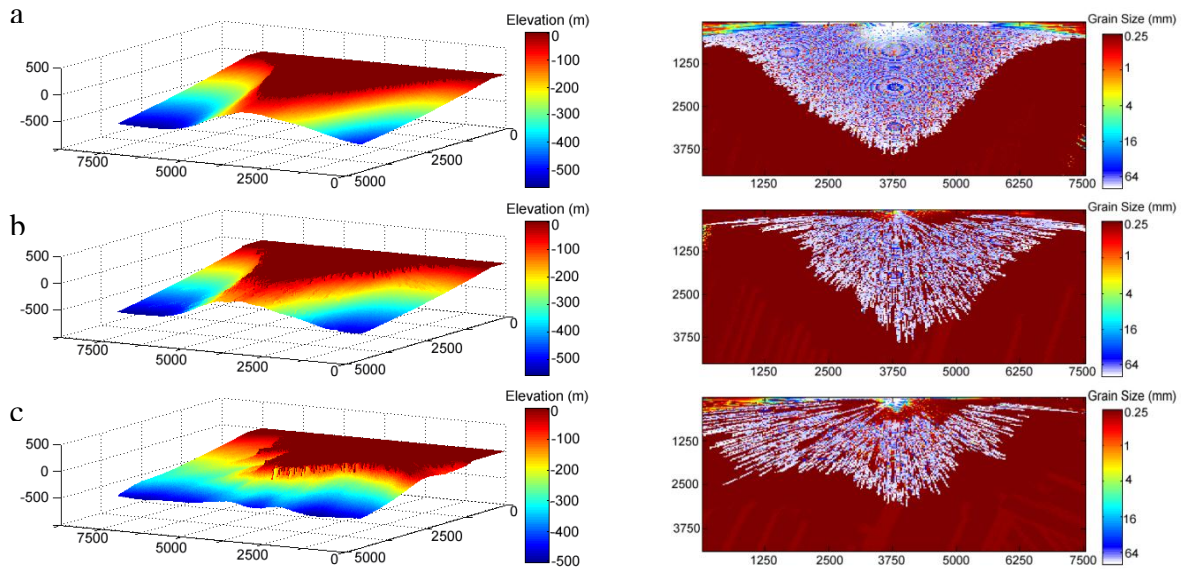
Figure 4. a) Dilute and b) dense sediment concentrations in a 10m-deep continuous river result in similar 4 km³ deltas (elevation, left column). c) A 10-m deep continuous river experiencing temporary increases in concentration from dilute (95% of the time) to dense (5% of the time) produces a delta having a more irregular shape due to the varying sediment supply. Grain sizes within the deltas (mm, right column) include a greater range of deposited grain sizes (sand to cobble) for the higher concentrated flows (middle and bottom) than for the diluted flows (gravel to cobble, top). The continuous dilute river formed the 4 km³ delta in approximately 28 years, while the continuous dense river formed the 4 km³ delta in approximately 6 years, and the river with changing sediment concentrations formed the 4 km³ delta in approximately 20 years.

with suspended load transport systems having fine-grained (sand, dust, clay) and coarse-grained (boulder and gravel) sediments. Even continuous, single-event formation scenarios likely had varying sediment concentrations that were initially dense and then progressed to dilute (Kleinhans et al., 2010; Kraal et al., 2008). These conditions should produce deltas with irregular outlines. This is not seen in the stair stepped deltas on Mars that have been interpreted by some as having formed by single event continuous flows (Kleinhans et al., 2010; Kraal et al., 2008). While this is interesting to note, this work did not incorporate all the conditions associated with stair-stepped delta formation. Our companion paper (Di Achille et al) has investigated these scenarios more thoroughly.
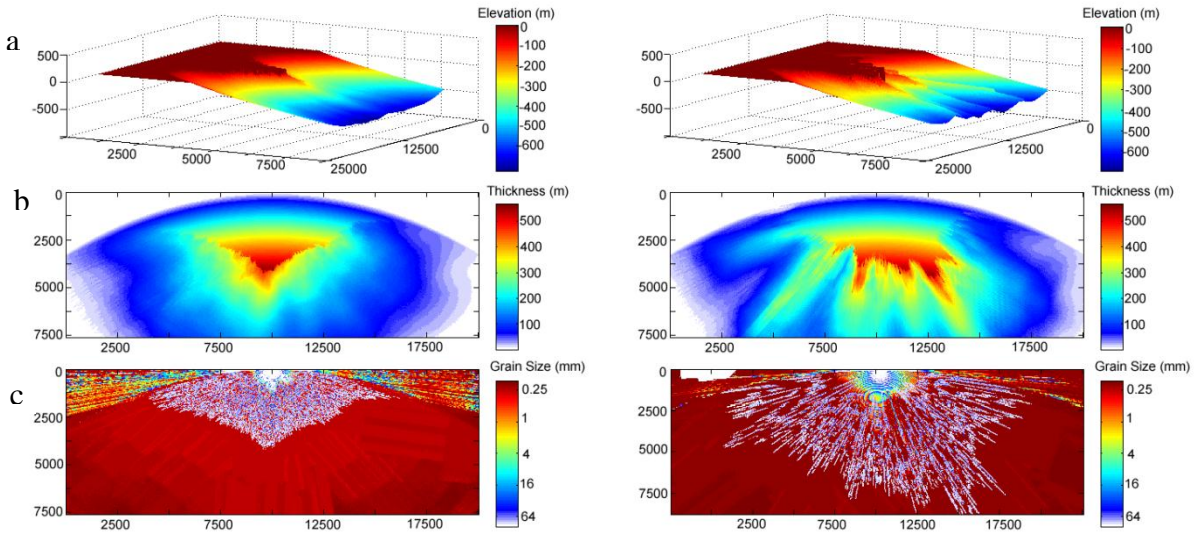
Figure 5. This figure illustrates the a) elevation, b) deposit thickness, and c) grain size for two variable-river scenarios that produced 10 km^3 deltas of irregular shape and structure that reflect their changing flood stage and sediment concentrations. The scenario in the left column is of a delta that formed from a dilute river that experienced episodes of flooding (5 m deep for 95% of the time, 20 m deep for 5% of the time) while the scenario in the right column is the same river but with increased sediment concentrations for the first 1/3rd of the flood event. The river flood scenario on the left formed a 1 km^3 delta in 27 years that grew to 5 km^3 in 78 years and 10 km^3 in 120 years. The river flood with temporary increased sediment concentration scenario on the right formed a delta of the same volumes in 12 years, 27 years, and 44 years.

The shape of the ephemeral delta is smoothed and more rounded as compared with the continuous delta scenarios. This is a result of diffusion of the deposited sediment within the lake. Since we held lake levels constant after filling, the ephemeral scenario may not capture the actual variability such a delta would experience. However, as some paleolakes on Mars are associated with significant contribution by groundwater sources (Fassett and Head, 2008a), it is conceivable a lake would remain despite a lack of precipitation.

4.3.2   Effects of river discharge on grain distribution

As river depth and discharge were increased, the faster flows transported more suspended sediment further into the basin beyond the delta-forming region. The slower settling rates of the smaller grains allowed them to reach greater distances before being deposited onto the

crater floor (Figure 6). Indeed, most of the modeled deltas had topset material that consists of

larger grain sizes transported primarily by bedload, while significant amounts of fine-grained,

suspended-load material was deposited further into the basin beyond the delta. The fine-

grained material transported beyond the deltas in our results may represent the thinly layered

deposits seen beyond some deltas on Mars as well as represent thicker offshore sedimentation

that hypothetically make many deltas difficult to identify (Howard, 2007). The difference

between thinly layered distal deposits and thicker offshore sedimentation lies in the discharge

rates and concentrations of the supply-river.

The off shore sedimentation is an important consideration for Martian deltas that have

been interpreted to have rapid formation timescales as a result of high discharge rates (e.g.

Hauber et al., 2008; Kleinhans et al., 2010; Kraal et al., 2008). Although the rivers in those

scenarios are capable of supplying the delta-forming zones with sediment at a rapid rate, much

of that sediment may be transported past the delta forming zones. If the Martian deltas were

composed primarily of larger-grained bedload material, their formation would fit with

continuous high discharge scenarios. However, most of the deltas on Mars were characterized

by finer sediment (e.g. Hauber et al., 2009; Pondrelli et al., 2008), suggesting the flows had to

have been of low enough energy to allow deposition in the coastal region.

Grain size distributions within the modeled deltas changed as concentrations in the river

increased. For example, a continuous 10-m deep river with dilute concentrations produced a

modeled delta composed primarily of 1 mm to 0.1 m grains representative of the largest

suspended load grains and the bedload material. The same scenario but with dense

concentrations produced a delta of 200 μm to 0.1 m, indicating that with the denser flows,

more sand grains were deposited in the delta. A similar range of grain sizes was in the
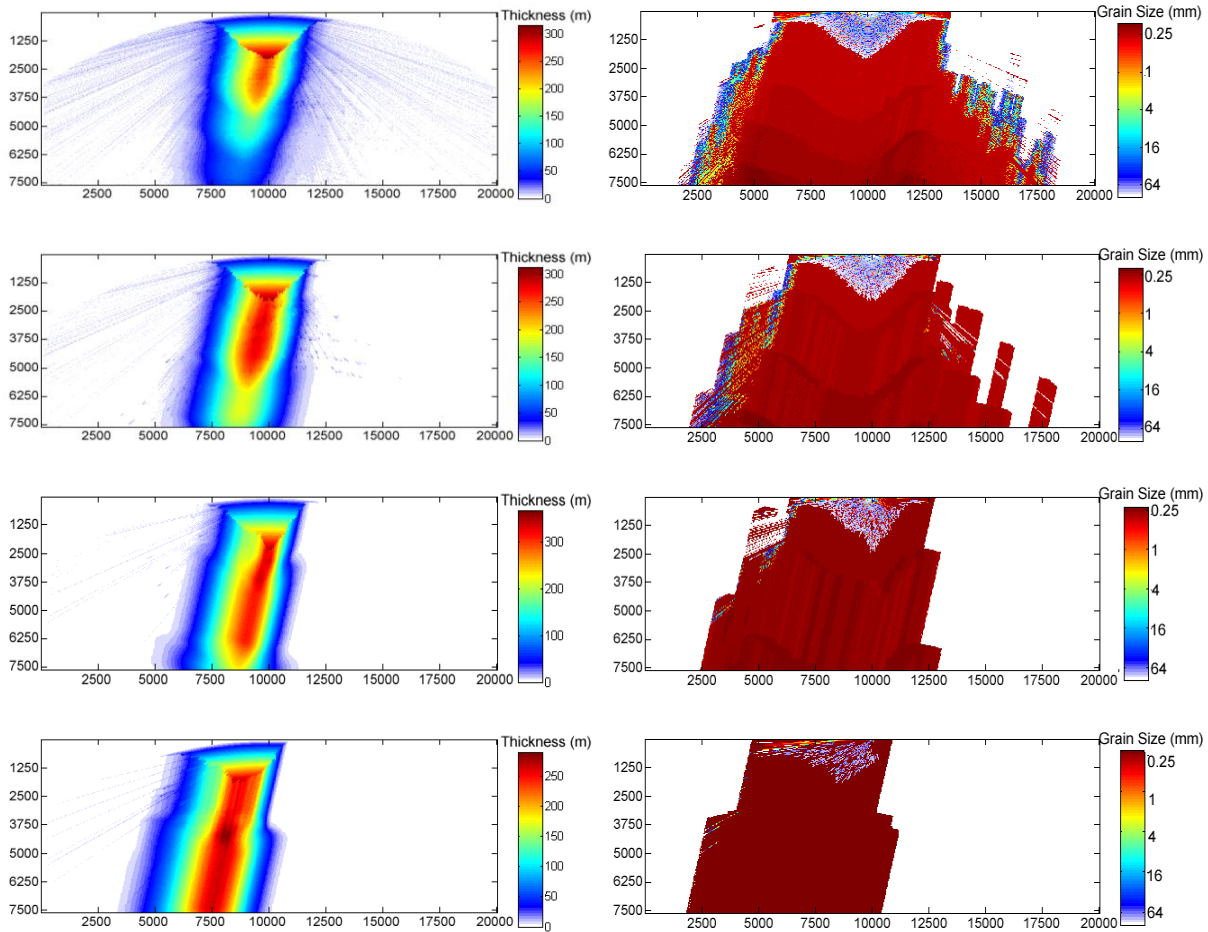
Figure 6. Delta thicknesses (meters) that correspond to total volumes of 1 km³ are formed in 45 years (5m-deep continuous river, 1st row), 12 years (10m-deep continuous river, 2nd row), 3 years (20m-deep continuous river, 3rd row), and 0.8 years (40m-deep continuous river, 4th row). The grain size distributions within the basin (mm) show most of the smaller material being transported beyond the delta in all discharge scenarios. The deltas are composed of bedload (0.1 m) and large suspended load (1mm) grains, and increased discharge rates, represented here by deeper flow depths in the contributing river, correspond to a greater range in grain sizes to include smaller grains (down to 0.3 mm) deposited in the delta. All spatial resolutions are 25 m by 25 m in the horizontal and 0.5 m in the vertical.

delta scenario that formed from a continuous 10-m deep river that experienced occasional

increases in concentration from dilute (95% of the time) to dense (5% of the time) conditions.

This scenario may result from a wall collapse along the valley feeding the delta or from impact

or volcanic ejecta. This suggests sediment concentrations did not need to be continuously

dense, which would be difficult to produce as a river naturally progresses to dilute conditions

125

(Kleinhans et al., 2010). Rather, occasional dense concentrations will produce the mix of grains from sand to boulders seen in some layers in Martian deltas, such as Eberswalde, assuming a flow capable of transporting those grain sizes.

Kleinhans et al. (2010) discussed the formation of thin drapes of deposited sediment from dilute rivers. They explain that for events shorter than the time to fill the lake, the deposited sediment forms either a thin drape or an alluvial fan, depending on whether the river sediment concentration was dilute or dense, respectively. However, the Late Noachian and Early Hesperian are often characterized by terrestrial-like arid or semi-arid precipitation (e.g. Barnhart et al., 2009; Howard, 2007; Stepinski and Stepinski, 2005). If this time in Martian history was characterized by hyper-arid conditions with high evaporation rates and intermittent valley-incising precipitation, it is possible there was little ponding. In that case, each episode of precipitation would transport sediment that could be deposited subaerially. However, there is abundant evidence for the formation of paleolakes fed by precipitation and surface runoff with volumes comparable to their watersheds (e.g. Fassett and Head, 2008a).

Alternatively, reworking of deposited delta sediments during fluctuations in lake level may have obscured delta boundaries, making them difficult to identify today (Howard, 2007). Though deltaic deposits in the Great Basin region of the United States remain distinct from their basins, suggesting fluctuating lake levels may not explain the lack of deltas on Mars (Howard, 2007), the widespread resurfacing on Mars since their formation (Fassett and Head, 2008a) may compound the difficulty in identifying many deltas.

4.3.3 Formation Timescales

Continuous formation scenarios of Martian deltas within Sedflux are capable of producing surprisingly fast formation timescales, even with the loss of smaller sediment

beyond the delta. A continuous 40-m deep deluge emptying into a basin would form a 1 km^3 delta in 0.8 years. This timescale is 10 times longer than was calculated based on sediment supply to the basin due to loss of sediment beyond the delta-forming region. Other recent work has produced Martian deltas in days to hundreds of years depending on the type of delta and methods used. Those results are comparable to some of our continuous formation timescales for Martian-sized deltas. Though some of the conditions that the Kleinhans et al. (2010) model uses includes much steeper slopes and at times extreme flow depths (up to 100 m) that produce such short timescales. Continuous formation scenarios of deeper flows and higher discharge rates, however, are not required for the formation of fluvio-features during this time in Martian history; these conditions are much more extreme than the conditions required for the formation of the contemporaneous valley networks. The large valley networks formed as a result of precipitation and surface runoff during the Late Noachian and Early Hesperian over periods of 10^5 to 10^7 years with runoff rates similar to intense storms in arid regions on Earth (Hoke et al., 2011). The deltas that formed during this time were likely exposed to the same climatic conditions and formation scenarios. Therefore, intermittent formation requiring smaller flows is a more realistic scenario for the Martian deltas than continuous deluges. On that end of the spectrum, a 1-m deep continuous river would form a 1 km^3 delta in 4750 years, compared with a calculated formation timescale of 3780 years. If the river was ephemeral, formation timescales could approach 500,000 years, placing it within the duration of clement conditions in the Late Noachian and Early Hesperian on Mars.

The dense 10 m deep flow scenario produced a delta in less time than the similar dilute flow scenario, though the increase in the range of deposited grain sizes contributed only minorly to the faster formation timescale of the dense-flow scenario. Rather the
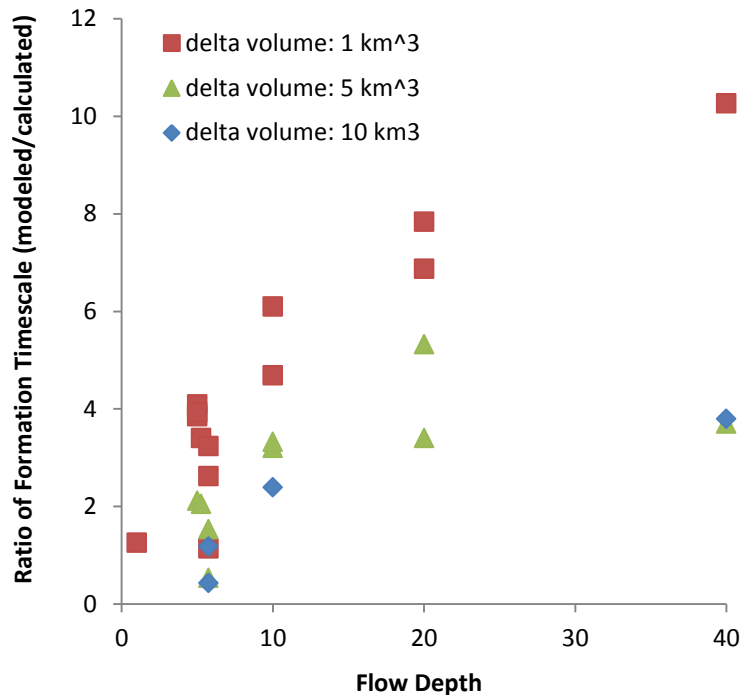
Figure 7. The modeled formation timescales were in most cases longer than the calculated formation timescales (Equation 11) by up to a factor of 10, depending on the modeled scenario. Red squares correspond to deltas of 1 km^3, green triangles correspond to deltas of 5 km^3, and blue diamonds correspond to deltas of 10 km^3. The difference between modeled and calculated formation timescales was greater for rivers with higher discharges (represented here by deeper flow depths) due to the increased transport of material beyond the delta-forming region.

decrease in time it took to form a 5 km^3 delta from 32 years (dilute concentrations) to 6 years (dense concentrations) was primarily a result of the increase in total supplied sediment within the flow. The delta that formed from the continuous 10-m deep river that experienced both dilute and dense concentration (Figure 4c) resulted in formation timescales that are dominated by the all-dilute flow scenario (Figure 4a), though the grain size distribution more closely resembled the all-dense scenario (Figure 4b).

By adding more detail into Martian delta formation modeling through the use of increased grain size distributions and various process-response modules that Sedflux offers, we see different results than if we used bulk flow and transport calculations. With the ability to

track sediment as it is transported throughout the basin, it is apparent that non-negligible amounts are moved beyond the delta-forming region. This loss of sediment increased with greater river discharges (Figure 6), increasing the gap between the calculated and modeled formation timescales (Figure 7). Therefore, formation timescales that consider only the supply of sediment to the system and don't take into account factors affecting deposition and delta formation are underestimates of the actual amount of time needed to form the deposits.

4.4   Conclusions

We have investigated the effects of changing the hydrologic and sedimentary conditions on the formation timescales required to produce Martian delta volumes. Our results indicate that significant off shore sedimentation is common with the various formation scenarios we explored, particularly with high river discharge scenarios. These results have important implications for the formation timescales of the deltas and the lack of identifiable deltas on Mars today.

Our delta modeling indicates that formation timescales of Martian deltas were likely longer than that determined by bulk flow calculations due to the significant sediment transported beyond the delta-forming region. The assumptions of continuous delta formation with extreme discharges in a single event (e.g. Kleinhans et al., 2010; Kraal et al., 2008) are not consistent with recent work describing Martian conditions for valley network formation that suggest precipitation during the Late Noachian was comparable to that in arid or semi-arid regions on Earth (e.g. Barnhart et al., 2009; Hoke et al., 2011; Howard, 2007; Irwin et al., 2011). A complicated formative history for the Martian deltas, with changing lake levels, varying sediment and river characteristics (e.g Di Achille et al., 2006; Fassett and Head, 2005, 2008a; Moore et al., 2003; Pondrelli et al., 2010; Wood, 2006), and formation timescales comparable to

the duration of clement conditions (e.g. Hoke et al., 2011) would place the deltas under the same formation conditions as their coeval paleolakes and valley networks. The lack of identifiable deltas in many locations that would have supported their formation (e.g. Fassett and Head, 2008a) are likely a result of significant sediment transport beyond the coastal delta-forming region (Howard, 2007). With significant offshore sedimentation, the elevation of a delta above the basin floor becomes less recognizable (Howard, 2007). Combined with reworking of deposits during fluctuating lake levels associated with an arid- to semi-arid environment (Barnhart et al., 2009) and post-formation resurfacing by impact and eolian processes (e.g. Howard, 2007), these results could explain the lack of deltas seen on Mars.

5   Conclusions

The presence of valley networks across much of the ancient surface of Mars (e.g. Hynek et al., 2010), together with the locations and morphologies of the Martian deltas (e.g. Di Achille and Hynek, 2010b) and ancient paleolakes (e.g. Fassett and Head, 2008a; Irwin et al., 2005a), provides strong evidence that the Martian surface environment was once capable of sustaining liquid water at the surface. Many of the largest Martian valley networks, with their meandering trunks, densely dendritic form, and tributaries that reach up to drainage divides, appear to have formed primarily from surface runoff of precipitated water (e.g. Craddock and Howard, 2002; Hoke and Hynek, 2009; Howard et al., 2005; Hynek and Phillips, 2003; Hynek et al., 2010). These same valley networks have crater densities that place their formation in the Late Noachian and Early Hesperian (~3.5-3.8 Ga) (Fassett and Head, 2008b; Hoke and Hynek, 2009), consistent with their formation during a period of enhanced fluvial erosion and incision on Mars (e.g. Craddock and Howard, 2002; Howard et al., 2005; Hynek and Phillips, 2001, 2003; Hynek et al., 2010).

Runoff and evaporation rates on Mars during this time in its history may have resembled those in arid to semi-arid regions on Earth, characterized by numerous and repeated moderate floods separated by periods of evaporation (e.g. Barnhart et al., 2009; Howard, 2007; Irwin et al., 2011; Stepinski and Stepinski, 2005). Assuming intermittent formation in an arid or semi-arid environment, calculated formation timescales for each of several of the large Martian valley networks range from 10^5 to 10^7 years (Barnhart et al., 2009; Hoke et al., 2011). This suggests the Martian climate was capable of supporting terrestrial desert-like precipitation for a hundred thousand to tens of millions of years. Based on relative crater densities between the large valley networks (Hoke and Hynek, 2009) and evidence that many areas on Mars experienced multiple

episodes of fluvial modification (e.g. Baker and Partridge, 1986; Ehlmann et al., 2008; Grant, 2000; Grant and Schultz, 1990; Harrison and Grimm, 2005; Hoke and Hynek, 2009; Howard et al., 2005; Irwin et al., 2005a; Williams and Phillips, 2001), these warmer, wetter periods came and went at least three times in places over the 10^8 years of valley formation (Hoke and Hynek, 2009). Though, considering the large uncertainty in these calculations and the combination of parameters that produced minimum timescales, it is possible the formation timescales of the valley networks approach durations similar to their span in ages, and therefore terrestrial desert-like conditions may have persisted for a few hundred million years.

The formation timescales we have determined for these large valley networks are significantly longer than formation timescales that have been calculated for Martian deltas in other recent work (e.g. Hauber et al., 2009; Kleinhans et al., 2010; Kraal et al., 2008). Those studies produce Martian deltas in days to hundreds of years depending on the type of delta and methods used. The difference in formation timescale between the valley networks and deltas is not surprising due to the steep channel slopes, smaller sediment volumes, and at times extreme flow depths (up to 100 m) that produce delta formation on such short timescales (e.g. Hauber et al., 2009; Kleinhans et al., 2010; Kraal et al., 2008).

Our delta modeling indicates that formation timescales of Martian deltas were likely longer than that determined by bulk flow calculations due to the significant sediment transported beyond the delta-forming region. The assumptions of continuous delta formation with extreme discharges in a single event (e.g. Kleinhans et al., 2010; Kraal et al., 2008) are not consistent with recent work describing Martian conditions for valley network formation that suggest precipitation during the Late Noachian was comparable to that in arid or semi-arid regions on Earth (e.g. Barnhart et al., 2009; Hoke et al., 2011; Howard, 2007; Irwin et al., 2011). A

complicated formative history for the Martian deltas, with changing lake levels, varying

sediment and river characteristics (e.g Di Achille et al., 2006; Fassett and Head, 2005, 2008a;

Moore et al., 2003; Pondrelli et al., 2008; Wood, 2006), and formation timescales comparable to

the duration of clement conditions (e.g. Hoke et al., 2011) would place the deltas under the same

formation conditions as their coeval paleolakes and valley networks. The lack of identifiable

deltas in many locations that would have supported their formation (e.g. Fassett and Head,

2008a) are likely a result of significant sediment transport beyond the coastal delta-forming

region (Howard, 2007). With significant offshore sedimentation, the elevation of a delta above

the basin floor becomes less recognizable (Howard, 2007). Combined with reworking of

deposits during fluctuating lake levels associated with an arid- to semi-arid environment

(Barnhart et al., 2009) and post-formation resurfacing by impact and eolian processes (e.g.

Howard, 2007), these results could explain the lack of deltas seen on Mars.

Regardless, the amount of time required to form the deltas (Chapter 4) and the large

valley networks (Hoke et al., 2011) does not extend the timing of precipitation on Mars to earlier

than the Late Noachian and few identified valleys and deltas formed much after ~3.0 billion

years ago (e.g., Di Achille and Hynek, 2010b; Hynek et al., 2010). Collectively, these results are

consistent with hypotheses that the majority of valley incision was constrained to a relatively

short period of Martian history near the Noachian-Hesperian boundary (e.g. Howard et al., 2005;

Hynek and Phillips, 2001; Irwin et al, 2005a, 2011).

Valley networks share similar ages (Hoke and Hynek, 2009) and formation timescales

(Hoke et al., 2011) as their neighboring networks. This observation is consistent with regional

weather patterns delivering precipitation of sufficient magnitude to form the valleys while other

non-incising regions received minor precipitation, if any. These zones of precipitation appear to

have roamed throughout the equatorial regions of the ancient Martian surface, sometimes returning to previously rainy regions (Hoke and Hynek, 2009).

A geographic region may experience changing levels of precipitation over time, driven by changes in topography and relative locations of source bodies of water, changes in atmospheric circulation patterns, and/or changes in orbit and obliquity (e.g. Colaprete et al., 2004; Soto et al., 2011). An example of this can be seen in the Basin and Range province within Nevada. At present, conditions are extremely arid and desert-like, whereas the Pleistocene climate permitted vigorous hydrological activity and long-lived lakes covering much of north and west Nevada (e.g. Hostetler and Benson, 1990). The Chad basin in the African Sahara Desert also likely experienced alternating periods of aridity and heavy rainfall in response to changing global ice coverage since its formation approximately 25 million years ago (Burke, 1976). Given the rapidly changing conditions on early Mars, it is not surprising that valley formation would occur in different regions at different times. These episodes of clement conditions (by Martian standards) may have been driven by impact events, volcanic outgassing, and/or any other event that changed the atmospheric temperature, density, and composition.

The Segura et al. (2002, 2008) model of impact-induced climate change produces episodes of precipitation that likely resulted in erosion and sediment transport early in Martian history. However, the timing of the impact events (e.g. Fassett and Head, 2011; Werner, 2008) overall do not coincide with the timing of valley network formation (Fassett and Head, 2008b; Hoke and Hynek, 2009), nor do they provide long enough durations of precipitation to form the large valley networks (e.g. Barnhart et al., 2009; Hoke et al., 2011).

All of the valley networks analyzed in Hoke and Hynek (2009) and Hoke et al. (2011) have valley lengths that range from about 5000 km to 15,000 km, placing them with the largest

valley network systems on Mars and similar to larger contemporary rivers on Earth. These valley networks have crater ages that place their formation 3.63 to 3.72 (+/- 0.03) Ga (Hoke and Hynek, 2009) or 3.69 to 3.76 (+/- 0.08) Ga (Fassett and Head, 2008b). Since most of the impact basin formation events occurred between about 3.9 to 4.1 Ga (e.g. Fassett and Head, 2011; Nimmo and Tanaka, 2005; Werner, 2008) during the Early and Middle Noachian, the impact-related climate change described by Segura et al. (2008) occurred at least 100 million to 200 million years before the greatest degree of valley incision. Since, each impact event produced only a few centuries, at best, of active hydrologic cycles and precipitation (Segura et al., 2008), the impact-induced climate change would not have been present at the time of valley incision. Therefore, the timing of valley incision and impact-related climate change are not contemporaneous.

Further, the impact-induced climate change model would suggest that significant valley formation happened earlier in the Noachian when larger and more frequent impacts were occurring (Hartmann and Neukum, 2001). Valley network formation should have waned over time as impacts diminished in size and frequency, producing a relationship between age and valley size (e.g. total valley length, stream order, drainage density); none of which is evident in our results (Hoke and Hynek, 2009). In fact, just the opposite is observed. The greatest degree of valley incision, which presumably coincides with the greatest degree of precipitation and surface runoff (e.g. Irwin et al., 2011), occurred at least 100 to 200 million years after the impact-related climate change described by Segura et al. (2008).

Finally, all of the valley networks in this study require several orders of magnitude longer durations of clement conditions to form than can be provided by the impact events. Even considering unrealistic scenarios of continuously high discharge rates, which give the shortest

135

formation timescales, these valley networks require 200-5000 years to form (Hoke et al., 2011).

Studies done on the morphology of fluvially-modified craters that date to the Late Noachian and

Early Hesperian note the low occurrence of exit breaches in crater rims in the southern

highlands, which suggests these surfaces did not experience deluge-like conditions (e.g. Barnhart

et al., 2009; Craddock and Howard, 2002). Rather, these studies describe moderate, episodic

periods of precipitation and evaporation that characterized valley network formation. Given

more realistic flow depths and runoff rates and assuming intermittent formation similar to that on

Earth, our formation timescales become 10^5-10^7 years, or at least three orders of magnitude longer

than what could be produced by the impacts alone (Hoke et al., 2011). Therefore, the few tens to

hundreds of years of precipitation related to any large impact event that may have occurred in the

Late Noachian is insufficient to form these large valley networks.

The timing of valley network formation on ancient Mars coincides well with the

accumulation of CO_2, H_2O, H_2S, and SO_2 from Tharsis volcanic outgassing, providing a possible

explanation for the climate change necessary for liquid water to be stable on the surface of Mars

and the formation of dense valley networks. Many researchers have determined that the

quantities of greenhouse gasses released during Tharsis formation may have been sufficient to

warm the atmosphere during the Late Noachian to the point that liquid water was stable at the

surface (e.g. Forget and Pierrehumbert, 1997; Johnson et al., 2008; Phillips et al., 2001). The

relatively short duration of warm conditions produced by some greenhouse models would have

been continuously repeated throughout the Late Noachian with each volcanic event (Johnson et

al., 2008). This scenario, just as with the impact-induced climate change scenario, would likely

also have produced valley network formation earlier in the Noachian that waned over time as

atmospheric loses to space outpaced the decreasing volcanic supply. Though, as Tian et al.

(2009) describe, the early Martian climate may have been significantly affected by the strong solar extreme ultraviolet (EUV) flux from the young sun during the first several hundred million years of solar system history. This strong EUV flux would have led to increased thermal escape of carbon from early Mars, keeping the early Martian climate relatively cold and dry (Tian et al., 2009). Eventually, the decrease in solar EUV flux as the sun matured may have allowed a build-up of atmospheric carbon that, combined with a possible release of volatiles trapped in ices on the surface of Mars, could have led to a warm, wet period lasting a few hundred Myr in the mid to late Noachian (Tian et al., 2009).

Many recent studies have concluded that evaporation from the northern lowlands, as from an ocean, would provide the humidity needed to produce the extensive valley networks seen on the north slope of the dichotomy boundary (e.g. Hynek et al., 2010; Irwin et al., 2011; Lou and Stepinski, 2009; Soto et al., 2010). Results by Soto et al. (2010) that modified an Earth climate model with Martian topography and various amounts of surface water indicate that an ocean is required to produce any significant precipitation on the surface of Mars. Without an ocean, neither a saturated regolith nor the presence of lakes associated with valley networks (Fassett and Head, 2008a) are sufficient to drive the precipitation needed for valley network formation as the water quickly becomes trapped in the colder polar and higher elevation regions of the surface (Soto et al., 2010). Their scenario that filled the northern hemisphere to 3 km below the Martian geoid produced precipitation patterns that best matches the distribution of valley networks.

Comparing the elevations of 52 deltaic deposits in open and closed basins across Mars, Di Achille and Hynek (2010a) found that their elevations varied by only a few km, consistent with their formation near a global water table. Further, when they considered only the deltas in open basins that border the northern lowlands, the range in elevations varied by less than a

kilometer from the -3km equipotential line relative to the Martian geoid (Di Achille and Hynek, 2010a). The inferred equipotential surface created by these deltas marks a potential shoreline that is similar to previously proposed shorelines for a northern ocean (Clifford and Parker, 2001), suggesting that these deltas may have formed where rivers emptied into an ocean. Similarly, by comparing the elevations of the global distribution of valley networks' highest tributaries and lowest outlets (Hynek et al., 2010) showed that less than 1% of Noachian-aged valleys extended to lower elevations than the equipotential surface derived from the open basin deltas (Di Achille and Hynek, 2010a), consistent with their formation upslope from a northern ocean.

Regardless of how the early Martian climate was able to support precipitation and surface runoff of liquid water on the surface for extended periods of time, we find abundant evidence that it did. This observation has important implications for any life that may have existed on early Mars. Although the surface was evidently warmer, wetter, and more habitable for some period of time during the Late Noachian and Early Hesperian, the variability in the location and amount of water at the surface would have made it difficult for life to evolve if it required a stable environment to do so. The terrestrial arid-like environment that may have characterized the Late Noachian on Mars (e.g. Irwin et al., 2011; Stepinski and Stepinski, 2005) may have made it difficult for life to survive. The declining impact rate would have improved the habitability in the Late Noachian, but the loss of the dynamo-induced magnetic field would have exposed the surface to more harmful radiation that would have made it difficult for life to survive on the surface. These conditions may have forced life, if it ever existed, to adapt to extreme conditions or seek refuge within the Martian crust in order to survive (Sleep and Zahnle, 1998).

References

Acuna, M. H., J. E. P. Connerney, N. F. Ness, R. P. Lin, D. Mitchell, C. W. Carlson, J. McFadden, K. A. Anderson, H. Reme, C. Mazelle, D. Vignes, P. Wasilewski, P. Cloutier 1999. Global distribution of crustal magnetization discovered by the Mars Global Surveyor MAG/ER experiment. Science 284, 790-793, doi:10.1126/science.284.5415.790.

Anderson, R. C., J. M. Dohm, M. P. Golombek, A. F. C Haldemann, B. J. Franklin, D. L. Tanaka, J. Lias, B. Peer, 2001. Primary centers and secondary concentrations of tectonic activity through time in the western hemisphere of Mars. J. Geophys. Res., 106(E9), 20563-20586, doi:10.1029/2000JE001278.

Arvidson, R., J. Boyce, C. Chapman, M. Cintala, M. Fulchignoni, H. Moore, G. Neukum, P. Schultz, L. Soderblom, R. Strom, A. Woronow, R. Young, 1979. Standard techniques for presentation and analysis of crater size-frequency data. Icarus, 37(2), 467-474, doi:10.1016/0019-1035(79)90009-5.

Baker, V. R., 1982 *The Channels of Mars*: Univ. Texas Press., Austin.

Baker V. R., 2001. Water and the Martian landscape. Nature, 412, 228-236.

Baker, V.R., Partridge, J.B., 1986. Small Martian valleys: Pristine and degraded morphology. J. Geophys. Res., 91, 3561–3572, doi:10.1029/JB091iB03p03561.

Baker, V. R., R. G. Strom, V. C. Gulick, J. S. Kargel, G. Komatsu, and V. S. Kale, 1991. Ancient oceans, ice sheets and the hydrological cycle on Mars. Nature, 352, 589-594, doi:10.1038/352589a0.

Baker et al., 1992 in *Mars* (eds Kieffer, H.H., Jakosky, B.M., Snyder, C.W., Matthews, M.S.). Univ. Arizona Press, Tucson, 493-522.

Baker, V. R., Gulick, V. C., and Kargel, J. S., 1993 in *Resources of Near-Earth Space* (eds Lewis, J. s., Matthews, M. S., and Guerrieri, M. L.). Univ. Arizona Press, Tucson, 765-797.

Bandfield, J. L., Glotch, T. D., Christensen, P. R., 2003. Spectroscopic Identification of Carbonate Minerals in the Martian Dust. Science 301, 1084, doi:10.1126/science.1088054

Barnhart, C.J., Howard, A.D., Moore, J.M., 2009. Long-term precipitation and late-stage valley network formation: Landform simulations of Parana Basin, Mars. J. Geophys. Res. 114, doi:10.1029/2008JE003122.

Bates, C. D., 1953. Rational theory of delta formation. Am. Assoc. Petrol. Geol. Bull. 37, 2119–2162.

Bhattacharya, J.P., Payenberg, T.H.D., Lang, S.C., Bourke, M., 2005. Dynamic river channels suggest a long-lived Noachian crater lake on Mars. Geophys. Res. Lett. 32, L10201.

Bibring, J. P., Y. Langevin, J. F. Mustard, F. Poulet, R. Arvidson, A. Gendrin, B. Gondet, N. Mangold, P. Pinet, F. Forget and the OMEGA team, 2006. Global mineralogical and aqueous Mars history derived from OMEGA/Mars Express data. Science, 312, 400-404.

Bierhaus, E. B., C. R. Chapman, W. J. Merline, S. M. Brooks, E. Asphaug, 2001. Pwyll secondaries and other small craters on Europa. Icarus, 153, 264-276.

Bjerklie, D.M., Dingman, S.L., Vorosmarty, C.J., Bolster, C.H., Congalton, R.G., 2003. Evaluating the potential for measuring river discharge from space. J. Hydrology 278, 17-38, doi:10.1016/S0022-1694(03)00129-X.

Boynton, W.V., Feldman, W.C., Squyres, S.W., Prettyman, T.H., Bruckner, J., Evans, L.G., Reedy, R.C., Starr, R., Arnold, J.R., Drake, D.M., Englert, P.A.J., Metzger, A.E., Mitrofanov, I., Trombka, J.I., d'Uston, C., Wanke, H., Gasnault, O., Hamara, D.K., Janes, D.M., Marcialis, R.L., Maurice, S., Mikheeva, I., Taylor, G.J., Tokar, R., Shinohara, C., 2002. Distribution of hydrogen in the near surface of Mars: Evidence for subsurface ice deposits. Science 297, 81-85.

Brain, D. A. and B. M. Jakosky, 1998. Atmospheric loss since the onset of the Martian geologic record: Combined role of impact erosion and sputtering. J. Geophys. Res., 103(E10), 22689-22694.

Burke, K., 1976. The Chad Basin: An Active Intra-Continental Basin. Tectonophys. 36, 197-206.

Bursik, M. I., 1995. Theory of the sedimentation of suspended particles from fluvial plumes. Sedimentology 42, 831-838.

Cabrol, N., Grin, E., 1999. Distribution, classification, and ages of Martian impact crater lakes. Icarus 142, 160–172.

Cabrol, N., Grin, E., 2001. The evolution of lacustrine environments on Mars: Is Mars only hydrologically dormant? Icarus 149, 291-328. doi:10.1006/icar.2000.6530.

Carr, M. H., 1995. The Martian drainage system and the origin of valley networks and fretted channels. J. Geophys. Res., 100(E4), 7479-7507.

Carr, M.H., 1996. *Water on Mars*: New York, Oxford University Press, 229 p.

Carr, M. H., 1999. Retention of an atmosphere on early Mars. J. Geophys. Res., 104, 21897-21909.

Carr, M.H., Chuang, F.C., 1997. Martian drainage densities. J. Geophys. Res. 102, 9145-9152.

Carr, M. H. and G. D. Clow, 1981. Martian channels and valleys: Their characteristics, distributions, and age. Icarus, 48(1), 91-117, doi:10.1016/0019-1035(81)90156-1.

Carr, M.H., Malin, M.C., 2000. Meter-scale characteristics of Martian channels and valleys. Icarus 146, 366-386, doi:10.1006/icar.2000.6428

Carr, M.H. and G.G. Schaber, 1977. Martian permafrost features. J. Geophys. Res., 82, 4,039-4,065.

Catling, D.C, 1999. A chemical model for evaporates on early Mars: Possible sedimentary tracers of the early climate and implications for exploration. J. Geophy. Res. 104, 16453-16469.

Christensen, P.R., 1986. Regional Dust Deposits on Mars: Physical Properties, Age, and History. J. Geophys. Res., 91, 3533–3545, doi:10.1029/JB091iB03p03533.

Christensen, P.R., Jakosky, B.M., Kieffer, H.H., Malin, M.C., McSween, H.Y., Nealson, K., Mehall, G.L., Silverman, S.H., Ferry, S., Caplinger, M., Ravine, M., 2004. The Thermal Emission Imaging System (THEMIS) for the Mars 2001 Odyssey Mission. Space Sci. Rev. 110, 85–130, doi:10.1023/B:SPAC.0000021008.16305.94.

Clark, B. C., 1979. Solar-driven chemicals energy sources for a martian biota. Origins Life 9, 645– 665.

Clark, B. C., 1999. On the non-observability of carbonates on Mars, Fifth Int. Conf. on Mars, abstract 6214, Lunar and Planet. Inst., Houston, Tex.

Colaprete, A., R. M. Haberle, T. L. Segura, O. B. Toon, K. Zahnle, 2004. The effect of impacts on the early martian climate. Second Conference on Early Mars, Abstract 8016, Lunar and Planet. Inst., Houston, Tex.

Coppus, R., Imeson, A.C., 2002. Extreme events controlling erosion and sediment transport in a semi-arid sub-andean valley. Earth Surf. Process. Landforms 27, 1365-1375, doi:10.1002/esp.435.

Craddock, R. A. and A. D. Howard, 2002. The case for rainfall on a warm, wet early Mars. J. Geophys. Res., 107(Ell), 5111, doi:10.1029/2001JE001505.

Craddock, R. A., and T. A. Maxwell, 1993. Geomorphic evolution of the Martian highlands through ancient fluvial process. J. Geophys. Res., 98, 3453–3468.

Craddock, R. A., T. A. Maxwell, and A. D. Howard, 1997. Crater morphometry and modification in the Sinus Sabaeus and Margaritifer Sinus regions of Mars. J. Geophys. Res., 102(E6), 13,321-13,340, doi:10.1029/97JE01084.

De Pablo, M., Pacifici, A., 2008. Geomorphological Evidence of Water Level Changes in Nepenthes Mensae, Mars. Icarus.

Di Achille, G., Hynek, B.M., 2010a. Ancient ocean on Mars supported by global distribution of deltas and valleys. Nature Geoscience 3, doi:10.1038/NGEO891.

Di Achille, G., and B. M. Hynek, 2010b. Deltas and valley networks on Mars: Implications for a global hydrosphere, in *Lakes on Mars*, edited by N. Cabrol, chap. 10, Elsevier, New York.

Di Achille, G., Marinangeli, L., Ori, G. G., Hauber, E., Gwinner, K., Reiss, D., Neukum, G., 2006. Geological evolution of the Tyras Vallis paleolacustrine system, Mars. J. Geophys. Res. 111, doi:10.1029/2005JE002561.

Dundas, C. and A. S. McEwen, 2005. Secondary craters and rays of Tycho, Geol. Soc. Am. Abstr. Programs, 37, Abstract 348.

Edgett, K. S., Christensen, P. R., 1991. The particle size of Martian aeolian dunes. J. Geophys Res 96, 22765-22776.

Ehlmann, B. L., Mustard, J. F., Fassett, C. I. Schon, S. C., Head, J. W., Des Marais, D. J., Grant, J. A., Murchie, S. L., 2008. Clay minerals in delta deposits and organic preservation potential on Mars. Nature Geoscience 1, doi:10.1038/ngeo207.

Fairen, A. G., Fernandez-Remolar, D., Dohm, J. M., Baker, V. R., Amils, R., 2004. Inhibition of carbonate synthesis in acidic oceans on early Mars. Nature 431, 423-426.

Farr, T.G., Rosen, P. A., Caro, E., et al., 2007. The Shuttle Radar Topography Mission. Rev. Geophys., 45, RG2004, doi:10.1029/2005RG000183.

Fassett, C. L., Head, J. W., 2005. Fluvial sedimentary deposits on Mars: Ancient deltas in crater lake in the Nili Fossae region. Geophy. Res. Lett 32, doi:10.1029/2005GL023456.

Fassett, C.I., Head III, J.W., 2008a. Valley network-fed, open-basin lakes on Mars: Distribution and implications for Noachian surface and subsurface hydrology. Icarus 198, 37-56, doi:10.1016/j.icarus.2008.06.016.

Fassett, C.I., Head III, J.W., 2008b. The timing of Martian valley network activity: Constraints from buffered crater counting. Icarus 195, 61-89, doi: 10.1016/j.icarus.2007.12.009.

Fassett, C. I., Head, J. W., 2011. Sequence and timing of conditions on early Mars. Icarus 211, 1204–1214, doi:10.1016/j.icarus.2010.11.014.

Fenton, L.K., Bandfield, J.L., Ward, A.W., 2003. Aeolian processes in Proctor Crater on Mars: Sedimentary history as analyzed from multiple data sets. Journal of Geophys. Res., 108 (E12), 5129, doi:10.1029/2002JE002015.

Fergason, R.L., Christensen, P. R., Kieffer, H. H., 2006. High-Resolution Thermal Inertia Derived from the Thermal Emission Imaging System (THEMIS): Thermal Model and Applications, J. Geophys. Res. 111, E12004, doi:10.1029/2006JE002735.

Finnegan, N.J., Roe, G., Montgomery, D.R., Hallet, B., 2005. Controls on the channel width of rivers: Implications for modeling fluvial incision of bedrock. Geology 33, 229–232, doi: 10.1130/G21171.1.

Forget, F. and R. T. Pierrehumbert, 1997. Warming early Mars with carbon dioxide clouds that scatter infrared radiation. Science, 278, 1273, doi:10.1126/science.278.5341.1273.

Forsberg-Taylor, N.K., Howard, A. D., Craddock, R.A, 2004. Crater degradation in the Martian highlands: Morphometric analysis fo the Sinus Sabaeus region and simulation modeling suggest fluvial processes. J. Geophys. Res. 109, E05002, doi:10.1029/2004JE002242.

Garvin, J., Frawley, J., 1998. Geometric properties of Martian impact craters: preliminary results from the Mars Orbiter Laser Altimeter. Geophys. Res. Lett. 25 (24), 4405–4408.

Ghatan, G. J. & Zimbelman, J. R., 2006. Paucity of candidate coastal constructional landforms along proposed shorelines on Mars: Implications for a northern lowlands-filling ocean. Icarus 185, 171-196.

Gilbert G. K., 1885. The topographic features of lake shores. U.S. Geol. Surv. Annu. Rep. 5, 69–123.

Gioia, G., Bombardelli, F.A., 2002. Scaling and similarity in rough channel flows. Phys. Rev. Lett., 88, doi:10.1103/PhysRevLett88.014501.

Goldspiel, J. M. and S. W. Squyres, 1991. Ancient aqueous sedimentation on Mars. Icarus, 89(2), 392-410, doi :10.1016/0019-1035(91)90186-W.

Goldspiel, J. M. and S. W. Squyres, 2000. Groundwater sapping and valley formation on Mars. Icarus, 148(1), 176-192, doi:10.1006/icar.2000.6465.

Goldspiel, J. M., S. W. Squyres, and D. G. Jankowski, 1993. Topography of small Martian valleys. Icarus, 105, 479– 500.

Golombek, M., Rapp, D., 1997. Size-frequency distribution of rocks on Mars and Earth analog sites: Implications for future landed missions. J. Geophys. Res., 102(E2), 4117– 4129.

Golombek, M.P., Haldermann, A.F.C., Forsberg-Taylor, N.K., DiMaggio, E.N., Schroeder, R.D., Jakosky, B.M., Mellon, M.T., Matijevic, J.R., 2003. Rock size-frequency distributions on Mars and implications for Mars Exploration Rover landing safety and operations. J. Geophys. Res., 108, E12, 8086, doi:10.1029/2002JE002035.

Golombek, M.P., Arvidson, R.E., Bell III, J.F., Christensen, P.R., Crisp, J.A., Crumpler, L.S., Ehlmann, B.L., Fergason, R.L., Grant, J.A., Greeley, R., Haldemann, A.F.C., Kass, D.M., Parker, T.J., Schofield, J.T., Squyres, S.W., Zurek, R.W., 2005. Assessment of Mars Exploration Rover landing site predictions. Nature 436, 44-48, doi:10.1038/nature03600.

Golombek, M.P., Crumpler, L.S., Grant, J.A., Greeley, R., Cabrol, N.A., Parker, T.J., Rice Jr., J.W., Ward, J.G., Arvidson, R.E., Moersch, J.E., Fergason, R.L., Christensen, P.R., Castan, A., Castan, R., Haldemann, A.F.C., Li, R., Bell III, J.F., Squyres, S.W., 2006. Geology of the Gusev cratered plains from the Spirit rover transverse. J. Geophys. Res. 100, doi:10.1029/2005JE002503.

Gomez, B., Church, M., 1989. An assessment of bed load sediment transport formulae for gravel bed rivers. Water Resources Research 25, 1161-1186.

Gough, D. O., 1981. Solar interior structure and luminosity variations. Solar Phys., 74, 21–34.

Graf, J. B., 1995. Measured and predicted velocity and longitudinal dispersion at steady and unsteady flow, Colorado River, Glen Canyon Dam to Lake Mead: Water Resources Bulletin, v. 31, no. 2, p. 265-281.

Grant, J. A., 2000. Valley formation in Margaritifer Sinus, Mars, by precipitation-recharged ground-water sapping. Geology, 28(3), 223-226, doi:10.1130/0091-7613(2000)28<223:VFIMSM>2.0.CO;2.

Grant, J. A. and P. H. Schultz, 1990. Gradational epochs on Mars: Evidence from West-Northwest of Isidis Basin and Electris. Icarus, 84(1), 166-195, doi:10.1016/0019-1035(90)90164-5.

Gulick, V. C., 2001., Origin of the valley networks on Mars: a hydrological perspective. Geomorphology, 37, 241-268, doi:10.1016/S0169-555X(00)00086-6.

Gulick, V. C., and V. R. Baker, 1990. Origin and evolution of valleys on Martian volcanoes. J. Geophys. Res., 95, 14325-14344.

Haberle, R. M., D. Tyler, C. P. McKay, and W. L. Davis, 1994. A model for the evolution of CO_2 on Mars. Icarus, 109, 102– 120.

Haberle, R.M., Murphy, J.R., Schaffer, J., 2003; Orbital change experiments with a Mars general circulation model. Icarus 161, 66-89.

Harrison, K. P, and R. E. Grimm, 2005. Groundwater-controlled valley networks and the decline of surface runoff on early Mars. J. Geophys. Res., 110, E12S16, doi:10.1029/2005JE002455.

Hartmann, W. K., 2005. Martian cratering 8: Isochron refinement and the chronology of Mars. Icarus, 174(2), 294-320, doi:10.1016/j.icarus.2004.11.023.

Hartmann, W. K. and Neukum, G., 2001. Cratering chronology and the evolution of Mars. Space Sci. Rev., 96, 165-194. doi:10.1023/A:1011945222010.

Hauber, E., Gwinner, K., Kleinhans, M., Reiss, D., Di Achille, G., Ori, G.-G., Scholten, F., Marinangeli, L., Jaumann, R., Neukum, G., 2009. Sedimentary deposits in Xanthe Terra: Implications for the ancient climate on Mars. Planetary and Space Science 57, 944–957, doi:10.1016/j.pss.2008.06.009.

Head et al., J. W., Hiesinger, H., Ivanov, M. A., Kreslavsky, M. A., Pratt, S., Thomson, B. J., 1999. Possible Ancient Oceans on Mars: Evidence from Mars Orbiter Laser Altimeter Data. Science286, 5447, 2134-2137, doi:10.1126/science.286.5447.2134

Head, J. W., Neukum, G., Jaumann, R, Hiesinger, H., Hauber, E., Carr, M., Masson, P., Foing, B., Hoffmann, H., Kreslavsky, M., Werner, S., Milkovich, S., van Gasselt, S., and the HRSC Co-Investigator Team, 2005. Tropical to mid-latitiude snow and ice accumulation, flow and glaciation on Mars. Nature, 434.

Herkenoff, K., Squyres, S. W, Arvidson, R., Bass, D. S., Bell III, J. F., Bertelsen, P., Cabrol, N. A., Gaddis, L., Hayes, A. G., Hviid, S. F., Johnson, J. R., Kinch, K. M., Madsen, M. B., Maki, J. N., McLennan, S. M., McSween, H. Y., Rice Jr., J. W., Sims, M., Smith, P. H., Soderblom, L. A., Spanovich, N., Sullivan, R., and Wang, A., 2004. Textures of the soils and rocks at Gusev Crater from Spirit's Microscopic Imager, Science, 305, 824-826, doi:10.1126/science.1100015.

Hoke, M. R. T. and B. M. Hynek, 2007. Valley Network Age Determinations: Multiple Periods of Formation. in 38th Lunar and Planetary Science Conference, Abstract 1338, Lunar and Planet. Inst., Houston, TX.

Hoke, M. R. T. and B. M. Hynek, 2008. Analyzing and dating valley networks in Arabia Terra and Terra Meridiani. Mars, in 39th Lunar and Planetary Science Conference, Abstract 1391, Lunar and Planet. Inst., Houston, Tex.

Hoke, M.R.T., Hynek, B.M., 2009. Roaming zones of precipitation on ancient Mars as recorded in valley networks. J. Geophys. Res. 114, doi:10.1029/2008JE003247.

Hoke, M. R. T., Hynek, B. M., Tucker, G. E., 2011. Formation timescales of large Martian valley networks. Earth and Planetary Science Letters 312, 1-12, doi:10.1016/j.epsl.2011.09.053.

Hostetler, S.W., and L.V. Benson, 1990. Paleoclimatic implications of the high stand of Lake Lahontan derived from models of evaporation and lake level. Climate dynamics, 4, 207-217, doi:10.1007/BF00209522.

Howard, A.D., 2007. Simulating the development of Martian highland landscapes through the interaction of impact cratering, fluvial erosion, and variable hydrologic forcing. Geomorphology 91, 332-363, doi:10.1016/j.geomorph.2007.04.017.

Howard, A.D., Moore, J.M., Irwin III, R.P., 2005. An intense terminal epoch of widespread fluvial activity on early Mars: 1. Valley network incision and associated deposits. Journal of Geophysical Research, 110, E12S14. , doi:10.1029/2005JE002460

Howard, A. D., Moore, J. M., Irwin III, R. P., Dietrich, W. E., 2007. Boulder transport across the Eberswalde delta, Lunar and Planetary Science 2007, 1168.Hynek, B.M., Phillips, R.J., 2001. Evidence for extensive denudation of the Martian highlands. Geology, 29, 407-410, doi:10.1130/0091-7613(2001)029<0407:EFEDOT>2.0CO;2.

Hutton, E.W.H., Syvitski, J.P.M., 2004. Advances in the numerical modeling of sediment failure during the development of a continental margin. Mar. Geol. 203, 367–380.

Hutton, E. W. H., Syvitski, J. P. M., 2008. Sedflux 2.0: An advanced process-response model that generates three-dimensional stratigraphy. Computer and Geosciences 34. 1319-1337, doi:10.1016/j.cageo.2008.02.013.

Hynek, B. M., and R. J. Phillips, 2001. Evidence for extensive denudation of the Martian highlands. Geology, 29(5), 407–410.

Hynek, B.M., Phillips, R.J., 2003. New data reveal mature, integrated drainage systems on Mars indicative of past precipitation. Geology, 31, 757-760, doi:10.1130/G19607.1

Hynek, B. M., M. Beach, and M. R. T. Hoke, 2008. Updated global map of martian valley networks and implications for hydrologic processes. in 39th Lunar and Planetary Science Conference, Abstract 1391, Lunar and Planet. Inst., Houston, Tex.

Hynek, B.M., Beach, M., Hoke, M.R.T., 2010. Updated global map of Martian valley networks and implications for climate and hydrologic processes. J. Geophys. Res. 115, doi:10.1029/2009JE003548.

Irwin, R. P., and A. D. Howard, 2002. Drainage basin evolution in Noachian Terra Cimmeria, Mars. J. Geophys. Res., 107(E7), 5056, doi:10.1029/2001JE001818.

Irwin, R.P., III, Howard, A.D., Craddock, R.A., Moore, J.M., 2005a. An intense terminal epoch of widespread fluvial activity on early Mars. 2. Increased runoff and paleolake development, J. Geophys. Res., 110, doi:10.1029/2005JE002460.

Irwin, R.P., III, Craddock, R.A., Howard, A.D., 2005b. Interior channels in Martian valley networks: Discharge and runoff production. Geology 33, 489-492, doi:10.1130/G21333.1.

Irwin, R. P., C. M. Fortezzo, S. E. Tooth, A. D. Howard, J. R. Zimbelman, C. J. Barnhart, A. J. Benthem, C. C. Brown, R. A. Parsons, 2008. Origin of theater-headed tributaries to Escalante and Glen Canyons, Utah: Analogs to martian valley networks. American Geophysical Union Fall Meeting 2008, abstract P41A-1351.

Irwin, R.P., III, Craddock, R.A., Howard, A.D., Flemming, H.L., 2011. Topographic influences on development of Martian valley networks. J. Geophys. Res., 116, doi:10.1029/2010JE003620.

Ivanov, B. A, 2001. Mars/Moon Cratering Rate Ratio Estimates. Space Science Reviews, 96(1-4), 87-104, doi:10.1023/A:1011941121102.

Ivanov, M.A. and Head, J.W., 2001. Chryse Planitia, Mars: Topographic configuration, outflow channel continuity and sequence, and tests for hypothesized ancient bodies of water using Mars Orbiter Laser Altimeter (MOLA) data. J. Geophys. Res. 106, 3275-3295.

Jakosky, B. M., 1986. On the thermal properties of Martian fines. Icarus 66, 117–124.

Jakosky, B. M. and R. J. Phillips, 2001. Mars' volatile and climate history. Nature, 412, 237-244.

Jakosky, B. M., B. G. Henderson, M. T. Mellon, 1995. Chaotic obliquity and the nature of the Martian climate. J. Geophys. Res., 100, 1579-1584.

Jakosky, B.M., Haberle, R.M., Arvidson, R.E., 2005. The changing picture of volatiles and climate on Mars. Science 310, 1439-1440.

Jaumann, R., D. Reiss, S. Frei, G. Neukum, F. Scholten, K. Gwinner, T. Roatsch, K.-D. Matz, V. Mertens, E. Hauber, H. Hoffmann, U. Kohler, J. W. Head, H. Hiesinger, and M. H. Carr, 2005. Interior channels in Martian valleys: Constraints on fluvial erosion by measurements of the Mars Express High Resolution Stereo Camera, Geophys. Res. Letters 32, doi:10.1029/2005GL023415.

Jaumann, R., Neukum, G., Behnke, T., Duxbury, T.C., Eichentopf, K., Flohrer, J., van Gasselt, S., Giese, B., Gwinner, K., Hauber, E., Hoffmann, H., Hoffmeister, A., Kohler, U., Matz, K.-D., McCord, T.B., Mertens, V., Oberst, J., Pischel, R., Reiss, D., Ress, E., Roatsch, T., Saiger, P., Scholten, F., Schwarz, G., Stephan, K., Wahlisch, M., the HRSC Co-Investigator Team, 2007. The high-resolution stereo camera (HRSC) experiment on Mars Express: instrument aspects and experiment conduct from interplanetary cruise through the nominal mission: planet. Space Sci. 55, 928–952.

Jerolmack, D.J., Mohrig, D., Zuber, M.T., Byrne, S., 2004. A minimum time for the formation of Holden Northeast fan, Mars. Geophys. Res. Lett. 31, L21701.

Johnson, C. L. and R. J. Phillips, 2005. Evolution of the Tharsis region of Mars: insights from magnetic field observations. Earth and Planetary Science Letters, 230(3-4), 241-254, doi:10.1016/j.epsl.2004.10.038.

Johnson, S.S., Mischna, M.A., Grove, T.L., Zuber, M.T., 2008. Sulfur-induced greenhouse warming on early Mars. J. Geophys Res 113, E08005, doi:10.1029/2007JE2962.

Kargel, J.S., Baker, V.R., Beget, J.E., Lockwood, J.F., Pewe, T.L., Shaw, J.S., Strom, R.G., 1995. Evidence of ancient continental glaciation in the Martian northern plains. J. Geophys. Res 100, 5351-5368.

Kasting, J. F., 1991. CO2 condensation and the climate of early Mars. Icarus, 94, 1–13.

Kasting, J. F., 1997. Warming early Earth and Mars. Science 276, 1213–1215.

Kieffer, H. H., Chase Jr., S. C., Miner, E., Munch, G., Neugebauer, G., 1973. Preliminary report on infrared radiometric measurements from the Mariner 9 spacecraft, J. Geophys. Res. 78, 4291-4312.

Kleinhans, M. G., 2005. Flow discharge and sediment transport models for estimating a minimum timescale of hydrological activity and channel and delta formation on Mars. J. Geophys. Res., 110, E12003.

Kleinhans, M. G., van de Kasteele, H. E., and Hauber, E., 2010. Paleoflow reconstruction from fan delta morphology on Mars. Earth Planet. Sci. Lett. 294, 378-392, doi:10.1016/j.epsl.2009.11.025.

Kleinhans, M. G. and Van den Berg, J. H., 2011. River channel and bar patterns explained and predicted by an empirical and physics-based method. Earth Surf. Process. Landforms 36, 721-738, doi:10,1002/esp.2090.

Komar, P., 1979. Comparisons of the hydraulics of water flows in Martian outflow channels with flows of similar scale on Earth. Icarus, 37, 156-181.

Komar, P., 1980. Modes of sediment transport in channelized water flows, with ramifications to the erosion of the Martian outflow channels. Icarus, 42, 317-329.

Konieczki, A. D., Graf, J. B., and Carpenter, M. C., 1997. Streamflow and sediment data collected to determine the effects of a controlled flood in March and April 1996 on the Colorado River between Lees Ferry and Diamond Creek, Arizona: U. S. Geological Survey Open-File Report 97-224, 55p.

Kraal, E. R., van Dijk, M., Postma, G., Kleinhans, M. G., 2008. Martian stepped-delta formation by rapid water release. Nature 451, doi:10.1038/nature06615.

Kubo, Y., Syvitski, J.P.M., Hutton, E.W.H., Paola, C., 2005. Advance and application of the stratigraphic simulation model 2D-SedFlux: from tank experiment to geological scale simulation. Sediment. Geol. 178, 187–195.

Kubo, Y., Syvitski, J.P.M., Hutton, E.W.H., Kettner, C., 2006. Inverse modeling of Post Glacial Maximum transgressive sedimentation using 2d-Sedflux: Application to the northern Adriatic Sea. Marine. Geol. 234, 233–243.

Lamb, M.P., Howard, A.D., Johnson, J., Whipple, K.X., Dietrich, W.E., Perron, J.T., 2006. Can springs cut canyons into rock? J. Geophys. Res. 111, E07002, doi:10.1029/2005JE002663.

Leighton, R.B. and Murray, B.C., 1966. Behavior of carbon dioxide and other volatiles on Mars. Science 153, 136–144, doi:10.1126/science.153.3732.136.

Leverington, D.W., Maxwell, T.A., 2004. An igneous origin for features of a candidate craterlake system in western Memnonia, Mars. J. Geophys. Res. 109, E06006, doi:10.1029/2004JE002237

Lowell, P. 1906. *Mars and its canals*. New York, MacMillan Company

Lucchitta, B.K., H.M. Ferguson, and C. Summers, 1986. Sedimentary deposits in the northern lowland plains, Mars. J. Geophys. Res. 91, E166-E174.

Malin, M. C., and M. H. Carr, 1999. Groundwater formation of martian valleys. Nature, 397, 589–591.

Malin, M.C. and Edgett, K.S., 1999. Oceans or seas in the martian northern lowlands: High resolution imaging tests of proposed coastlines. Geophys. Res. Lett. 26, 3049-3052, 1999.

Malin, M.C. and Edgett, K.S., 2001. Mars Global Surveyor Mars Orbiter Camera: Interplanetary cruise through primary mission. J. Geophys. Res., 106(E10), 23,429-23,570.

Malin, M. C., Edgett, K. S., 2003. Evidence for persistent flow and aqueous sedimentation on early Mars. Science 302, 1931– 1934.

Malin, M. C., Bell III, J. F., Cantor, B. A., Caplinger, M. A., Calvin, W. M., Clancy, R. T., Edgett, K. S., Edwards, L., Haberle, R. M., James, P. B., Lee, S. W., Ravine, M. A., Thomas, P. C., and Wolff, M. J., 2007. Context Camera Investigation on board the Mars Reconnaissance Orbiter. J. Geophys. Res., 112, E05S04, doi:10.1029/2006JE002808.

Mangold, N., C. Quantin, V. Ansan, C, Delacourt, P. Allemand, 2004. Evidence for precipitation on Mars from dendritic valleys in the Valles Marineris area. Science, 305(5680), 78-81, doi:10.1126/science.1097549.

Manning, R., 1891. On the flow of water in *Open channels and pipes*. Institute of Civil Engineers of Ireland Transactions, v. 20, p. 161–207.

Masursky, H., 1973. An overview of geologic results from Mariner 9. J. Geophys. Res., 78, 4009–4038.

McEwen, A. S., B. S. Preblich, E. P. Turtle, N. A. Artemieva, M. P. Golombek, M. Hurst, R. L. Kirk, D. M. Burr, P. R. Christensen, 2005. The rayed crater Zunil and interpretations of small impact craters on Mars. Icarus, 176, 351-381, doi:10.1016/j.icarus.2005.02.009

McEwen, A. S. and E. B. Bierhaus, 2006. The importance of secondary cratering to age constraints on planetary surfaces. Annu. Rev. Earth Planet. Sci., 34, 535-567, doi:10.1146/annurev.earth.34.031405.125018.

McEwen, A. S., et al. (2007), Mars Reconnaissance Orbiter's High Resolution Imaging Science Experiment (HiRISE), J. Geophys. Res., 112, E05S02, doi:10.1029/2005JE002605.

Mellon, M.T. and Jakosky, B.M, 1995. The distribution and behavior of Martian ground ice during past and present epochs. J. Geophys. Res. 100, 11781-11799.

Melosh, H. J., 1989. Impact Cratering: A Geologic Process. 253 pp., Oxford Univ. Press, New York.

Meyer-Peter E, and R. Muller, 1948. Formulas for bed-load transport. Proc., 3rd Conf. Int. Association of Hydraulic Research, Stockholm, Sweden, 39-64.

Michalski, J.R. and Niles, P.B., 2010. Deep crustal carbonate rocks exposed by meteor impact on Mars. Nature Geoscience 3, 751-755, doi:10.1038/NGE0971.

Milliken, R.E., Grotzinger, J., Murchie, S., Grant, J.A., the CRISM Team, 2007. Evidence for hydrated phyllosilicates in Holden Crater, Mars using hyperspec- tral CRISM data. Lunar Planet. Sci. XXXIII (abstract 1913).

Milton, D. J., 1973. Water and process of degradation in the Martian landscape. J. Geophys. Res. 78(20), 4037-4047.

Mischna, M. A., J. F. Kasting, A. Pavlov, and R. Freedman, 2000. Influence of carbon dioxide on early martian climate. Icarus, 145, 546– 554.

Mischna, M. A., M. I. Richardson, R. J.Wilson, and D. J. McCleese, 2003. On the orbital forcing of Martian water and CO2 cycles: A general circulation model study with simplified volatile schemes. J. Geophys. Res., 108(E6), 5062, doi:10.1029/2003JE002051.

Molnar, P., 2001. Climate change, flooding in arid environments, and erosion rates. Geology 29 (12), 1071-1074.

Moore, J.M., Howard, A.D., Dietrich, W.E., Schenk, P.M., 2003. Martian layered fluvial deposits: implications for Noachian climate scenarios. Geophys. Res. Lett. 30, 2292.

Morehead, M.D., Syvitski, J.P.M., Hutton, E.W.H., 2001. The link between abrupt climate change and basin stratigraphy: a numerical approach. Glob. Planet. Change 28, 107–127.

Mukhin, L. M., A. P. Koscheev, Yu. P. Dikov, J. Huth, and H. Wanke, 1996. Experimental simulations of the photodecomposition of carbonates and sulphates on Mars. Nature, 379, 141– 143.

Murchie, S. L., et al., 2009. A synthesis of Martian aqueous mineralogy after one Mars year of observations from the Mars Reconnaissance Orbiter. J. Geophys. Res., 114, E00D06, doi:10.1029/2009JE003342.

Mutch, T.A., Arvidson, R.E., Jones, K.L., Head, J.W., Saunders, R.S., 1976. *The Geology of Mars,* Princeton Univ. Press, Princeton, New Jersey.

Nelson, D.M. and Greeley, R., 1999. Geology of Xanthe Terra outflow channels and the Mars Pathfinder landing site. J. Geophys Res. 104, 8653-8669, doi:10.1029/98JE01900.

Neukum, G., R. Jaumann, and the HRSC Co-Investigator and Experiment Team, 2004. HRSC: The High Resolution Stereo Camera of Mars Express, in *Mars Express: The scientific payload*, edited by A. Wilson, pp. 17-35, ESA, Noordwijk, The Netherlands.

Newman, M. J., and R. T. Rood, 1977. Implications of solar evolution for the Earth's early atmosphere, Science, 198, 1035– 1037.

Nimmo, F. and K. Tanaka, 2005. Early crustal evolution of Mars. Annual Review of Earth and Planetary Science, 33, 133-161, doi:10.1146/annurev.earth.33.092203.122637.

Ori, G., Marinangeli, L., Baliva, A., 2000. Terraces and Gilbert-type deltas in crater lakes in Ismenius and Memnonia (Mars). J. Geophys. Res. 105, 17629–17641.

Osterkamp, W. R., and E. R. Hedman, 1982. Perennial-streamflow characteristics related to channel geometry and sediment in Missouri River basin. U. S. Geological Survey Professional Paper 1242, 37.p

Osterloo, M. M. et al., 2008. Chloride-bearing materials in the southern highlands of Mars. Science 319, 1651–1654.

Osterloo, M. M., F. S. Anderson, V. E. Hamilton, and B. M. Hynek, 2010. The geologic context of proposed chloride-bearing materials on Mars. J. Geophys. Res., doi:10.1029/2010JE003613.

Paola, C. and D. Mohrig, 1996. Palaeohydraulics revisited: palaeoslope estimation in coarse-grained braided rivers. Basin Research 8, 243-254.

Parker, G. 1978. Self-formed straight rivers with equilibrium banks and mobile bed. Part 2. The gravel river. J. Fluid Mech. 89, 127-146.

Parker, T. J., R. S. Saunders, and D. M. Schneeberger, 1989. Transitional morphology in west Deuteronilus Mensae, Mars: Implications for modification of the lowland/upland boundary. Icarus, 82, 111 – 145.

Parker, T. J., D. S. Gorsline, R. S. Saunders, D. C. Pieri, and D. M. Schneeberger, 1993. Coastal geomorphology of the martian northern plains. J. Geophys. Res., 98, 11,061– 11,078.

Pelkey, S. M., B. M. Jakosky, and M. T. Mellon, 2001. Thermal inertia of crater-related wind streaks on Mars. J. Geophys. Res. 106, 23909-23920.

Phillips, R. J., M. T. Zuber, S. C. Solomon, M. P. Golombek, B. M. Jakosky, W. B. Banerdt, R. M. E. Williams, B. M. Hynek, O. Aharonson, and S. A. Hauck II, 2001. Ancient geodynamics and global-scale hydrology on Mars, Science, 291(5513), 2587-2591, doi:10.1126/science.1058701.

Pieri, D., 1976. Distribution of small channels on the martian surface. Icarus, 27, 25– 50.

Pieri, D. C., 1980. Martian valleys: morphology, distribution, age, and origin, Science 210(4472), 895-897, doi:10.1126/science.210.4472.895.

Pollack, J. B., J. F. Kasting, S. M. Richardson, and K. Poliakoff, 1987. The case for a wet, warm climate on early Mars, Icarus, 71, 203–224.

Pondrelli, M., Rossi, A. P., Marinangeli, L., Hauber, E., Gwinner, K., Baliva, A., Di Lorenzo, S., 2008. Evolution and depositional environments of the Eberswalde fan delta, Mars, Icarus 197, 429-451, doi: 10.1016/j.icarus.2008.05.018.

Pondrelli, M., Rossi, A. P., Platz, T., Ivanov, A., Marinangeli, L., Baliva, A., 2010. Geological, geomorphological, facies and allostratigraphic maps of the Eberswalde fan delta. Planet. Space Sci., doi:10.1016/j.pss.2010.10.009.

Presley, M. A. and P. R. Christensen, 1997. Thermal conductivity measurements of particulate materials 2. Results. J. Geophys. Res.102, 6551-6566.

Putzig, N. E., Mellon, M. T., 2007. Apparent thermal inertia and the surface heterogeneity of Mars, Icarus, 191, 68-94, doi: 10.1016/j.icarus.2007.05.013.

Quantin, C., P. Allemand, N. Mangold, G. Dromart, C. Delacourt, 2005. Fluvial and lacustrine activity on layered deposits in Melas Chasma, Valles Marineris, Mars. J. Geophys. Res., 110, E12S19, doi:10.1029/2005JE002440.

Ribas, I., Guinan, E. F., Gudel, M. and Audard, M. 2005. Evolution of the solar activity over time and effects on planetary atmospheres. I. High-energy irradiances (1-1700 A), Astrophys. J. 622, 680.

Ribberink, J. S., 1998. Bed-load transport for steady flows and unsteady oscillatory flows, Coastal Eng., 34, 59-82.

Ritter, D. F., 1978. *Process Geomorphology*, 603 pp., Wm. C. Brown Company Publishers, Dubuque, IA.

Rotto, S. and Tanaka, K. L., 1995. Geologic/geomorphic map of the Chryse Planitia region of Mars, U.S. Geol. Surv. Misc. Invest. Ser., Map I-2441.

Schick, A. P., 1988. Hydrologic aspects of floods in extreme arid environments. *Flood Geomorphology*, eds. V. R. Baker, R. C. Kochel, P. C. Patton.

Schieber, J., 2007. Reinterpretation of the Martian Eberswalde Delta in the light of new HiRISE images (abstract). Lunar Planet. Sci. XXXVIII (abstract 1982).

Schubert, G., C. T. Russell, W. B. Moore, 2000. Timing of the martian dynamo, Nature, 408, 666-667.

Scott, D. H., J. M. Dohm, and J. W. Rice Jr., 1995. Map of Mars showing channels and possible paleolake basins. U.S. Geol. Surv. Misc. Invest. Ser., Map I-1350, 1:30,000,000.

Segura, T. L., O. B. Toon, A. Colaprete, K. Zahnle, 2002. Environmental effects of large impacts on Mars, Science 298(5600), 1977-1980, doi:10.1126/science.1073586.

Segura, T. L., O. B. Toon, A. Colaprete, 2008. Modeling the environmental effects of moderate-sized impacts on Mars. J. Geophys. Res. 113, E11007, doi:10.1029/2008JE003147.

Seibert, N.M. and Kargel, J.S., 2001. Small-scale Martian polygonal terrain : Implications for liquid surface water. Geophys Res Let 28, 899-902, doi :10.1029/2000GL012093.

Sharp, R. P., and M. C. Malin, 1975. Channels on Mars. Geol. Soc. Am. Bull., 86, 593-609.

Shoemaker, E. M., 1965. Preliminary analysis of the fine structure of the lunar surface in Mare Cognitum, JPL Tech. Report No. 32-700, in *The Nature of the Lunar Surface*, ed. W. N. Hess, D. H. Menzel, J. A. O'Keefe, p 23-77, Johns Hopkins Press, Baltimore.

Silberman, E., R. Carter, H. Einstein, J. Hinds, R. Powell, and ASCE Task Force on Friction Factors in Open Channels. 1963. Friction factors in open channels, J. Hydraul. Eng, 89 (HY2), 97-143.

Skinner, J. A., Jr., T. M. Hare, K. L. Tanaka, 2006. Digital renovation of the atlas of Mars 1:15,000,000-scale global geologic series maps, 37th Lunar and Planetary Science Conference, Abstract 2331, Lunar and Planet. Inst., Houston, Tex.

Sklar, L. S., Dietrich, W. E., 2004. A mechanistic model for river incision into bedrock by saltating bed load. Water Resources Res. 40, W06301, doi:10.1029/2003WR002496

Sleep, N. H., and K. Zahnle, 1998. Refugia from asteroid impacts on early Mars and the early Earth. J. Geophys. Res,. 103, pp. 28,529-28,544.

Smith, M.D., 2002. The annual cycle of water vapor on Mars as observed by the Thermal Emission Spectrometer. J. Geophys. Res 107, doi:10.1029/2001JE001522.

Smith, D. E., M. T. Zuber, H. V. Frey, J. B. Garvin, J. W. Head, D. O. Muhleman, G. H. Pettengill, R. J. Phillips, S. C. Solomon, H. J. Zwally, W. B. Bandert, T. C. Duxbury, M. P. Golombek, F. G. Lemoine, G. A. Newmann, D. D. Rowlands, O. Aharonson, P. G. Ford, A. B. Ivanov, C. L. Johnson, P. J. McGovern, J. B. Abshire, R. S. Afzal, X. Sun (2001), Mars Orbiter Laser Altimeter: Experiment summary after the first year of global mapping of Mars, J. Geophys. Res., 106(E10), 23,689-23,722,. doi :10.1029/2000JE001364

Smith, P.H., L. K. Tamppari, R. E. Arvidson, D. Bass, D. Blaney, W. V. Boynton, A. Carswell, D. C. Catling, B. C. Clark, T. Duck, E. DeJong, D. Fisher, W. Goetz, H. P. Gunnlaugsson, M. H. Hecht, V. Hipkin, J. Hoffman, S. F. Hviid, H. U. Keller, S. P. Kounaves, C. F. Lange, M. T. Lemmon, M. B. Madsen, W. J. Markiewicz, J. Marshall, C. P. McKay, M. T. Mellon, D. W. Ming, R. V. Morris, W. T. Pike, N. Renno, U. Staufer, C. Stoker, P. Taylor, J. A. Whiteway, A. P. Zent, 2009. H2O at the Phoenix Landing Site. Science 325, 58, doi:10.1126/science.1172339

Solyom, P. B. and G. E. Tucker, 2004. Effect of limited storm duration on landscape evolution, drainage basin geometry, and hydrograph shapes. J. Geophys. Res., 109, F03012, doi:10.1029/2003JF000032.

Som, S. M., D. R. Montgomery, H. M. Greenberg. 2009. Scaling relations for large Martian valleys. J. Geophys. Res. 114, E02005, doi:10.1029/2008JE003132.

Soto, A. and M.I. Richardson, Water at the Surface of Mars. Second Workshop on Mars Valley Network*s*, pp. 66-68, Smithsonian Institute, 2009

Soto, A., M. I. Richardson, and C. E. Newman, 2010. Global constraints on rainfall on ancient Mars: Oceans, lakes, and valley networks. Lunar Planet. Sci., XLI, Abstract 2397.

Squyres, S. W., Arvidson, R. E., Bell III, et. al., 2004. The Opportunity Rover's Athena Science Investigation at Meridiani Planum, Mars. Science, 306, 1698-1703. doi:10.1126/science.1106171.

Stepinski, T. F. and M. L. Collier, 2004. Extraction of Martian valley networks from digital topography. J. Geophys. Res., 109, E11005, doi:10.1029/2004JE002269.

Stepinski, T. F., A. P. Stepinski., 2005. Morphology of drainage basins as an indicator of climate on early Mars. J. Geophys. Res 110, E12S12, doi :10.1029/2005JE002448.

Stevenson. D. J., 2001. Mars' core and magnetism. Nature, 412, 214-219.

Strahler, A. N., 1958. Dimensional analysis applied to fluvially eroded landforms. Geol. Soc. Am. Bull., 69, p 279-300.

Strom, R.G., Croft, S.K., Barlow, N.G., 1992. in *Mars* (eds Kieffer, H.H., Jakosky, B.M., Snyder, C.W., Matthews, M.S.) 383-423. Univ Arizona Press, Tucson.

Syvitski, J.P.M., Hutton, E., 2001. 2D SEDFLUX 1.0C: An advanced process-response numerical model for the fill of marine sedimentary basins. Computers and Geosciences, 27. doi:10.1016/S0098-3004(00)00139-4.

Syvitski, J.P.M., Smith, J.N., Calabrese, E.A., Boudreau, B.P., 1988. Basin sedimentation and the growth of prograding deltas. Journal of Geophysical Research 93 (6), 6895-6908.

Tanaka, K. L., 1982. A new time-saving crater-counting technique, with application to narrow features. NASA Tech. Memo. 85127, 123-125.

Tanaka, K. L., 1986. The stratigraphy of Mars. J. Geophys. Res., 91, E139-E158.

Tanaka, K.L., 1999, Debris-flow origin for the Simud/Tiu deposit on Mars, J Geophys Res 104, p. 8637–8652.

Taylor, G. J., et al., 2006. Variations in K/Th on Mars. J. Geophys. Res., 111, E03S06, doi:10.1029/2006JE002676.

Tian, F., J. F. Kasting, and S. C Solomon, 2009. Thermal escape of carbon from the early Martian atmosphere. Geophys. Res. Lett., 36, doi:10.1029/2008GL036513.

Toon, O. B., Segura, T., and Zhanle, K., 2010. The formation of Martian river valleys by impacts. Annu. Rev. Earth Planet. Sci. 38, 303-322, doi :10.1146/annurev-earth-040809-152354.

Tucker, G. E. and R. L. Bras, 1998. Hillslope processes, drainage density, and landscape morphology, Water Resources Research, 34(10), 2751-2764.

Tucker, G. E. and R. Slingerland, 1997. Drainage basin responses to climate change, Water Resources Research, 33, 2031-2047.

Tucker, G. E., L. Arnold. R. L. Bras, H. Flores, E. Istanbulluoglu, P. Solyom, 2006. Headwater channel dynamics in semiarid rangelands, Colorado high plains, USA. GSA Bulletin 118, 959-974, doi :10.1130B25928.1.

USGS and NASA, 2009, Global Land Survey 2005, Sioux Falls, SD USA: USGS Center for Earth Resources Observation and Science (EROS).

van Rijn, L. C, 1984a. Sediment transport, Part I: Bed load transport., J. Hydraul. Eng. 110, 1431-1456.

van Rijn, L. C, 1984b. Sediment transport, Part II: Suspended load transport., J. Hydraul. Eng. 110, 1613-1641.

Werner, S. C., 2008. The early Martian evolution – Constraints from basin formation ages. Icarus 195, 45-60, doi:10.1016/j.icarus.2007.12.008.

Wilhelms, D. E., V. R. Oberbeck, H. R. Aggarwal, 1978. Size-frequency distributions of primary and secondary lunar impact craters, Proc. Lunar Planet. Sci, 9, 3735-3762.

Williams, R. M. E., and R. J. Phillips, 2001. Morphometric measurements of martian valley networks from Mars Orbiter Laser Altimeter (MOLA) data, J. Geophys. Res., 106(E10), 23737-23752.

Wilson, L., G. J. Ghatan, J. W. Head III, K. L. Mitchell., 2004. Mars outflow channels: A reappraisal of the estimation of water flow velocities from water depths, regional slopes, and channel floor properties. J. Geophys. Res., 109, E09003.

Withers, P. and Neumann, G.A., 2001. Enigmatic northern plains of Mars. Nature 410, 651.

Wolman, M. G., and J. P. Miller., 1960. Magnitude and frequency of forces in geomorphic process. J. Geol. 68. 54-74.

Wong, M. and Parker, G., 2006. Reanalysis and correction of bed-load relation of Meyer-Peter and Muller using their own database. J. Hyrdaul. Eng. 132, 1159-1168, doi:10.1061/(ASCE)0733-9429(2006)132:11(1159).

Wood, L.J., 2006. Quantitative geomorphology of the Mars Eberswalde delta. Geol. Soc. Am. Bull. 118, 557–566.